Edgar Ângelo Jacinto Castanheira

Licenciado em Química Aplicada

Smart Mesoporous Silica Glyconanoparticles for Theranostics

Dissertação para obtenção do Grau de Mestre em

Química Bioorgânica

Orientador: Carlos Baleizão, Professor Auxiliar, IST-UL.

Co-orientador: Carina Crucho, Investigadora Pós-Doutoral, IST-UL.

Presidente: Prof. Doutora Paula Cristina de Sério Branco
Arguente: Doutora Sandra Maria Nunes Gago
Vogal: Prof. Doutor Carlos Miguel Calisto Baleizão

FACULDADE DE CIÊNCIAS E TECNOLOGIA
UNIVERSIDADE NOVA DE LISBOA

[Outubro 2018]

THIS

PAGE INTENTIONALLY

LEFT BLANK

“Smart Mesoporous Silica Glyconanoparticles for Theranostics”

THIS

PAGE INTENTIONALLY

LEFT BLANK

Acknowledgments

Gostaria de começar por agradecer aos meus orientadores, Prof. Dr. Carlos Baleizão e Dr. Carina Crucho, por me terem instruído uma grande parte do conhecimento que aqui espero demonstrar, a vossa orientação e apoio foi crucial para a conclusão deste trabalho. Durante este ano, não só me ensinaram o que é verdadeiramente trabalhar num ambiente académico, mas como também, incumbiram-me de valores que espero manter durante todo o meu percurso profissional. Gostaria de agradecer também ao Prof. Dr. José Farinha, por todas as opiniões e conhecimentos trespassados durante as reuniões e encontros de grupo.

De seguida, gostaria de agradecer a todos os meus colegas de laboratório, especialmente à Márcia, José, Bárbara, Tiago, Daniela e Filipa, pelo tempo que passamos juntos. A verdade, é que é dito que a ciência não é algo que se faça sozinho, é necessária muita colaboração, e o apoio que é transmitido dentro das quatro paredes (ou três e meia) e entre todos os colegas, é algo que deve ser devidamente mencionado e apreciado. Não importa o quanto o dia fosse difícil ou as coisas estivessem a correr mal, espero que tenha estado lá com um sorriso para vocês, tal como estiveram para mim. Não poderia deixar de agradecer aos restantes membros do *Optical & Multifunctional Materials group*, que embora a partilha de momentos não tenha sido tão abundante, mas foram de grande qualidade e que de alguma forma possibilitaram o desenvolvimento deste projeto.

Não poderia deixar de agradecer, ao Pedro, à Rita e à Adriana. A “concorrência” que esteve sempre lá para dar uma mãozinha. Agradecer aos inúmeros almoços, cafés e conversas permitiram conhecer três pessoas maravilhosas e que facilitaram bastante este percurso. À Rita, a santa das causas perdidas, que não perdeu um minuto para me vir socorrer sempre que precisava de ajuda ou companhia. Ao pedro, que com a sua descontração, criava um ambiente propicio a boa ciência, e duas horas de almoço se tivéssemos de esperar que ele acabasse de comer. Como último membro da “concorrência”, gostaria de agradecer à Adriana por estes últimos dois anos, por ser quem é, sem receios nem vergonhas. Houve muitas queixas, desabafos e preocupações, e tentei dar o melhor de mim para te ajudar, mas na verdade acho que eras tu que acabavas por me ajudar, não só a seguir em frente de cabeça erguida, mas também a tirar conclusões, sobre variados assuntos, que talvez sozinho não chegasse lá, obrigado.

Prosseguindo com os agradecimentos, não poderia deixar de mencionar as pessoas que não tiveram ligadas diretamente com este trabalho, mas que não deixaram de ser essenciais. Ao Cristiano, a minha companhia de workshops e congressos, que apesar de parecer desajeitado e na lua, é um amigo com que se pode contar, irá chegar atrasado, mas estará lá. Com o potencial que tens mostrado, vais chegar longe, não tenho dúvida, nem que seja aos 902 metros de altura da serra de Monchique. Por falar em alturas, à pequena grande guerreira Mariana, gostaria de

expressar um enorme agradecimento, por me mostrar o que significa não desistir, nem quando tudo parece que está a descambar, ela mostrou resistência. Nem sempre, o teu empenho foi bem recebido, mas olha para onde te trouxe, parabéns e continua assim. À Bibas e Gabi, as companheiras de curso, de escrita de tese, de coscuvilhices, de parvoíce e podia continuar por aí fora. Duas pessoas fundamentais quer na licenciatura, quer no mestrado, que se não fossem elas, nesta altura se calhar ainda andava de volta de elementos. Espero cultivar a vossa amizade por bastante tempo. Obrigado pelos últimos cinco anos. Em relação ainda ao ambiente de faculdade, gostaria de agradecer ao Bruno. Nunca pensei poder aprender tanto com uma pessoa e sucessivamente ser surpreendido pelo que ainda tem para ensinar. Obrigado pela quantidade de *E. buffer* dado e pelos empurrões para crescer melhor e mais rápido, se não fosses tu, se calhar nem estaria onde estou hoje. És um exemplo a seguir, quer a nível profissional, quer a nível pessoal, obrigado por tudo. Se realmente os amigos de faculdade são para toda a vida, estes são os que eu espero que façam parte da minha.

Continuando, com os amigos essenciais fora da faculdade, obrigado Chico, Dani, Inês, Bruno e Claudete. As rotas fora de rotina com vocês pelo Ama, golden moon, johnnys ou old mustache man's cakes tornaram-se algo simples e imprevisível, mas que serve sempre para meter todo o tipo de conversa em dia. Os momentos partilhados com vocês foram fundamentais para carregar baterias, aumentar a produtividade e ganhar novas perspetivas.

Para terminar gostaria de agradecer à família, que sempre esteve, está e estará presente, em momentos de alegria, tristeza ou de neutralidade. Aos meus irmãos, Dário e Rita, que embora não estejamos muito tempo juntos, estamos sempre cá uns para os outros. Como a minha avó diz, a Ritinha é uma grande mulher, e é uma grande verdade, estou orgulhoso de ti mana e obrigado por tudo. Ao meu irmão, os parabéns por ter vergado pelo seu próprio caminho e ter tido bastante sucesso, obrigado pelo exemplo dado. Desejo-te as maiores felicidades com a Natacha e o Rafa, e que eu esteja lá para instruir o miúdo a ir para ciências. Ao meu Pai babado, que dá tudo o que tem aos filhos e orgulha-se de quem são, mas por vezes não se orgulha de quem é, mas um filho só é aquilo que os pais fazem dele, por isso estou te grato do fundo do coração. E por último um agradecimento à minha mãe, sei que foi um ano difícil para ti, mas como sempre ultrapassaste, e com um sorriso na cara, porque é o que sempre fazes, encaras todo o tipo de obstáculos e sais a sorrir, se isto não é a definição de como ser uma heroína, não sei o que é. Sem vocês nada disto seria possível, obrigado a todos!

Um último agradecimento ao Instituto Superior Técnico e à Faculdade de Ciência e Tecnologia da Universidade Nova de Lisboa por cederem as infraestruturas necessárias à realização deste mestrado e à Fundação para a Ciência e Tecnologia no âmbito dos projetos PTDC/CTM-NAN/6249/2014 e UID/QUI/00100/2013.

"if you wish to move mountains tomorrow

you must start by lifting stones today" – African proverb

Resumo

As nanopartículas mesoporosas de sílica são uma plataforma adequada para entrega de fármacos devido às suas propriedades únicas, como a elevada capacidade de armazenar e proteger fármacos, e a possibilidade de ajustar o tamanho de partícula e diâmetro de poro. A imobilização de moléculas bioativas e polímeros com resposta a estímulos na superfície externa das partículas permite o aumento da biocompatibilidade e biodisponibilidade do fármaco, aumento da concentração no local de interesse e redução dos efeitos secundários.

Este trabalho consistiu na preparação de nanopartículas mesoporosas fluorescentes de sílica, com uma coroa polimérica de um *co*-polímero com unidades monossacarídicas e unidades responsivas ao pH. Assim, o diagnostico de células cancerígenas é realizado pelo bloco de açúcar e a terapia com recuso à libertação controlada pelo pH.

As nanopartículas fluorescentes de sílica foram preparadas através do método de Stöber, com incorporação na sua estrutura de um derivado de perilenodiimida (PDI). As nanopartículas foram caracterizadas por microscopia eletrónica de transmissão, apresentando diâmetros de 30 nm a 65 nm. Os homo e co-polímeros foram sintetizados por polimerização controlada por RAFT e caracterizados por UV-Vis e cromatografia por exclusão de tamanho (SEC), obtendo-se uma polidispersividade inferior a 1.2. A superfície externa das nanopartículas foi funcionalizada para permitir a imobilização dos polímeros. Estas modificações foram caracterizadas por ^{1}H-RMN, UV-Vis e potencial-ζ. Foram utilizados quatro métodos diferentes: “transfer to”, “graft to”, “graft from” e híbrido para imobilizar o polímero à partícula. Para as partículas com uma camada de polímero monossacarídica, foram obtidas percentagens em massa entre 0.5% a 4.3%.

A imobilização do co-polímero na superfície externa das nanopartículas foi obtida com uma percentagem mássica de 2% através do método “graft to”. A imobilização do *co*-polímero foi também obtida através do método híbrido, apresentando resultados promissores, mostrando o sucesso da estratégia utilizada nesta tese.

Palavras-Chave: Nanopartículas stöber de sílica; Nanopartículas mesoporosas de sílica; Polimerização por RAFT; nanopartículas monossacarídicas híbridas com resposta a estímulos; Terapia e diagnostico.

THIS

PAGE INTENTIONALLY

LEFT BLANK

Abstract

Mesoporous silica nanoparticles provide a versatile drug-delivery platform due to their exceptional properties, such as, high payload uptake, tunable pore width and particle size and protection over the guest molecule. The external surface can be functionalize with bioactive molecules and stimuli responsive polymers, improving the biocompatibility and drug bioavailability, increasing the local dose delivered and decreasing the side effects.

The objective of this work was to synthesize fluorescent hybrid MSNs, coated with a *co*-polymeric shell containing pH-responsive and carbohydrate blocks obtained through RAFT polymerization. Such combination opens the possibility of diagnosis, through carbohydrates recognition ability towards cancer cells, and therapy by a pH mediated controlled release.

The fluorescent silica nanoparticles were prepared by the Stöber method, incorporating a high quantum yield perylenediimide (PDI) in the silica structure. The nanoparticles were characterized by transmission electronic microscopy, with diameters of 30 nm and 65 nm with low size dispersity. The homo and *co*-polymers were synthesized by RAFT polymerization and characterized by UV-Vis and size exclusion chromatography (SEC), with a polydispersity below 1.2. The external surface of the MSNs was functionalized to allow the immobilization of the smart polymer. Surface modifications were assessed and quantified using ^{1}H-NMR, UV-Vis and ζ-Potential. Polymer immobilization on the MSNs external surface were performed using four different methods: “transfer to”, “graft to”, “graft from” and a hybrid method. The particles modified with the homo carbohydrate polymer were obtained with polymer weight percentage between 0.5% and 4.3%.

The immobilization of the final pH-responsive/carbohydrate co-polymer was achieved with a 2% polymer weight via “graft to” method. The immobilization by the hybrid method was also achieved, with promising results, indicating that our strategy is correct.

Key-Words: Stöber silica nanoparticles; Mesoporous silica nanoparticles; RAFT polymerization; Smart hybrid glyconanoparticles; Theranostics.

THIS

PAGE INTENTIONALLY

LEFT BLANK

Table of contents

1. Introduction 1

1.1. Drug Delivery Systems 2

1.2. Silica Nanoparticles 3

1.2.1. Mesoporous Silica Nanoparticles 5

1.2.2. Biocompatibility 6

1.3. Fluorescent Mesoporous Silica Nanoparticles 7

1.4. Controlled Radical Polymerization 8

1.4.1. Nitroxide-mediated polymerization 9

1.4.2. Atom Transfer Radical Polymerization 10

1.4.3. Reverse Addition-Fragmentation Chain Transfer 11

1.5. Hybrid Mesoporous Silica Nanoparticles 12

1.6. Smart fluorescent hybrid MSNs for cancer theranostic 13

1.6.1. Specificity and internalization 14

1.6.2. Tracking 15

1.6.3. Controlled release 15

1.7. Work Objective 17

2. Results and Discussion 21

2.1. Synthesis and characterization of fluorescent silica nanoparticles 21

2.2. Surface functionalization of silica nanoparticles 24

2.2.1. Amine modified silica nanoparticles 24

2.2.2. Functionalization with the chain transfer agent for RAFT polymerization 26

2.2.3. ζ-potential 29

2.3. Galactose-based monomer synthesis and polymerization 30

2.3.1. Synthesis of 2`-acrylamidoethyl-β-D-Galactose tetraacetate (AMEGalOAc) 30

2.4. Synthesis of 2-(diiso-propylamino) ethyl methacrylate (DPAEMA) 32

2.6. Synthesis of Stöber glyco-nanoparticles 36

2.6.1. Grafting densities 36

2.7. Stöber glyco-nanoparticles with dithiobenzoate as CTA 37

2.8. Improving "grafting from" polymerization onto stöber nanoparticles 39

2.9. Co-polymer synthesis 41

3. Conclusions and future work 45

4. Experimental section 47

4.1. Reagents and solvents 47

4.2. Equipment 47

4.2.1. Centrifuge 47
4.2.2. Transmission Electronic Microscopy (TEM) 47
4.2.3. Nuclear magnetic resonance (NMR) 48
4.2.4. UV-Vis spectroscopy 48
4.2.6. Size Exclusion Chromatography (SEC) 48
4.3. Experimental procedure 48
4.3.1. Synthesis of fluorescent stöber silica nanoparticles 48
4.3.2. Synthesis of fluorescent mesoporous silica nanoparticles 49
4.3.3. Modification of silica nanoparticles surface 49
4.3.4. Synthesis of 3-(benzylsulfanylthiocarbonylsulfanyl) propionic acid (BSPA) 50
4.3.5. Carbohydrate-based ethoxy acrylamide monomer 51
4.3.6. Synthesis of 2-(diisopropylamino) ethyl methacrylate (DPAEMA) 52
4.3.7. Deprotection of 2`-acrylamidoethyl-β-D-Galactose tetraacetate 52
4.3.8. RAFT polymerization in solution 52
4.3.9. Polymer graft at SiNPs surface 54
5. References 57
6. Attachments 63
6.1. NMR Spectra 63
6.1.1. BSPA 63
6.1.2. β-D-Galactose pentaacetate *(GalOAc)* 63
6.1.3.* 2`-acrylamidoethyl-β-D-Galactose tetraacetate *(AMEGalOAc) 65
6.1.4. 2-(diiso-propylamino) ethyl methacrylate (DPAEMA) 67
6.1.5.* 2`-acrylamidoethyl-β-D-Galactose *(AMEGal) 67
6.1.6. Particle grafted polymer 68
6.2. Calculation of the surface coverage 69
6.3. Chromatograms 69
6.3.1.* Polymer of 2`-acrylamidoethyl-β-D-Galactose tetraacetate *(PAMEGalOAc) 69
6.3.2.* Polymer of 2`-acrylamidoethyl-β-D-Galactose *(PAMEGal) 71
6.3.3. Polymer for 2-(diiso-propylamino) ethyl methacrylate (PDPAEMA) 72
6.3.4. Co-Polymerization of DPAEMA and AMEGal 73

Figure Index

Figure 1.1 – Different types of organic and inorganic drug delivery systems. 2
Figure 1.2 – Formation of the mesoporous. 6
Figure 1.3 – Chemical structure of the perylene diimide (PDI) derivative. 8
Figure 1.4 – Chemical structure for (2,2,6,6-Tetramethylpiperidin-1-yl) oxyl (TEMPO). 9
Figure 1.5 – Differences in grafting-from and transfer-to mechanisms. 13
Figure 1.6 – Receptor mediated endocytosis mechanism. 15
Figure 1.7 – Structures of tertiary amine-based methacrylate pH-responsive monomers. 17
Figure 1.8 – Schematic representation of the expected behavior for the co-polymer. 17
Figure 2.1 – TEM images for the stöber nanoparticles synthesized and their respective size distribution histogram. 22
Figure 2.2 – TEM image for the mesoporous silica nanoparticles synthesized and their respective size distribution histogram. 22
Figure 2.3 – Normalized abbsorption and emission spectra for perylenediimide derivative. 23
Figure 2.4 – ^{1}H-NMR obtained for the amine functionalized nanoparticles. 25
Figure 2.5 – TEM image of the synthesized mesoporous silica nanoparticles. 25
Figure 2.6 – ^{1}H-NMR obtained for 3-(benzylsulfanylthiocarbonylsulfanyl) propionic acid – compound **(1)**. 26
Figure 2.7 – Absorption spectra overlap for CTA-SiNp and NH_2-SiNp. 28
Figure 2.8 – Zeta-potential for NPs after the different surface modifications. 30
Figure 2.9 – ^{1}H-NMR obtained for compound 2`-acrylamidoethyl-β-D-Galactose tetraacetate (AMEGalOAc) – compound **(3)**. 32
Figure 2.10 – Synthesis of the pH-responsive, 2-(diiso-propylamino) ethyl methacrylate (DPAEMA) – compound **(4)** 32
Figure 2.11 – ^{1}H-NMR obtained for 2-(diiso-propylamino) ethyl methacrylate (DPAEMA) – compound (**4**). 33
Figure 2.12 – Kinetic plot of acrylamide galactose-based monomer – AMEGalOAc consumption over time. 34
Figure 2.13 – Absorption spectra for galactose-based polymer (PAMEGalOAc). 35
Figure 2.14 – Molecular weight distribution chromatogram for PAMEGalOAc. 35
Figure 2.15 – Stöber hybrid silica nanoparticle with a glycopolymeric shell by a “transfer to” approach. 36
Figure 2.16 – ^{1}H-NMR spectra for the SiNps before and after polymerization. 37
Figure 2.17 – Effect of the basic solution onto the mesoporous silica nanoparticles 40
Figure 2.18 – ^{1}H-NMR obtained for the co-polymer (PDPAEMAM and PAMEGal). 42
Figure 2.19 – SEC-MALS chromatogram for the *co*-polymer synthesized in solution. 43
Figure 2.20 – Representative illustration for the hybrid polymerization mechanisms and comparation with the graft-to method. 44
Figure 4.1 – Both CTAs chemical structure used to anchor at the particle surface. 50

THIS

PAGE INTENTIONALLY

LEFT BLANK

Scheme Index

Scheme 1.1 – Schematic representation for the main reactions involved on the synthesis of monodisperse silica nanoparticles using the sol-gel process. 4

Scheme 1.2 – Main reactions involved in the preparation of silica nanoparticles using the Stöber method, in basic or acidic conditions. 5

Scheme 1.3 – Species involved onto the propagation of a reversible deactivation radical polymerization for polystyrene. 9

Scheme 1.4 – Atom transfer radical addition (ATRA) mechanism based on the Kharasch addition. 10

Scheme 1.5 – Reactions involved in the reversible addition-fragmentation chain transfer (RAFT) mechanism. 12

Scheme 1.6 – Resume with a few examples of some of the CTA classes and their respective properties. 12

Scheme 1.7 – Schematic representation of the synthesis route planned for the smart hMSN. . 18

Scheme 2.1 – Fluorescent silica nanoparticles surface functionalization. 24

Scheme 2.2 – Synthesis of the trithiocarbonate chain transfer agent, 3-(benzyl sulfanyl thiocarbonyl sulfanyl) propionic acid (BSPA) **–** compound **(1)**. 26

Scheme 2.3 – Main reactions involved on the amine coupling with the CTA. 27

Scheme 2.4 – Reaction of amine modified silica nanoparticles with the reactive intermediate formed between o-acyl isourea and DMAP. 28

Scheme 2.5 – Synthesis route for the galactose-based acrylamide monomer. 2`-acrylamido ethyl-β-D-Galactose tetraacetate (AMEGalOAc) – compound (**3**). 31

Scheme 2.6 – Deprotection of the galactose-based monomer, 2`-acrylamidoethyl-β-D-Galactose tetraacetate (AMEGalOAc) – compound (**3**). 40

THIS

PAGE INTENTIONALLY

LEFT BLANK

Table Index

Table 2.1 – TEM diameter and shape factor obtained for the fluorescent silica nanoparticle. 23

Table 2.2 – APTES quantification for SiNps by ^{1}H-NMR. 25

Table 2.3 – Grafted CTA concentration onto SiNp. 28

Table 2.4 – Experimental conditions for a controlled polymerization by RAFT in solution, using the acrylamide galactose-based monomer, 2`-acrylamidoethyl-β-D-Galactose tetraacetate (AMEGalOAc) – compound **(3)**. 33

Table 2.5 – Molecular weight of the galactose-based polymer (PAMEGalOAc) synthesized in THF. 34

Table 2.6 – Quantification of the glycopolymer weight grafted onto the particle surface by ^{1}H-NMR. 36

Table 2.7 – Molecular weight for the DPAEMA polymer (PDPAEMA) synthesized in THF. 38

Table 2.8 – Grafted glycopolymer by controlled RAFT polymerization at stöber nanoparticles functionalized with BSPA or CPADB as the chain transfer agent. 38

Table 2.9 – Results obtained by SEC-MALS and UV-Vis for 2`-acrylamidoethyl-β-D-Galactose (AMEGal) monomer – compound (**5**) – in water. 41

Table 2.10 – Results obtained by SEC-MALS and UV-Vis for the polymer obtained in the supernatant of the hybrid RAFT method using the galactose-based deprotected monomer, 2`-acrylamidoethyl-β-D-Galactose (AMEGal) monomer – compound (**5**) – and stöber nanoparticles. 41

THIS

PAGE INTENTIONALLY

LEFT BLANK

Abbreviation List

^{13}C-NMR	Carbon Nuclear Magnetic Resonance
^{1}H-NMR	Proton Nuclear Magnetic Resonance
ACVA	4,4'-Azobis (4-cyanopentanoic acid)
AIBN	(2,2′-Azobis) 2-methylpropionitrile
AMEGal	2`-acrylamidoethyl-β-D-Galactose
AMEGalOAc	2`-acrylamidoethyl-β-D-Galactose tetraacetate
APTES	3-aminopropyl triethoxysilane
ASGPR	Asialoglycoprotein Receptor
ATRP	Atom Transfer Radical Polymerization
BSPA	3-(benzylsulfanylthiocarbonylsulfanyl) propionic acid
CMC	Critical Micellar Concentration
CPADB	4-Cyano-4-(phenylcarbonothioylthio)pentanoic acid
CPP	Critical Packing Parameter
CRD	Carbohydrate Recognition Domain
CTA	Chain Transfer Agent
CTAB	Hexadecyltrimethylammonium bromide
CTA-SiNPs	Silica nanoparticles functionalized with a chain transfer agent
DDS	Drug Delivery Systems
DMAP	4-Dimethylaminopyridine
DPAEMA	2-(diiso-propylamino) ethyl methacrylate
EDC	1-Ethyl-3-(3-dimethylaminopropyl) carbodiimide
EPR	Enhance Permeability Effect
SEC-MALS	Size Exclusion Chromatography Multi-Angle Light Scattering
hMSN	Hybrid Mesoporous Silica Nanoparticles
MCM-41	Mobil Composition of Matter Number 41
MSNs	Mesoporous Silica Nanoparticles
NH_2-SiNPs	Amine functionalized silica nanoparticles
NMP	Nitroxide-mediated polymerization
PAMEGal	Polymer of 2`-acrylamidoethyl-β-D-Galactose
PAMEGalOAc	Polymer of 2`-acrylamidoethyl-β-D-Galactose tetraacetate
PDI	Perylenediimide

PDPAEMA	Polymer of 2-(diiso-propylamino) ethyl methacrylate
PEG	Polyethylene Glycol
pK_a	Acid Dissociation Constant
PRE	Persistent Radical Effect
RAFT	Reversible Addition-Fragmentation Chain Transfer
RDRP	Reversible-Deactivation Radical Polymerization
SiNPs	Silica Nanoparticles
TEM	Transmission Electron Microscope
TEMPO	2,2,6,6-Tetramethylpiperidinyloxyl
TEOS	Tetraethoxysilane
UV	Ultraviolet
UV-Vis	Ultraviolet-Visible Spectroscopy

Unit List

m; cm; µm; nm	meter; centimeter (10^{-2} m); micrometer (10^{-6} m); nanometers (10^{-9} m)
L; mL; µL	Liter; milliliter (10^{-3} L); microliter (10^{-6} L)
kg; g; mg; µg	Kilogram; gram (10^{-3} kg); milligram (10^{-6} kg); microgram (10^{-9} kg)
h; min; s	Hours; minutes; seconds
M; mM	Molar; millimolar (10^{-3} M)
Da	Dalton
mV	Millivolts
°C	Degree Celsius
ppm	Parts per million
MHz	Megahertz
rpm	Rotations per minute
Eq	Equivalent
a.u.	Arbitrary unit

THIS

PAGE INTENTIONALLY

LEFT BLANK

Symbol List

[NaOH]	Sodium Hydroxide concentration
[NH3]	Ammonia concentration
[APTES]	3-aminopropyl triethoxysilane concentration
$[Initiator]_0$	Initial initiator concentration
$[CTA]_0$	Initial chain transfer agent concentration
$[M]_0$	Initial monomer concentration
ζ	Zeta
λ	Wavelength
ε	Molar absorption coefficient
M_w (SEC)	Weight Average Molecular weight obtained by SEC-MALS
M_w (UV-Vis)	Weight Average Molecular weight obtained by UV-Vis
M_n	Number Average Molecular weight

THIS

PAGE INTENTIONALLY

LEFT BLANK

1. Introduction

Nanotechnology can be defined as a multidisciplinary area of science and engineering that consists in planning, synthesizing, characterizing and testing the behavior of materials and macrostructured devices with an overall size below 100 nanometers (billionth of a meter). This brings novel approaches to different types of issues due to new properties unobservable at higher scales [1].

Over the years nanotechnology has been developing many applications in medicine to prevent, diagnose and treat different types of diseases, from nanoparticles for drug delivery, to gene therapy and tissue engineering [2]. Concerning the drug delivery systems (DDSs) various approaches have been pursued to obtain an effective DDS. The concept of drug targeting was introduced as the “magic bullet” by Paul Ehrlich at the beginning of the 20th century. A notion which describes a site-specific system to target receptors with a controlled release rate of therapeutic agent, taking down the pathogens or mutated cells and remaining harmless to healthy tissues [3]. Therefore, the use of nanoparticles is changing the way that drugs are formulated and delivered. By 2016 there were around nineteen thousand articles about nanoparticles technology and their aspects [4].

Cancer morbidity and mortality have been increasing, thus, the number of people undergoing chemotherapeutic treatment is growing [5]. Most anticancer drugs used in conventional therapeutic strategies have low aqueous solubility, instability, non-selective distribution and they are quickly metabolized. With so many drawbacks the doses are limited by the side effects, and even in a suboptimal therapeutic doses, their activity can still be dangerous due to systemic toxicity [6]. Hence, the quality of life of patients is severely compromised by the current used of cancer therapeutic agents.

DDSs emerge as a promising approach to diagnose and treat cancer due to the ability to reduce systemic toxicity from anticancer agents and improving their pharmacokinetics. In addition, they can increase drug target specificity and provide protection against biochemical degradation confining a longer circulation half-time [7].

DDS can even be pushed further into smart drug delivery systems that can react to specific endogenous or exogenous triggers, such as pH and temperature. The main advantage of these systems is the capacity of having a controlled release mechanism that reduces the drug concentration fluctuations. Therefore, a higher therapeutic efficacy is obtained by an outweighing of the side effects with the benefit of the treatment. As a consequence, of the nonspecific toxicity to healthy cells, a higher dose of therapeutic agents can be delivered, increasing the bioavailability and enhancing their efficacy [8].

1.1. Drug Delivery Systems

Nowadays bio-nanotechnology can divide DDSs into three distinct groups based on their composition: organic, inorganic and hybrid (Figure 1.1). For instance, a few examples of organic-based DDSs are polymeric micelles, dendrimers and carbon nanotubes. On the other hand, quantum dots, gold nanoparticles and silica nanoparticles are representative of the inorganic DDSs. Furthermore, hybrids are nanocomposites characterized with both organic and inorganic moieties, like silica nanoparticles coated with a polymeric shell [9] or gold nanoparticles complexed with dendrimers [10].

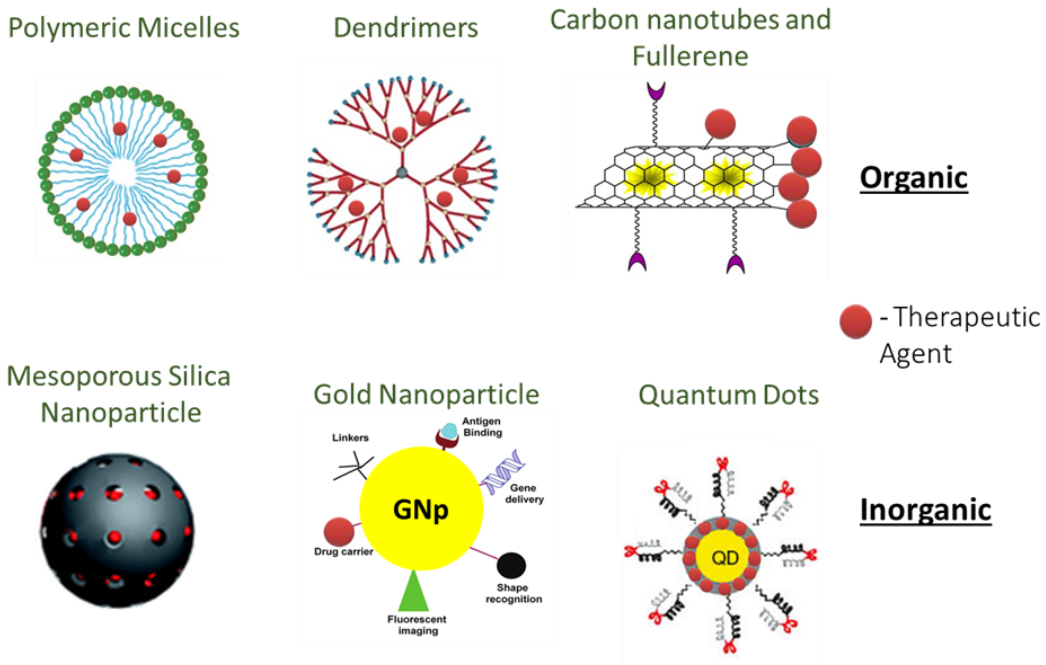

Figure 1.1 – Different types of organic and inorganic drug delivery systems. [Taken from (Micelles and Dendrimers) [11]]; [Adapted from (Carbon nanotube) [12]; (MSN) [13]; (Gold Nanoparticle) [14]; (Quantum Dots) [15]].

According to the intended final objective these systems can bring all kind of advantages. For instance, due to a hydrophobic core stabilized by a hydrophilic shell, polymeric micelles are suitable for various anticancer drugs that were previously abandoned by having low solubility and bioavailability [16].

Carbon nanotubes due to their cylindric shape have a similar behavior as polymeric micelles since they have a hydrophobic hollow. Also, they come with a large surface area that allow an external functionalization by chemical attachment or physical adsorption to the walls improving their biocompatibility and increasing therapeutic interest [17].

Quantum dots are semiconductor particles with unique optical properties such as, high stability, high quantum yield, water solubility and size-tunable emission. These assets when linked to biomolecules with appropriate lifetime for living systems creates an opportunity to study several bio-mechanisms, including *in vivo* and *in vitro* drug delivery [18].

In comparison with other inorganic drug delivery systems mesoporous silica nanoparticle (MSNs) exhibit several superior properties. A class of solid silica materials which contain an ordered or disordered arrangement of empty channels called mesopores (with sizes ca. 2nm to 20 nm), providing huge accessible specific volumes, in the order of 1 mL/g. MSNs feature unique physicochemical properties, such as high surface areas, high pore volume, uniform and tunable pore and particle sizes, good colloidal stability, and versatile surface functionalization. With the possibility of incorporating sensor molecules in the structure, adding surface targeting groups, and loading therapeutic agents into the free pore volume MSNs are expected to be a key player in the field of therapy and diagnosis (theranostics) [19]. Several types of responsive hybrid MSN-based DDS (hMSN) are reported according to the loaded and grafted groups [13].

1.2. Silica Nanoparticles

Silica nanoparticles are used in many industrial areas, such as catalysis, chromatography or ceramics [20]. For technological purposes a well-defined and reproductible synthesis procedure is crucial. In general, top-down and bottom-up are the two main approaches for nanoparticle synthesis. The top-down approach is characterized by reducing the original size of a material by a physical approach, while the bottom-up is defined by using chemical methods to produce nanoparticles from a molecular level.

Some of the most common approaches based on bottom-up are reverse microemulsion or sol-gel. Reverse microemulsion is based on the addition of the silica precursor onto microcavities formed by spherical micelles that surround water with their polar heads. Sol-gel is a more commonly used technique due to the fact that parameters such as particle size, size distribution and morphology are easily controlled by the reaction parameters, while reverse microemulsion comes with a higher cost and the removal of the surfactant from the final product is intricate [21].

In sol-gel, the process can be performed using acidic (inorganic salts) or basic (usually ammonia) conditions. There are three reactions that leads to a three-dimensional silica matrix (gel) and consequently to mature silica nanoparticles, and they are: hydrolysis of the silica precursor, water condensation and alcohol condensation (Scheme 1.1).

Hydrolysis

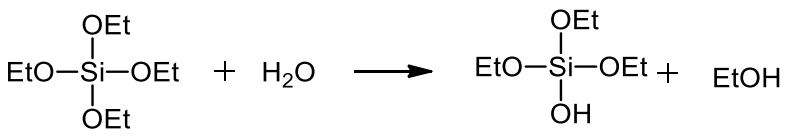

Water Condensation

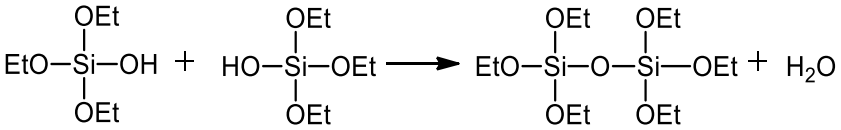

Alcohol Condensation

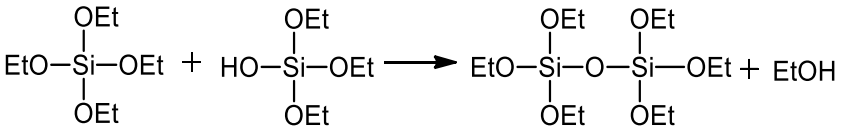

Scheme 1.1 – Schematic representation for the main reactions involved on the synthesis of monodisperse silica nanoparticles using the sol-gel process.

A colloidal solution of silica precursors condensate, initiating siloxane bridges (Si-O-Si) leading to a silica matrix (gel). The sol-gel mechanism can be divided into two main parts, nucleation and growth. After many years of investigation there is still some debate around these steps and how they really work. After simulations and scattering experiments, is believed that the first step relies on the formation of particles around 2 nm followed by two possible but contradictory theories (monomer addition and aggregation) [22].

Monomer addition theory suggest that particles grow by a balance of hydrolysis rate of the silica precursor and the rate of molecular addition to the particle surface. As a result, the number of particles are conserved during growth, limiting nucleation to the early stages of the process [23].

The growth model suggest that particle size distribution is determined by particle interaction potentials, not only reaction rates, but also size and colloidal stability of the primary particles. This model correlates the rate of loss and absolute concentration of hydrolyzed silica precursor with the number and size of the nanoparticles [24].

Particularly, the growth model has shown a good correlation between predicted and measured particle size, but still now there is no consensus on which leads to mature particles.

Stöber Synthesis

Based on the sol-gel process, in 1968 a method was developed for synthesizing monodisperse suspensions of compact silica spheres (Stöber) from 5 nm up to 2 microns. The process is based on the hydrolysis of metal alkoxides in a mixture of alcohol and water with different bases, just as described by Kolbe in 1956. After some changes in the ammonia concentrations catalyst, alcohol mixtures and ester concentration, the compact silica spheres were obtained with a predictable size and geometry [25].

With a careful control of the reaction parameters is possible to control the size and morphology of the nanoparticles (Scheme 1.2). The main difference between the two types of catalysis, is that in acidic medium, hydrolysis is favored leading to oligomeric chains that will fuse

and generate longer nanoparticles. However, in basic medium, condensation reactions are favored, leading to smaller particles, as no hydrolysis occurs before condensation. The ratio between the alcohol and water has also an influence in size, higher water percentages favor hydrolysis over condensation giving raise to larger and less round nanoparticles. The last parameter is temperature, by increasing the temperature, both reactions are enhanced leading to smaller particles [26].

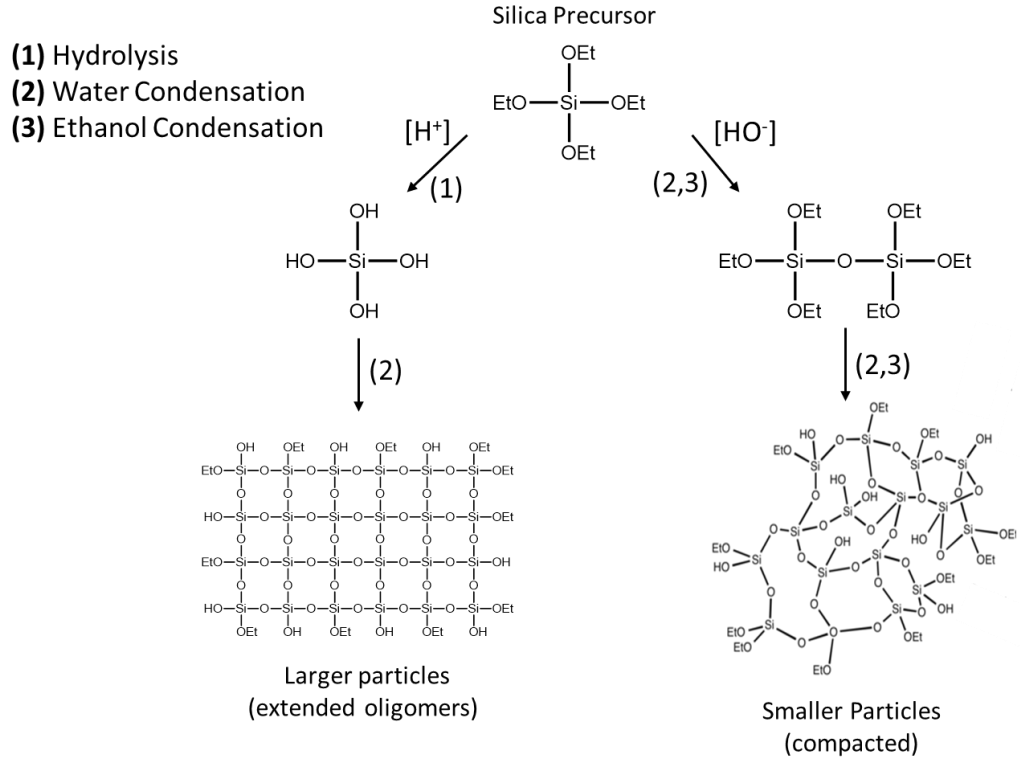

Scheme 1.2 – Main reactions involved in the preparation of silica nanoparticles using the Stöber method, in basic or acidic conditions.

1.2.1. Mesoporous Silica Nanoparticles

Advances in mesoporous silica materials started with the discovery of MCM41 family by Mobil Corporation Scientists in 1992 and so far, they are the most studied family of mesoporous inorganic materials. These materials are well known for their regular hexagonal array of uniform channels confirmed by diffraction patterns [27].

The synthesis of this type of materials is based on the stöber method with the addition of an extra component, a cationic surfactant. Surfactant-templated mesoporous silica nanoparticles can be tuned to several mesostructures (e.g. laminar, hexagonal and cubic), morphologies (e.g. spheres and fibers) and dimensions by controlling the reaction conditions (temperature, pH, template and silica source, etc.) (Figure 1.2). After the surfactant (1.2- A) reaches the critical micellar concentration (CMC), molecules start to aggregate and self-assemble as micelles (1.2- B). Macrostructures (e.g. hexagonal) (1.2- C) given by micelles are controlled by the surfactant critical packing parameter (CPP). This parameter (Equation 1.1) is dependent of the surfactant

tail volume (V), tail length (l) and head area (A). When this value is between 0.33 and 0.5, hexagonal packing becomes possibly [28]. Finally, the self-assembly process is followed by hydrolysis and condensation of the silica precursor around the micelles to create surfactant-templated mesoporous silica nanoparticles (1.2- D). The interaction between the silica nanocomposites and the head groups of surfactant occurs spontaneously between the inorganic and organic components [29].

Micelles formed by the surfactant control the pore size and structure, and thus according to the application or guest molecules the pore size can be tuned.

$$CPP = \frac{V}{A.l} \quad \textbf{(1)}$$

Pore tuning can be achievable by changing the alkyl chain length of the surfactant or by adding hydrocarbons, as micelles swelling agents (e.g. 1,3,5-trimethylbenzene). With the addition of hydrocarbons, that can be solubilized by the hydrophobic region, the micelle diameter increases. Since the micelle nucleus is based on the hydrophobic region of the surfactant, the micelle diameter increases with the tail length [30].

For surfactant such as hexadecyltrimethylammonium ion, hexagonal arrays are approximately spaced with 4 nm of distance and with a pore diameter around 3 nm [27].

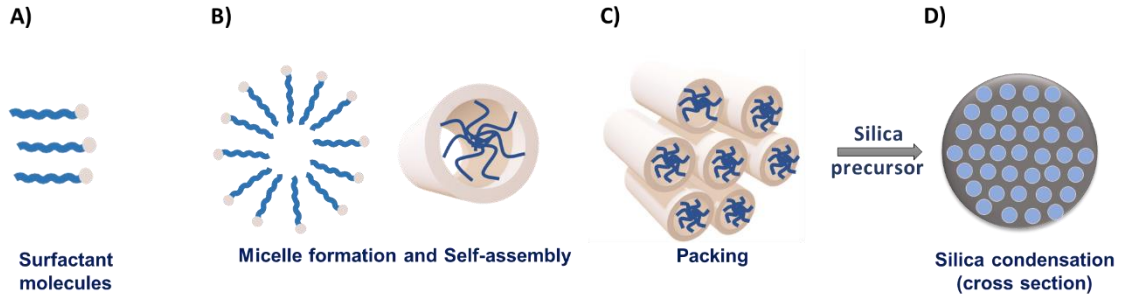

Figure 1.2 – Formation of the mesoporous channels. Surfactant micelle formation followed by a self-assembly and packing onto a hexagonal array of uniform channels. D) Hydrolysis and condensation of the silica precursor around the template.

1.2.2. Biocompatibility

Mesoporous silica nanoparticles (MSNs) have been used in several studies to evaluate the *in vivo* biocompatibility through biodistribution, toxicity and excretion. Once in a living system, MSNs can be hydrolyzed onto orthosilicic acid ($Si(OH)_4$), that consequently is absorbed and turned into elemental silica as a remainder. Biodistribution studies have shown that nanoparticles can accumulate in some organs but with no significant impact on the animal constitution or inflammatory response.

One of the early studies relating to biodistribution, performed by Ji-Ho Park in 2009, MSNs were injected intravenously into mice. The biodistribution profile shows that MSNs accumulate in liver and spleen, as in other organs related with the macrophages response to unusual

substances. Most MSNs were cleared from the system after four weeks due to degradation by lysosomes and excretion by the kidneys [31].

Two years later, a study by Qiajun He and his team, related the size and functionalization of MSN with their excretion. Again, the results shown that the particles distribute mainly in the liver and spleen. Small MSN quantities were also found over the lungs and in even smaller quantities at the kidneys and heart. After injection and following the MSN concentration over time, it was clear that larger particles can be more easily captured by the organs. In addition, a higher amount of particles were excreted due to faster biodegradation. Coating the surface of MSNs with polyethylene glycol (PEG) makes them less detectable by the organs, resulting in less accumulation and longer blood-circulation life time. This is a key factor when we compare hybrid MSNs (hMSN) with bare nanoparticles, since by a simple and easy surface modification, higher selectivity is achieved by avoiding the accumulation in other type of organs [32].

Regarding the safe administration dose, *in vivo* studies by the group of Fuyuhiko Tamanoi, determined that 50 $mg.kg^{-1}$ were a safe dosage (for particles around 130nm). In the same study, nanoparticles shown an enhanced permeability and retention effect (EPR), exhibiting higher accumulation on tumor tissues. After 4 days, 94% of the silicon injected had been excreted from the mice system [33].

All these studies were only possible since mesoporous silica nanoparticles can be modified during or pos-synthesis to include fluorescent dyes to a culmination of a good fluorescent probe for *in vivo* studies.

1.3. Fluorescent Mesoporous Silica Nanoparticles

MSNs are distinguished for multimodal application in drug delivery and bioimaging. They are suitable for biodegradable nanocarriers by excellently fulfill desired properties, such as high drug loading capacity, low toxicity and possibility to design gatekeeper systems for a controlled release. Furthermore, MSNs can also be tuned as imaging tools for biodistribution and precise cell targeting.

Radioactive labeling is generally used for bioimaging and tracking compounds through metabolic pathways, tissues and cells. Such technique can cause radioactive damage and lead to false (positive or negative) results. Therefore, there is an added interest on developing a highly sensitive and specific probe for cell imaging and medical diagnose. Regular fluorescent dye are often toxic to cells or lack in active functional groups for bioconjugation [34].

By connecting fluorescent dyes into the silica network, during condensation of the particle, photostability is increased and toxicity reduced. Furthermore, photobleaching is also reduced because silica can act as a barrier to oxygen.

Incorporation of PDI into silica network has been developed by the OM2-IST group. A symmetric derivative of perylene diimide (PDI) with two propyltriethoxysilane groups for possible

condensation with silica precursor has been used (Figure 1.3). The dye has been incorporated in stöber and MSN during the silica condensation [35]–[38].

PDI's dyes have a high quantum yield, high photostability, small stokes-shift and can be excited in a visible region, such properties are important for optical applications like fluorescence imaging and microscopy (Confocal Fluorescence Microscopy) [39].

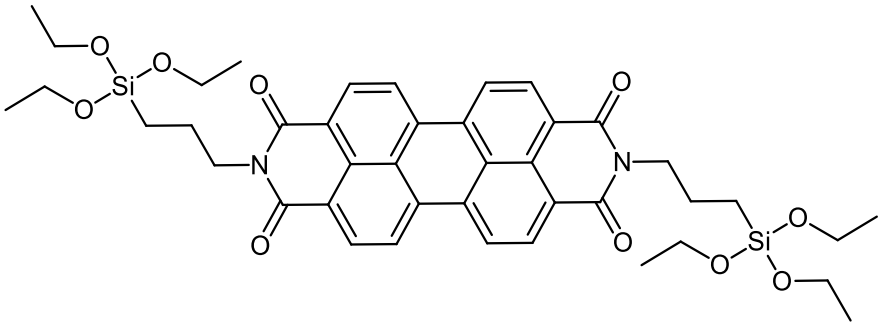

Figure 1.3 – Chemical structure of the perylene diimide (PDI) derivative previously used on MSN and Stöber nanoparticles

1.4. Controlled Radical Polymerization

The basic mechanism behind the preparation of polymers was established between the 1940 and 1950, where three different steps were distinguished: initiation, propagation and termination [40]. The polymerization can be mediated by different kinds of reactive species like carbanions, carbocations, metal complexes and free radicals. From the species above mentioned, carbanions are the only that do not share an extra step entitled chain transfer.

The principles behind every type of polymerization are essentially the same only the mechanism behind is changed. Radical polymerization is widely used in many industrial applications with advantages of being relatively simple, easy to implement and slightly resistant to impurities (stabilizer and oxygen).

Initiation is the process responsible by the generation of radicals by a precursor molecule. These free radicals can be produced by thermolysis, redox reactions or photolysis. The limiting step for initiation is the half-life of the initiator used, since the formation of primary radicals is much slower than the reaction of radical-radical (termination) or radical-monomer (propagation). Initiator half-life is given by the time required to decrease 50% of the initial concentration at a determined temperature. The most common type of radical initiators used are azobis derivatives and peroxides. The next step, propagation, is responsible by the chain growth of the polymer and is mediated by the rate of monomeric addition to active radical propagating chains relative to their termination.

In anionic polymerizations, due to the lack of termination events (charge repulsion), all chains grow at the same rate creating a narrow mass distribution (living polymerization). As the monomer is consumed an external termination agent is needed to end the polymerization. However, in radical polymerization the growth of radical chains can vary from a few seconds to a

few minutes leading to high mass distribution (free radical polymerization) and difficulties on controlling their macrostructured composition [41]. Chain transfer events happens when a growing chain is transfer to another growing chain, which is a common process in radical polymerization that interferes with mass distribution. To avoid this problem, several types of compounds are commonly added as chain transfer agent (CTA). This type of agents deactivates propagating chains by creating a dormant specie capable of generating new radicals that can initiate another chain (Scheme 1.3). From this process a control of active species concentration and a similar chain growth rate is achieved (living polymerization). Such process is called reversible deactivation radical polymerization (RDRP) and leads to narrow molar mass distribution with a good control of the final macrostructure.

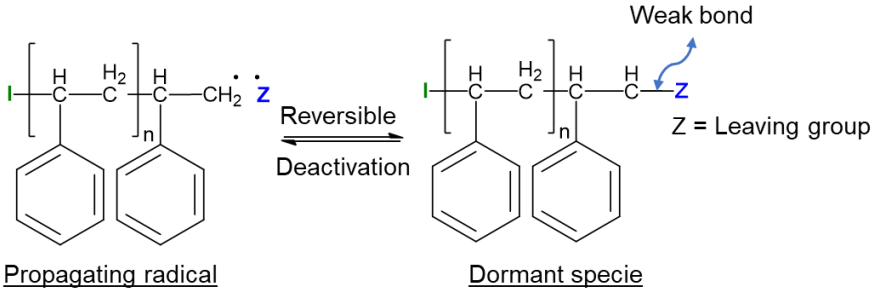

Scheme 1.3 – Species involved onto the propagation of a reversible deactivation radical polymerization for polystyrene. [Adapted from [34]].

1.4.1. Nitroxide-mediated polymerization

Procedures involving RDRP can be tracked back to 1982, where Otsu and his team used organic sulfur compounds as CTA for a living polymerization [42]. Three years later, nitroxide-mediated polymerization (NMP) appears through a patent [43] but went unnoticed, receiving proper attention in 1993 with the application of this method on the synthesis of low mass distribution polystyrene [44].

NMP consists in using a nitroxide stable radical and peroxides for radical initiators. One of the first set used was 2,2,6,6-tetramethyl-l-piperidinyloxy (TEMPO) (Figure 1.4) as the nitroxide stable radical and benzoyl peroxide (BPO) as the radical initiator.

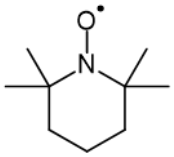

Figure 1.4 – Chemical structure for (2,2,6,6-Tetramethylpiperidin-1-yl) oxyl (TEMPO).

The dormant specie formed with TEMPO can be photo or thermally dissociated into the stable radical (nitroxide) and active propagating radical (usually carbon centered). TEMPO can act as a cap or a radical trap that protects the growing end of the chains avoiding termination effects. While transient species (active propagating radicals) reach a concentration maximum and decay due to bimolecular self-termination, persistent radicals (stable radicals) increase steadily to balance this termination. This self-regulation will cause a buildup of the persistent specie, also

known as persistent radical effect (PRE). The reversible binding originated by the persistent specie creates a “living” nature (no irreversible chain transfer or termination) leading to uniform mass distribution and controlled structure [45].

NMP is a simple technique with good results but can only be applicable to a limited set of monomers. Therefore, more versatile methods were developed such as, Atom Transfer Radical Polymerization (ATRP) and Reversible Addition-Fragmentation Chain Transfer (RAFT).

1.4.2. Atom Transfer Radical Polymerization

ATRP origin goes back to 1995 when Wang and Matyjaszewski applied a Kharasch addition as an expansion for atom transfer radical addition (ATRA). This reaction consists on the addition of polyhalogenated alkanes to an alkene catalyzed by redox reactions with transition metal salts (Scheme 1.4). The transition metals complexes allows an efficient reversible halogen transference [46].

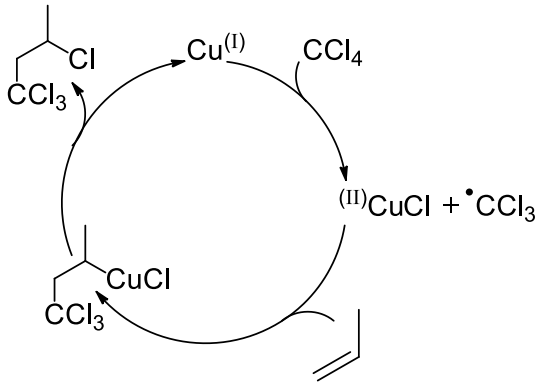

Scheme 1.4 – Atom transfer radical addition (ATRA) mechanism based on the Kharasch addition.

When alkyl halide radical species are stable enough and their reactivity is similar before and after the addition to the double bond, polymerization takes place. Therefore, the radical originally generated by the alkyl halide, can be a polymeric growing chain and the process is now denominated atom transfer radical polymerization (ATRP). Like NMP, ATRP shares the same principle of persistent radical effect. A shift of the equilibrium to the dormant specie occurs due to early termination processes, with an increase in metal oxidized species and reduction of the free radical concentration narrow mass distribution is achieved.

Several metal salts have been used as catalysts, including copper, ruthenium, iron and cobalt with counter ions ranging from chlorine to iodine. The most common used is copper due to its versatility and cheap price. Auxiliary ligands are also used, like triphenylphosphine and 2,2`-bipyridyl, to facilitate the salt solubilization. For initiation usually, alkyl bromides and alkyl chlorides are preferred. When compared with NMP, metal catalysts are not capable of initiating the polymerization or react with themselves, like TEMPO can, which decreases even further the irreversible termination.

ATRP is a versatile technique for a variety of monomers classes when proper initiator, catalyst, ligand and reaction conditions are picked. Otherwise, metal catalyst can have high binding constants with monomers leading to irreversible binding and consequently to higher mass distributions [47].

1.4.3. Reverse Addition-Fragmentation Chain Transfer

RAFT was reported in 1998 by Ezio Rizzardo and his team [48] and since then, it has attracted great attention as it can be applied in a multitude of monomers, just like ATRP. Contrary to ATRP, RAFT do not use any metals, offering a more suitable option to polymers used in biological applications.

Unlike NMP and ATRP that act on the principle of capping growing chains, creating the dormant species, RAFT goes by reversal chain transfer. The main difference between both mechanisms, is that the polymer grows on the chain transfer agent (dormant/active species) instead of being reversible capped to avoid termination.

To understand the living aspect of RAFT we need to comprehend the mechanism behind this polymerization (Scheme 1.5). It starts with the decomposition of the initiator and formation of the propagating chain, as explained before. The following step consists on the addition of the growing chain to the CTA. A pre-equilibrium is reached, where a radical adduct can undergo between two possibilities. The adduct can either fragmentate and form a polymeric CTA (dormant specie) plus a new radical or go back into the CTA agent plus the propagating chain. This last possibility (equilibrium between CTA and radical adduct) is what is normally observed on ATRP and NMP (cap/uncap). On the other hand, when the equilibrium goes for the dormant specie, the new radical has the possibility to generate new propagating radicals. With new propagating chains, the main equilibrium is reached, this step is responsible for the narrow mass distribution. Main equilibrium is characterized by a fast interchange between all the radical growing chains, the more the chains get to be transferred the higher will be the probability to grow equally [49].

The chain transfer agent structure plays a crucial role in the transference rate and consequent living aspect of the polymerization. Most common RAFT agents are based on thiocarbonylthio compounds, such as trithiocarbonates, dithiocarbamates, dithiobenzoate and xanthates (Scheme 1.6). The nature of the R and Z groups is very important for the RAFT process. Z groups are mediators of the thiocarbonyl group reactivity, they promote the radical addition during polymerization. Aryl groups have shown good results as Z group, while alkoxy and dialkylamino compounds lead to low transfer constants. R groups are compounds commonly capable of initiating new radicals and at the same time, good leaving groups. Cumyl and cyanoisopropyl are effective R groups, followed by benzyl a less effective group, as reported by Rizzardo [48]. According to the monomer type, it is possible to pick the appropriate chain transfer agent in order to obtain the best control of a polymerization by RAFT [50].

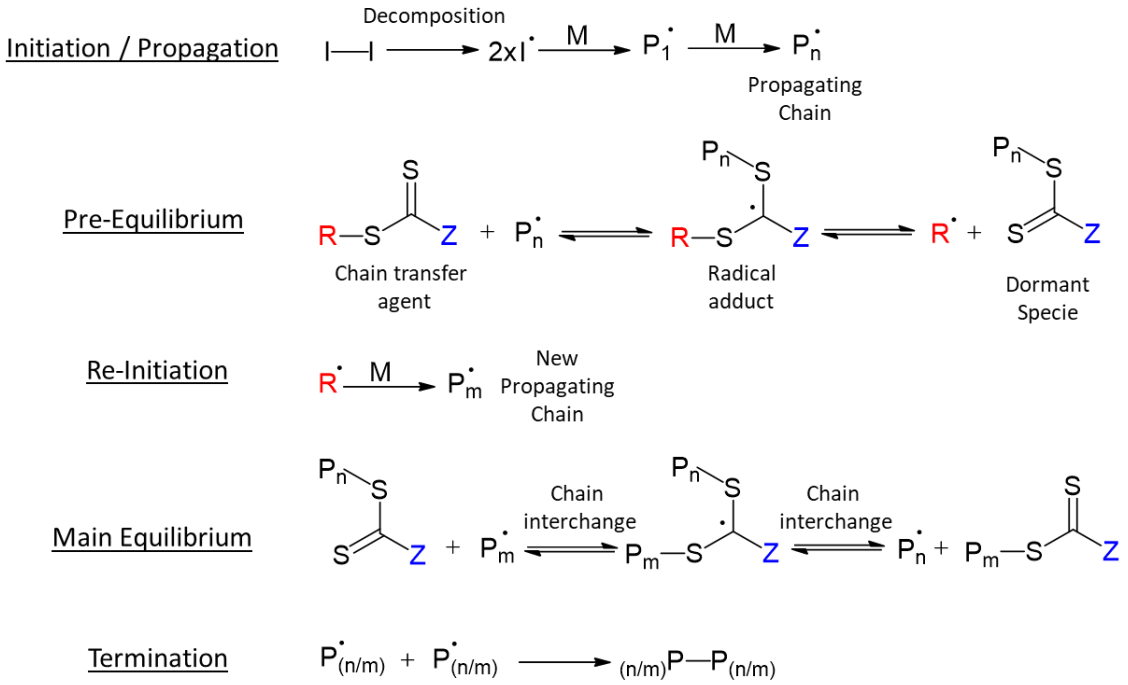

Scheme 1.5 – Reactions involved in the reversible addition-fragmentation chain transfer (RAFT) mechanism.

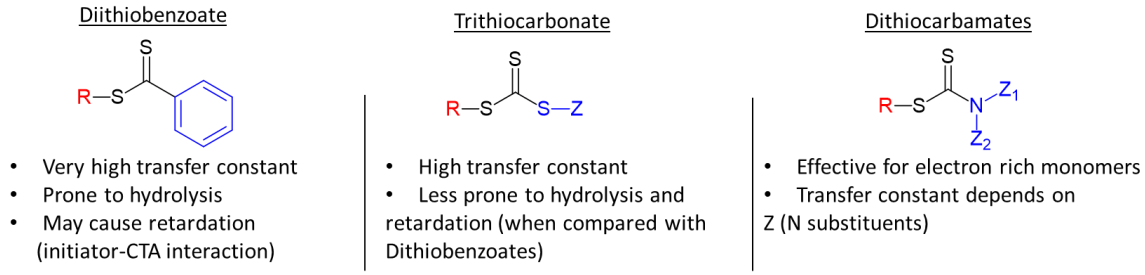

Scheme 1.6 – Resume with a few examples of some of the CTA compound classes and their respective properties. [Adapted from [41]].

1.5. Hybrid Mesoporous Silica Nanoparticles

With control polymerization we can achieve predetermined polymeric compositions, architecture and molar weight. Polymers are attached onto nanoparticles, proteins or other type of surfaces for endless type of applications, such as, protection from external environments (e.g. UV damage) [51], improve biocompatibility (e.g. prevent phagocytosis) [52] or even change their natural properties (e.g. hydrophobicity) [53]. Specifically, polymers are grafted into nanoparticles to increase stability and avoid aggregation, to link bioactive and non-bioactive molecules or to confine optical properties [54].

Hybrid mesoporous silica nanoparticles (hMSN) can be defined by combining inorganic nanoparticles with an organic shell (e.g. polymer). Nanoparticles grafted with polymers can be achieved mainly by two ways. The polymers can be previously synthesized and then linked covalently to the particles surface (grafting-to) or grown from a chain transfer agent or initiator covalently attached onto the particle surface (grafting-from). It is known that by using a grafting-from methodology a higher grafting density can be achieved but intermolecular coupling may occur [55]. In grafting-from if the CTA is attached by the Z-group to the nanoparticles is preferred to use the term “transfer-to” (Figure 1.5). Transfer-to is a combination between grafting-from and grafting-to methodologies. CTA fragments are released from the nanoparticle surface, allowing the propagating polymer chains to grow in solution and return to the particle surface by chain-transfer reactions. It is still a controlled manner of polymer growth but differs from grafting-from by having less side reactions that lead to unwanted defects, such as, intramolecular radical reaction (looping) and intermolecular coupling. In contrast, there is higher steric hindrance in transfer-to, that increases with the polymer molecular weight, leading to termination reactions of the active radical chains [56].

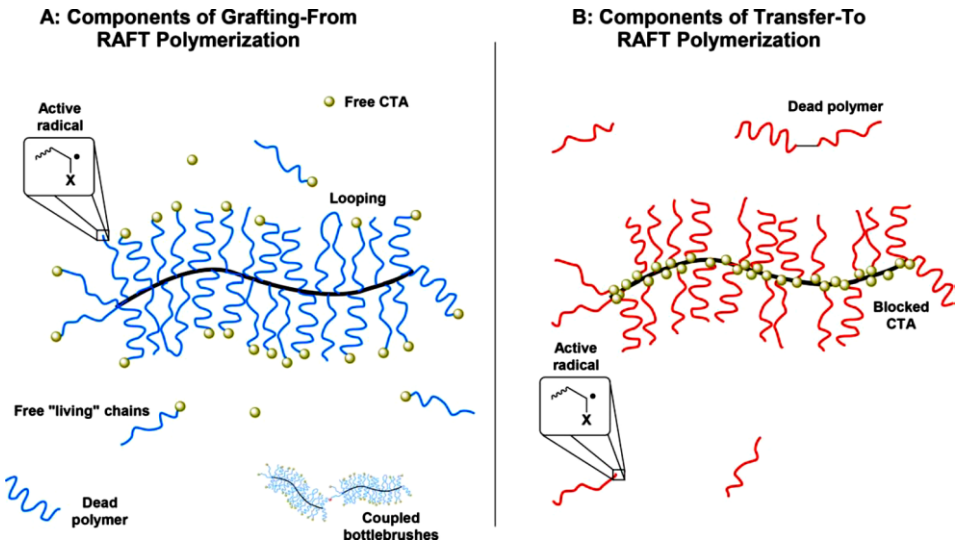

Figure 1.5 – Differences in grafting-from and transfer-to mechanisms. [Taken from [55]].

1.6. Smart fluorescent hybrid MSNs (hMSNs) for cancer theranostic

Hybrid MSNs are excellent nanocarriers for several biomedical applications such as, bioimaging, drug delivery systems [57], bone repair and tissue engineering [58]. Using hMSNs, most of the common conventional drug administration problems, like poor solubility, quick metabolization/excretion and undesired side effects are reduced [8]. This is due to hMSNs high load capacity for therapeutics encapsulation and high chemical/mechanical stability to protect the guest molecule. For the therapy and diagnosis (theranostic) approach, three factors must be defined, and they are, how do hMSN reaches the target with selectivity, how can we track it and finally how to obtain a controlled release.

1.6.1. Specificity and internalization

To target tumor cells, the nanoparticle surface could be modified with antibodies [59], folic acid [60] or carbohydrates (galactose/lactose) [61], taking advantage of the overexpressed receptors in cancer cells. Using *in vitro* studies hMSNs have shown target selectivity for cancer cells [62]. Concerning the carbohydrate specificity, C-type lectins are commonly used for cell recognition and uptake. Lectins are carbohydrate recognizing proteins, on the cell membrane, that bind reversible to monosaccharides or oligosaccharides with high specificity. The interaction between lectin and carbohydrates can be as specific as an enzyme and their substrate. Their carbohydrate-binding activity is a product of a limited amino acid residues group known as carbohydrate recognition domain (CRD). Depending on their family type they can have one or more CRD and be Ca^{2+} dependent [63].

Asialoglycoprotein receptors (ASGPR), a C-type lectin, are primarily expressed on hepatocytes and are responsible for recognizing and internalize asialoglycoproteins (glycoproteins with their sialic acid terminal removed). This receptor can distinguish between anomeric isomers and binds specifically to D-galactose and *N*-acetylgalactosamine. The interactions between receptor-carbohydrate occurs through coordination of the amino acids (receptor) and carbohydrate oxygens with the calcium cation. Besides, other types of bonding are formed for the recognition, hydrogen bonds are established between amides and carboxylates of amino acids side chains with the 3- and 4-hydroxil groups of the carbohydrate [64]. ASGPR has been characterized as efficacious for the hepatocellular carcinoma-targeted drug delivery systems [65]. As shown before in the biocompatibility section, MSNs tend to concentrate in the liver, creating a good pathway for target and cell recognition.

Particle internalization proceeds after the recognition through receptor-mediated endocytosis (Figure 1.6). This cellular process starts with the transference of the receptor-ligand to a coated pit on the external region of the lipid bilayer. The coated pit is rich on clathrin, an important protein for this type of internalization. With the arrival of the ligand to the pitch an invagination is formed with pos-release of a closed coated vesicle inside the cell. The clathrin coat is shed by heat sock proteins and end up fusing with other vesicles to form early endosomes. Then, early endosomes will also fuse and separate into two distinct organelles, late endosomes and recycling endosomes, the classification is based on a few physicochemical parameters (e.g. shape and material composition). Late endosome will end up with ligands and harmful molecules, while the recycling endosome engulfs the receptor. Posterior, the receptor goes back to the external surface of the cell membrane while the late endosome is combined with a lysosome to be digested by enzymes [66].

Relating the hybrid nanocarriers, it is important that they can permeate through the endosomes to efficient delivery the drug into the cytoplasm. Some anticancer drugs, like doxorubicin, can leave the endosome membrane, however some therapeutic agent and nanoparticles are retained due to their hydrophobicity [67]. Internalization efficiency will depend

on size and morphology of the particle, but also of the chain length and functional groups of the organic shell [8]. A known alternative for this problem is to use the “pH-buffering effect”, where macromolecules are used to protonate entrapped agents and promote osmotic swelling with posterior membrane rupture. Besides, other mechanisms can be performed such as, using cationic amphiphilic peptides to raise internal tension, leading to pores on the endosomal membrane or even taking advantage of photosensitizers, like dendrimer-based photosensitizer, that when exposed to light can produce oxygen singlet species to destroy the endosomal membrane [68].

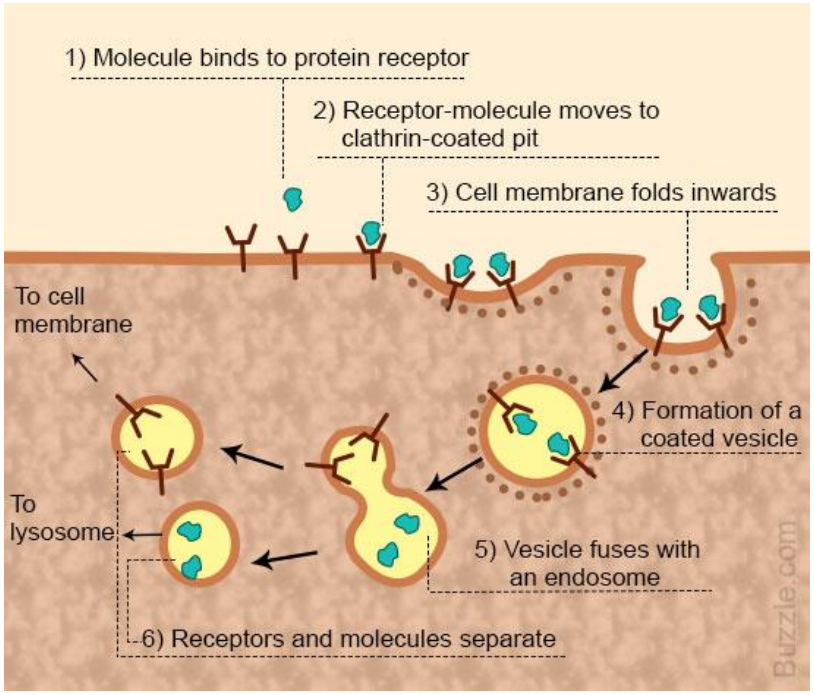

Figure 1.6 – Receptor mediated endocytosis mechanism. [Taken from [58]].

1.6.2. Tracking

Particle accumulation can be followed using fluorescent mesoporous nanoparticles. Fluorescent MSNs can be synthesized using external surface modification or during silica condensation to link fluorescent molecules [69]. It can also be done by encapsulation of fluorescent dyes or quantum dots using a covalently bound cap to block molecules from leaching out [70]. They are commonly used in optical resonance imaging and magnetic resonance imaging or a combination of both [71]. With the high resolution provided by fluorescent MSNs numerous processes can be studied (e.g. biodistribution, internalization mechanisms and cytotoxicity) [31], [57].

1.6.3. Controlled release

Desirable drug delivery systems are expected to release their cargo in an appropriate concentration on the desired target over a well-known time. MSNs show a “zero leakage”, meaning it cannot release their payload alone, therefore, external surface modifications are required for a controlled release. A gatekeeper is normally used to release the cargo over specific

internal (biomolecules, redox or pH) or external stimulus (light, temperature or magnetic). MSNs gatekeepers can either be nanoparticles, organic molecules or supramolecular assemblies.

Some of the work that uses nanoparticles as gatekeepers in mesoporous silica materials are based on disulfide linkers and transition metal-based nanoparticles. These linkers are chemically labile and allow the attachment of the two different types of nanoparticles. The linkage can then be cleaved with a redox stimulus, by artificial or cell produced antioxidants produced. Some examples of the nanoparticles used to cover the porous are cadmium sulfide and superparamagnetic iron oxide nanoparticles. Such combination of mesoporous silica materials with magnetic particles allow to the guidance of the nanoparticles to specific regions with a magnetic motor [72]. Gold nanoparticles also have been used to gatekeep MSN, using the same principle and stimuli, to deliver DNA and other chemicals into plant cells [73].

Supramolecular assemblies conjugated with MSNs are complex systems. There are a few examples in the literature, like reversible nanovalves based on rotaxanes to trap molecules intermediated by redox stimulus [74]. In addition, cyclodextrins combined with polyethyleneimine blocks were also reported as a pH mediated MSN porous cap [9].

Reversible gatekeeping based on organic molecules attached to the MSNs porous was also reported using photo induced dimerization of coumarins and cleavage of their respective dimers. The system takes advantage of the molecule size that when dimerizes its bulky enough to cover the porous [75]. Other authors have used polyamines to control the gate effect and studied its response to pH and anions. MSN porous were functionalized with mercaptothiol groups and the external surface with amines following the response of the system through a reaction of squaraines with the thiol groups. With the anions (ATP, sulfate and chloride) a correlation was found between their binding affinity with the amines and the time with no significant release, the higher their binding affinity with the amines was, the longer the gate would stay closed. Regarding the pH stimuli, an effect of swelling/deswelling was observed for gating the MSN porous [76].

Considering the different types of strategies, pH responsive is a convenient method for cancer therapy due to difference in cytosolic pH (ca. 7.2) on healthy cells and in tumor cells (ca. 6.6). Besides that, organelles like endosomes and lysosomes are also acidic [77]. Ideally polymers with ionizable molecules and a pK_a around those values are good candidates for a controlled release. Stimuli-responsive polymers can be divided into three groups, acidic polymers, basic polymers and natural polymers. Acidic polymers are characterized by having acid functional groups (boronic; phosphoric and carboxylic acids) that accept protons at low pH and release them at high pH. Basic polymers transitions are around pH 7-11, and are based on functional groups like tertiary amines, heterocyclic amine groups and dendrimers. Lastly, natural polymers like chitosan and dextran, show good biocompatibility, biodegradability and are easy to modify [78]. Tertiary amine-based methacrylate monomers (Figure 1.7) show a pK_a between 5-7. Special attention should be given to 2-(diiso-propylamino) ethyl methacrylate (DPAEMA; pK_a=6.4) and 2-(piperidino) ethyl methacrylate (PPDEMA; pK_a=6.8), which proceed to a phase change by

ionization on a very similar pH range to the healthy/cancer cells pH difference. The monomer and polymer pK_a is expected to be similar since the pK_a is determined by the same ionizable functionals groups [79].

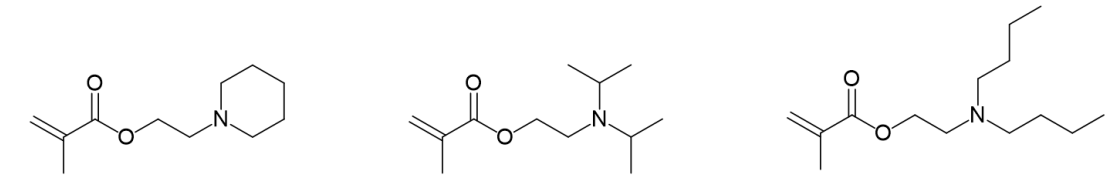

2-(piperidino)ethyl methacrylate (PPDEMA) pK_a~ 6.8

2-(diiso-propylamino)ethyl methacrylate (DPAEMA) pK_a~ 6.4

2-(dibutylamino)ethyl methacrylate (DBAEMA) pK_a~ 5.1

Figure 1.7 – Structures of tertiary amine-based methacrylate pH-responsive monomers suitable for biomedical applications and the approximation for their pK_a [72].

Tertiary amine-based methacrylate monomers can alternate between two distinguish shapes. When the amines are protonated (below their pK_a) the chains remain extended due to coulomb repulsions. However, when deprotonated, the amines can establish hydrogen bonds and create micelles with hydrophilic cores (e.g. MSN) creating a polymeric collapsed structure [80] (Figure 1.8). The uniform polymeric mass distribution given by living processes like RAFT or ATRP is crucial, since there is a need to have a homogeneous shell to cover the porous.

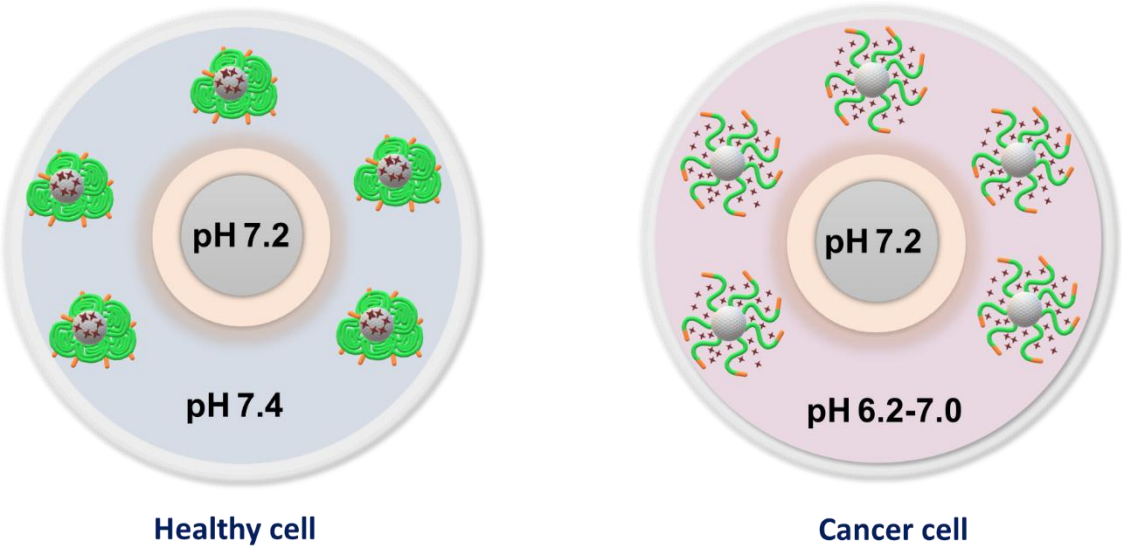

Figure 1.8 – Schematic representation of the expected behavior for the co-polymer with an inner block of pH-responsive polymer (green) and outer block of glycopolymer (orange) grafted to MSN in healthy and cancer cells. The values represent the pH inside the nucleus and cytoplasm.

1.7. Work Objective

The objective of this thesis is to prepare fluorescent smart hybrid mesoporous silica nanoparticle (hMSNs) suitable for theranostic. Smart hMSNs are exceptional candidates due to

high drug uptake capacity, regulable cell targeting and controlled drug release. Combining both therapeutic and diagnosis functions most conventional systemic drug administration problems (e.g. limited stability and lack of selectivity) are expected to be surpassed. Specific ligands can be attached onto MSNs as a targeting strategy to cancer cells overexpression of some well-known receptors and antigens [81].

Synthesis of MSNs from the MCM-41 family, with organized pore structure, controlled morphology and diameter under 100 nm will be performed using the sol-gel process catalyzed in basic medium. Strategy for fluorescent nanoparticles goes by physical adsorption of a symmetric derivative of perylene diimide (PDI) with two propyltriethoxysilane groups to the surfactant hexadecyltrimethylammonium bromide (CTAB). Thus, synthesis of fluorescent MCM-41 nanoparticles will proceed with the hydrolysis and condensation of the silica precursor, tetraethoxysilane (TEOS), around the polar head of the surfactant adsorbed to PDI.

After nanoparticle synthesis, external surface will be modified with 3-aminopropyl triethoxysilane (APTES) to obtain surface amine groups, followed by the removal of the template from the porous using an acidified ethanolic solution. This strategy will allow the coupling of the chain transfer agent (e.g. trithiocarbonate or dithiobenzoate) and the polymerization controlled by RAFT at the particle surface.

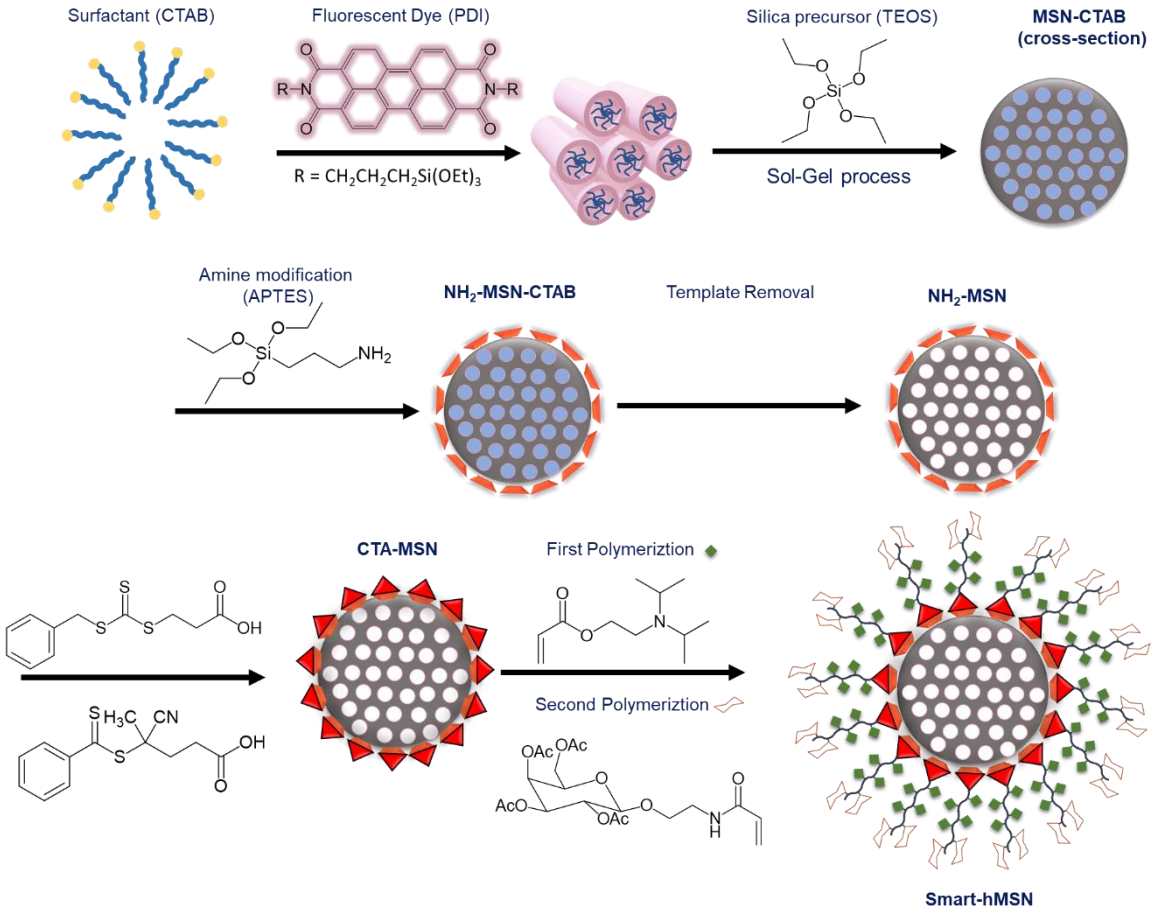

Scheme 1.7 – Schematic representation of the synthesis route planned for the smart hMSN.

Smart hMSNs will be prepared by a “graft from” methodology, growing the co-polymer from the particle surface. Co-polymer will be based on an inner block of 2-(diiso-propylamino) ethyl methacrylate units (pH-responsive) and an outer block of acrylamide ethoxy D-galactose based units (site-specific ligand). Responsive behavior of this co-polymer is expected to change conformation between the pH range of tumor cells. This novel combination of MSNs with responsive and site targeting polymers is expected to be capable of executing diagnosis and therapy. Finally, for evaluation of hMSNs, *in vitro* studies of the release mechanism and uptake are envisioned to be conducted in tumorous hepatic cells.

Characterization of the materials and their respective modifications will be performed through transmission electron microscopy (TEM), nuclear magnetic resonance (NMR), zeta-potential, UV-Vis spectra and size exclusion chromatography (SEC).

A schematic representation of the methodology that will be implemented for the synthesis of the smart hMSN can be observed in scheme 1.7.

THIS

PAGE INTENTIONALLY

LEFT BLANK

2. Results and Discussion

2.1. Synthesis and characterization of fluorescent silica nanoparticles

In the last years there has been an intensive research on the development of silica nanoparticles as suitable carriers for controlled drug release and targeting. Two types of silica nanoparticles (SiNPs) were involved in this study: the non-porous nanoparticles (Stöber NPs) and the mesoporous silica nanoparticles (MSNs). We started by the synthesis of Stöber NPs before moving to the more challenging MSNs. This approach enabled us to identify the optimal nanoparticle structure parameters and experimental conditions for polymerizations. In addition, Stöber nanoparticles present more silanol groups available to react, simpler synthesis procedure and less possible complications with undesired surfactant interactions.

The Stöber nanoparticles were prepared following a strict but very reproductible sol-gel procedure. For the preparation of traceable fluorescent silica NPs, we incorporated a perylenediimide (PDI) dye derivative in the structure of the silica pore walls, during the NPs synthesis. The synthesis of PDI derivatives with silica precursor groups is well established in this research group [39].

The morphology and dimensions of NPs are crucial parameters due to the size and form-dependence of uptake by cells and distribution in biological tissues. It was also found that the uptake of NPs by cells was higher for particles of 50 nm, being 2.5 times higher when compared with particles of 30 nm [39]. In order to investigate whether silica NPs with different sizes have distinctive uptake behavior, Stöber NPs between 30 nm and 60 nm were selected. These particles were obtained by changing the ammonia concentration used for the sol-gel catalysis [25]. By increasing the number of hydroxyls groups in solution, the condensation process is accelerated leading to smaller particles. The particles were characterized by TEM, revealing that the silica NPs have uniform spherical morphology and narrow size distribution. (Figure 2.1).

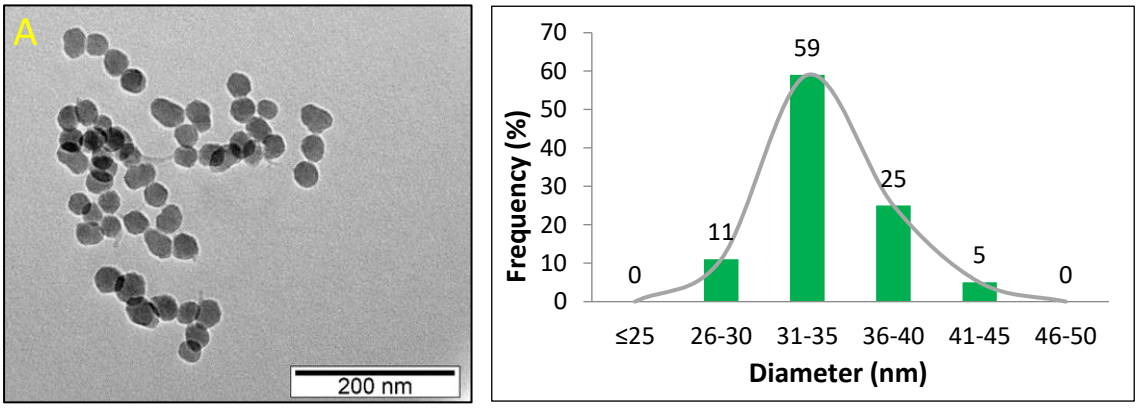

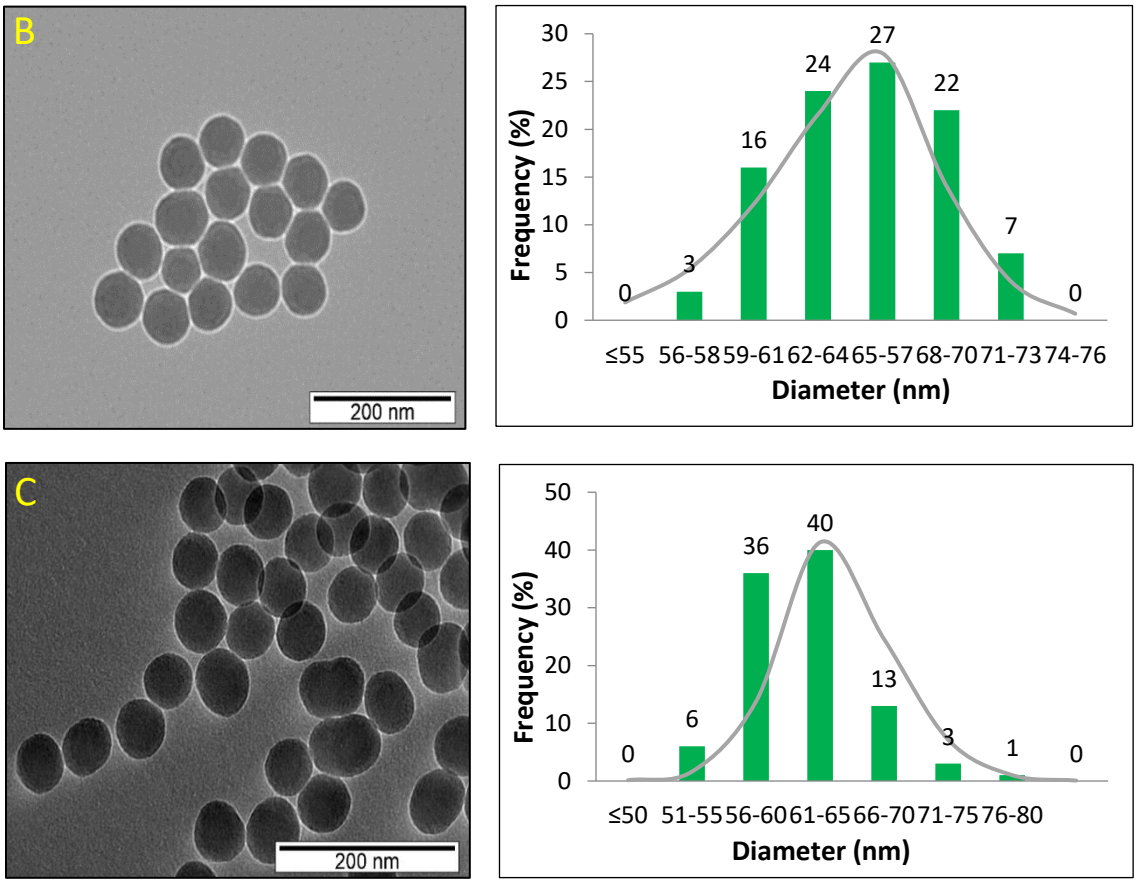

Figure 2.1 – TEM images (200 nm scale) for the stöber nanoparticles synthesized A: Stöber1 (S1); B: Stöber2 (S2) and C: Stöber3 (S3) (Left) and their respective size distribution histogram (Right).

Mesoporous silica nanoparticles (MSN) were synthesized by a modified sol-gel procedure in an aqueous medium, with CTAB as an ionic surfactant, TEOS as the silica source and NaOH as the base catalyst. MSNs with a particle size of 50 nm were obtained by carefully controlling the pH and temperature of the synthesis by a method recently developed in our group (unpublished results). The size of as-prepared MSNs was measured by TEM and was statistically analyzed and found to be 50 ± 6 nm.

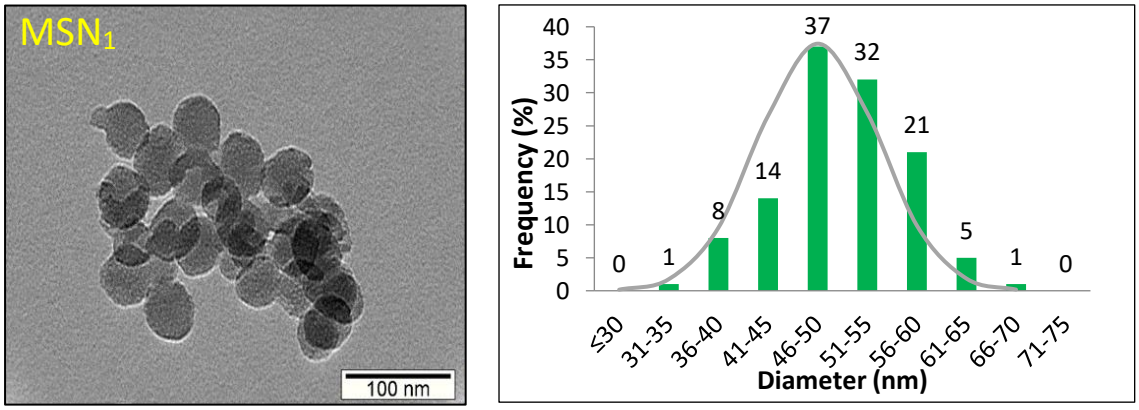

Figure 2.2 – TEM image (100 nm scale) for the mesoporous silica nanoparticles synthesized (Left) and their respective size distribution histogram (Right).

Besides size, information related to NPs sphericity can also be withdrawn from TEM images. NPs morphology was evaluated by the shape factor, when the values are close to one, sphericity resembles to a perfect sphere (Table 2.1).

Table 2.1 – TEM diameter and shape factor obtained for the fluorescent silica nanoparticle.

Particle Batch	[NH_3]	[NaOH] (M)	Shape Factor	D_{TEM} (nm)
S_1	X (<25%)	-	1.14	34 ± 3
S_2	Y (25-28%)	-	1.06	61 ± 5
S_3	Y (25-28%)	-	1.07	64 ± 4
MSN_1	-	1.7	1.12	50 ± 6

From the results and looking at S_2 and S_3, approximately the same size and shape were obtained and with a narrow polydispersity, confirming the reproducibility of the method. A slightly difference in roundness can be pointed out. These results may be correlated with condensation rate and aggregation. Smaller initial nanoparticles tend to aggregate and co-exist in larger clusters stabilized by Van der Walls forces, which can lead to imperfections in morphology. These interactions are then oppressed by electrostatic repulsions from the hydroxyl groups in mature particles obtaining dispersed particles [82]. As expected, to lower concentrations of ammonia (X) smaller particles were synthesized. MSNs were obtained with the desired size and with a relatively good size distribution and shape factor.

Due to the low solubility of the fluorescent dye in water, the dye was first dissolved in ethanol, followed by a filtration before adding it to the silica precursor. An absorption spectrum (Figure 2.3) was made to determine the concentration of PDI added to the nanoparticle synthesis. Absorption was not measured after synthesis as it was assumed that most of it went under condensation simultaneous with the silica precursor. A total of 37 µg were added during the synthesis, which was revealed to be enough for bioimaging studies, as shown in the literature [35]. Now, regarding the MSN synthesis, the fluorescent dye was previously adsorbed to the surfactant and added to the synthesis.

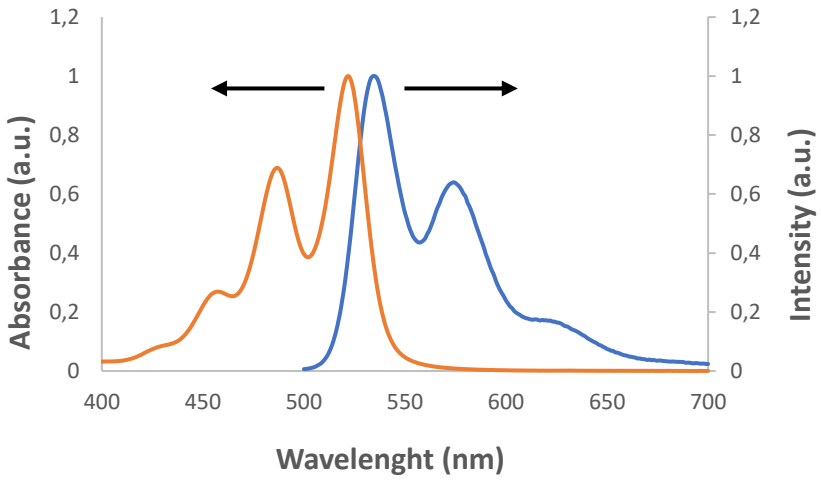

Figure 2.3 – Normalized absorption (orange) and emission (blue) spectra for perylene diimide derivative in ethanol. Extinction coefficient (ε) at absorption maxima = 56,162 $M^{-1}cm^{-1}$ [29].

2.2. Surface functionalization of silica nanoparticles

The synthetic route for surface functionalization with the corresponding trithiocarbonate as RAFT chain transfer agent (CTA) is given in Scheme 2.1. The external surface of the silica NPs will be modified with (3-aminopropyl) triethoxysilane) (APTES) to obtain amine groups at the particle surface. This surface modification will be used to couple the chain transfer agent for RAFT controlled polymerization, followed by the grafting of a *co*-polymeric chain. An extra step was necessary during the MSNs synthesis, to uncover the MSN porous was used an acidified ethanolic solution.

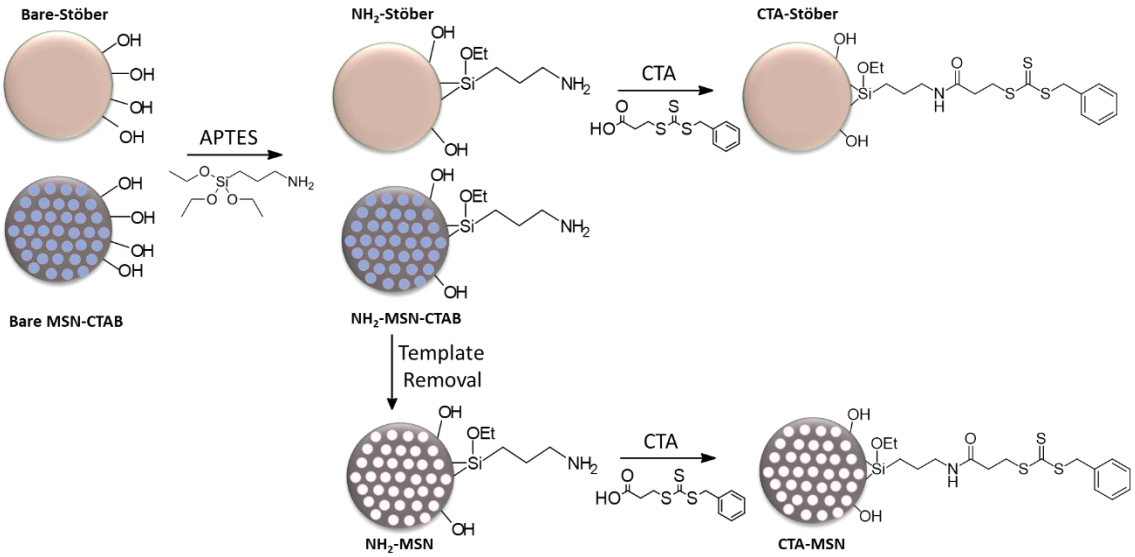

Scheme 2.1 – Fluorescent silica nanoparticles surface functionalization. First step - amine surface modification; Second step - chain transfer agent coupling. Extra step of template (surfactant) removal for the mesoporous silica nanoparticle (MSN).

2.2.1. Amine modified silica nanoparticles

Functionalization of the outer surface of the silica NPs with amine was performed using APTES through siloxane chemistry. The reaction was performed under inert atmosphere and with dry solvent to prevent spontaneous hydrolysis of the reagent. To avoid self-condensation of APTES molecules, the APTES concentration were judiciously calculated. Ideally self-condensation of APTES is avoided and only condensation with silanol groups occurs.

To know the exact amount of APTES needed to a determined concentration per particle it was necessary to calculate the surface coverage (molecules/nm^2). The surface coverage of two molecules per nm^2 was pointed out (calculation in attachment 6.13). This value was picked to create an amine monolayer and still avoid hinderance effects during the polymerization.

Solution NMR was used for the identification and quantification of the covalently bound ligands by a method recently developed in the group [83]. The particles were first washed several times to make sure that the result obtained was from amines covalently attached at the surface and not from entrapped molecules in the silica matrix. First, the particles require to be hydrolyzed by sonication in basic medium (pH=13), followed by the addition of an internal standard (1,3,5-

Trioxane) to quantify the amines. This method avoids the usage of solid-state NMR, that demands a higher amount of sample and is less accessible when compared with solution NMR. The APTES concentrations obtained for the nanoparticles, is shown at Table 2.2.

Table 2.2 – APTES quantification for SiNps by ^{1}H-NMR, spectra in D_2O (pH=13).

Particle Batch	[APTES] (mmol/g SiNp)	APTES Molecules / nm^2
S_1 (33 nm)	0.4	2.2
S_2 (61 nm)	0.4	2.2
S_3 (64 nm)	0.2	2.3
MSN_1 (50 nm)	1.1	1.9

APTES concentrations were determined by ^{1}H-NMR (Figure 2.4) using an internal standard as reference. The number of molecules obtained were very similar to the pre-determined value of 2 molecules per nm^2. Besides the grafted APTES molecules to the SiNPs, at 5.2 ppm we can see a singlet from the internal standard (1,3,5 – trioxane). Also, at 3.7 ppm a quartet and at 1.2 ppm a triplet corresponding to ethanol CH_2 and CH_3 groups respectively can be observed. The obtained ethanol is a result from the hydrolysis of unreacted ethoxy silane groups as consequence of the basic pH during the NMR sample preparation.

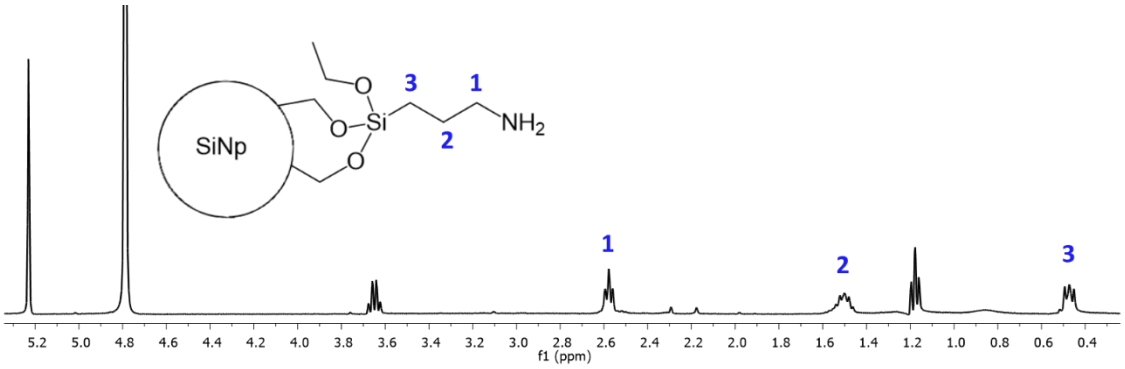

Figure 2.4 – ^{1}H-NMR (400MHz; D_2O) obtained for the amine functionalized nanoparticles.

In MSN synthesis, before proceeding with the next modification, the surfactant was removed by extraction with an acidified ethanolic solution. Surfactant was removed after amine functionalization to avoid amine functionalization inside the porous, remaining only at the particle surface. By having amines only at the particle surface, CTA coupling, and further polymerization will not interfere with drug encapsulation. Consequently, the well-ordered porous structure became more evident, as shown by the TEM images (Figure 2.5).

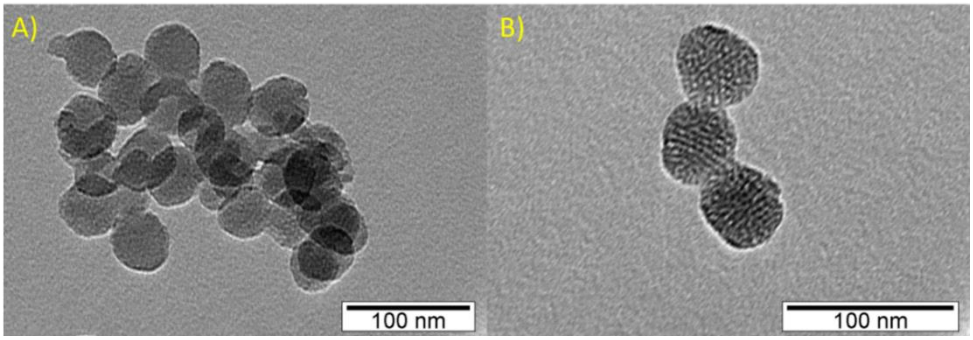

Figure 2.5 – TEM image (100 nm scale) of the synthesized mesoporous silica nanoparticles. A) before surfactant removal; B) after surfactant removal.

2.2.2. Functionalization with the chain transfer agent for RAFT polymerization

Synthesis of 3-(benzylsulfanylthiocarbonylsulfanyl) propionic acid (BSPA), a trithiobased chain transfer agent for amine coupling was performed by one-pot synthesis. Reaction occurs by an addition of the mercaptopropionic acid to carbon disulfide, with KOH as the base catalyst, followed by a nucleophilic substitution of the trithio group to the benzyl bromide. Combination of trithiocarbonate compounds and propionic acid as thiocarbonyl activator (Z group) have shown to provide controlled molecular weight and narrow polydispersity for acrylamide monomers in water and organic solvents [84]. Besides functional group such as carboxyl, enables the attachment to the nanoparticles via coupling with the amines. As the group R, benzyl was picked as a good leaving group for the polymerization controlled by RAFT [85]. Thus, the chain transfer agent **(1)** was synthesized as shown in Scheme 2.2.

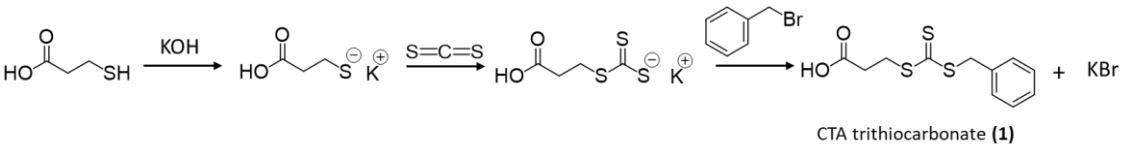

Scheme 2.2 – Synthesis of the trithiocarbonate chain transfer agent, 3-(benzylsulfanylthiocarbonylsulfanyl) propionic acid (BSPA) **–** compound **(1)**.

A yellow powder with a pungent odor was obtained from recrystallization in dichloromethane with a yield of 33%. This yield is low compared to the literature [86] but can be explained by extraction and recrystallization efficiency. The structure of the chain transfer agent **(1)** was confirmed by ^{1}H-NMR (Figure 2.6) and ^{13}C-NMR (Attachment 6.1).

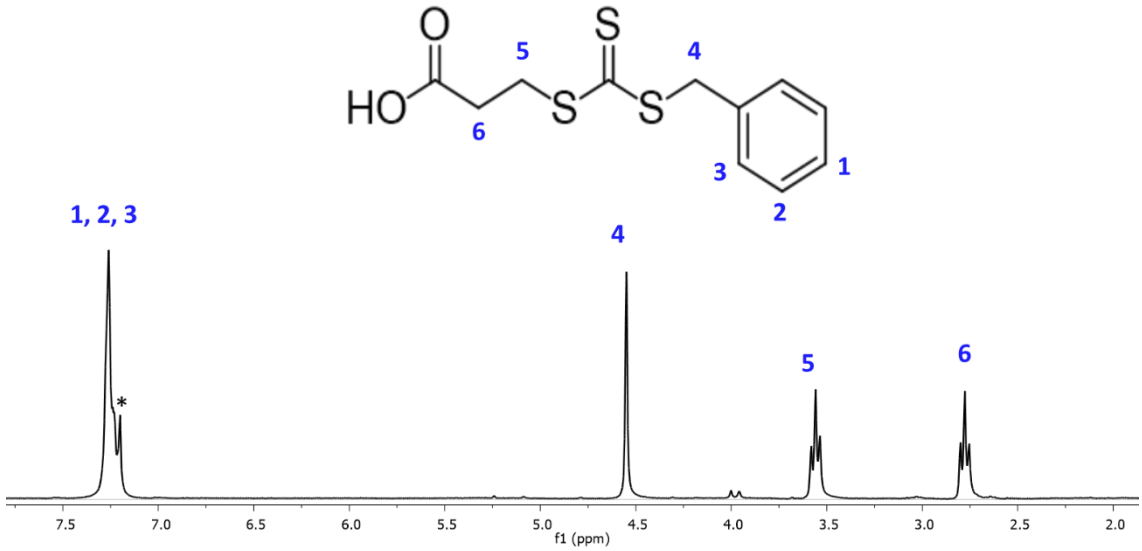

Figure 2.6 – ^{1}H-NMR (400MHz;($CDCl_3$)) obtained for 3-(benzylsulfanylthiocarbonylsulfanyl) propionic acid – compound **(1)**.

After the synthesis of the chain transfer agent we proceed to the next step of the surface functionalization. The amine groups were covalently reacted with the carboxylic acid group of CTA to form amide linkages by standard EDC coupling chemistry. As carboxyl activating agent coupling agent 1-Ethyl-3-(3-dimethylaminopropyl) carbodiimide (EDC) was used to react with CTA, creating a reactive intermediate of O-acyl isourea (Scheme 2.3). This intermediate creates an ester with a good leaving group that in the presence of primary amines leads to the desired

amide and urea as a by-product. A less likely reaction to produce the desire amide can also occur by an indirect method, in which the acid reacts with O-acyl isourea followed by an addition of the primary amine. O-acyl isourea can also rearrange through a N-acyl transference, creating a stable undesired urea as sub-product. Besides lowering the yield of the reaction, the urea by-product is not a problem since particles are then washed in ethanol and centrifuged, removing all possible urea.

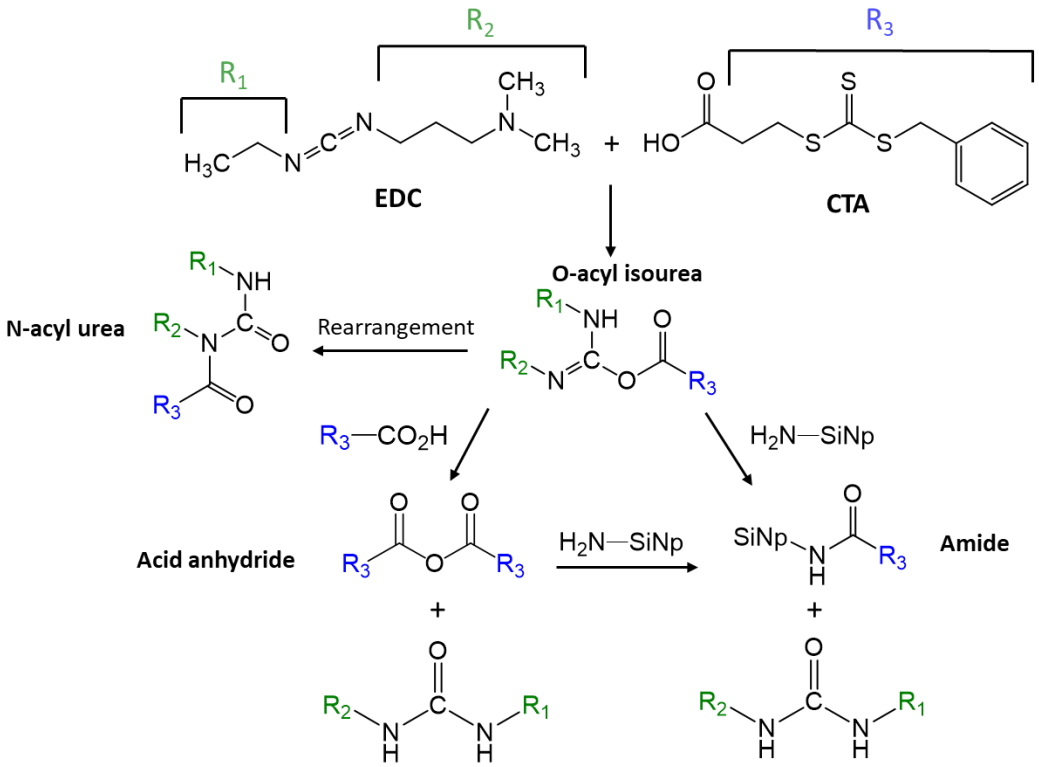

Scheme 2.3 – Main reactions involved on the amine coupling using EDC as carboxyl activating agent for the CTA and NH_2-SiNp as the primary amine source.

The CTA surface density was calculated from the absorption spectra of CTA-SiNp dispersed in 1,4-dioxane. Based on the Beer-Lambert equation, it was possible to calculate the CTA concentration (ε = 13.98 mM^{-1} cm^{-1}; A_{max}: 310nm). Correction of light scattering by the nanoparticles was applied using NH_2-SiNp as baseline and adjusting it for wavelengths below 260 nm and over 360 nm using SOLVER (Figure 2.7). This procedure was performed just as reported in 2015 using the same type of particles and CTA agent [87].

CTA coupling reaction was performed on the amine functionalize particles, reaching to obtain different grafted CTA concentrations (Table 2.3). Different grafting concentrations of CTA agent were used to study their effect on growing the polymer from the particle surface (grafting from).

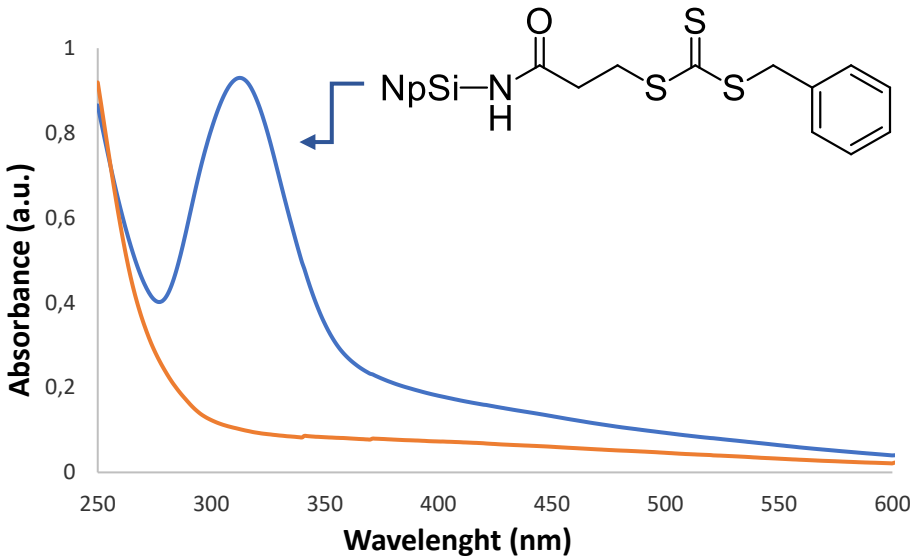

Figure 2.7 – Absorption spectra overlap for CTA-SiNp (blue) and NH_2-SiNp (orange) in 1,4-dioxane.

Although at least two different CTA-stöber concentrations were achieved, other experiences were performed to reach a higher concentration. We started by duplicating the quantities of CTA from equimolar to two equivalents, but the same amount of CTA was obtained (0.08 mmol per gram of silica nanoparticles). This result led us to believe that the problem was not on the transfer agent but on the amine susceptibility to react. Taking that in consideration, 4-Dimethylaminopyridine (DMAP) was added in equimolar amount as a nucleophilic catalyst. DMAP reacts rapidly with O-acyl isourea creating an instable intermediary and promoting the amine coupling (Scheme 2.4).

Table 2.3 – Grafted CTA concentration onto SiNp, characterized by UV-Vis.

Particle Batch	[CTA] (mmol/g SiNp)	CTA Molecules / nm²
S_1 (33 nm)	0.08	0.4
S_1 (33 nm) + DMAP	0.04	0.2
S_2 (61 nm)	0.08	0.4
S_3 (64 nm)	0.01	0.1
MSN_1 (50 nm)	0.05	0.1

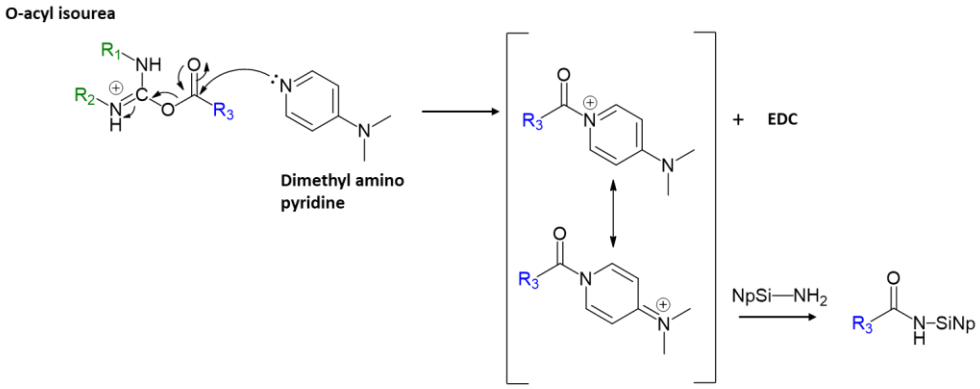

Scheme 2.4 – Reaction of amine modified silica nanoparticles with the reactive intermediate formed between o-acyl isourea and DMAP.

Although, the addition of DMAP did not increased the CTA concentration, in fact, it decreased by almost one half, reaching a concentration of about 0.03 mmol per gram of silica nanoparticles. This might have to do with the positively charged DMAP intermediate can possible aggregate around the hydroxyl groups of the nanoparticle surface. Blocked chains would be incapable to further react due to steric hindrance leading to lower grafted CTA concentrations. These aggregates would be removed during work-up and only covalently attached chains would be measured by absorption spectra. Although the higher CTA concentration was only half than what is reported in the literature [87] this value is strongly influenced by APTES concentration at the silica nanoparticle surface, thus a direct comparation between both works is not possible to establish.

For the MSNs, the CTA grafting density was lower than expected. Two methods were tested to improve the CTA grafted density. First, the amine coupling reaction was repeated onto the particles containing 0.05 mmol of CTA per gram of particle. The grafted density doubled from 0.05 mmol/g of SiNp to 0.1 mmol/g of SiNp. In the second approach it was found that while removing the surfactant with an acidic solution some of the amines would stay protonated decreasing their nucleophilicity. By washing the particles with a basic ammonia solution before proceeding with the amine coupling, it was possible to increase the CTA grafted density up to 0.15 mmol/g of SiNp.

It was reported in the literature that a lower CTA graft concentration would lead to an higher degree of polymerization [88]. This principle was explained by a “reaction-diffusion” mechanism, where it stated that, two active radicals will get closer as the chain transfer reactions occurs. The rate of chain transfer reactions will increase with higher surface CTA densities, promoting more termination events. Therefore, a grafting density of 0.08 chains per nm^2 (equivalent to 0.05 mmol/g of SiNp) was recommended by the authors to minimize termination reactions. As a consequence, higher CTA grafted densities were not pursued.

2.2.3. ζ-potential Determination

When charged, a double layer of ions (*Stern layer* and *Debye`s Law*) is adsorbed to the surface of charged dispersed particles. The double layer composition is based on both negative and positively charged ions that depends on a few factors (pH, ionic strength, concentration, etc.). By applying an electric field charged particles move towards opposite charged electrodes. The potential at the hypothetical plane (interface) between the moving particles and the layer of dispersant is known as zeta (ζ) potential. Zeta acts as a colloidal dispersion stability evaluator by a balance of attractive and repulsion forces between adjacent similar particles. With a low zeta-potential, attractive forces may exceed repulsion and particles flocculate [89]. Therefore, zeta-potential was measured for each particle functionalization as qualitative method for differences in surface charge (Figure 2.8).

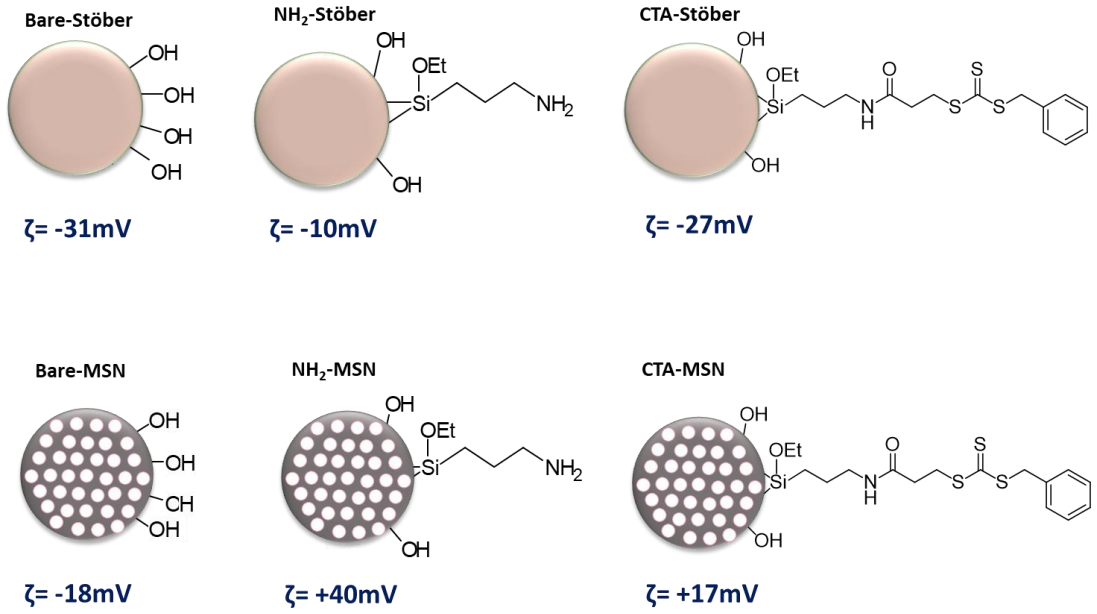

Figure 2.8 – Zeta-potential (mV) for NPs after the different surface modifications. Measures at pH=5 and concentration of 0.2 mg per mL.

By looking at the changes in zeta-potential we can conclude that all three different modifications occurred. For MSN, the template was always removed to eliminate the charge influence of the surfactant. In bare nanoparticles due to the eletrowithdrawing hydroxyl groups at the particle surface, a negative value was registered. When functionalized with APTES, amines reduce the electronegativity around the particles increasing the value of the zeta potential. For MSN, as the template was removed with an acidic solution, the primary amines may be charged, increasing drastically the zeta potential value. After CTA modification ζ-potential decreased due to a reduction of the primary amine effect, because of the amine coupling with the chain transfer agent. To sum up, it was observed that the ζ-potential increased upon amine functionalization and later changed to a less positive value upon CTA grafting, this clearly indicates that the modifications were successfully performed.

2.3. Galactose-based monomer synthesis and polymerization

Following the simpler approach, the “graft from” polymerization controlled by RAFT, was performed using a carbohydrate-based monomer instead of the *co*-polymer. The *co*-polymer composition was based on an inner block of 2-(diiso-propylamino) ethyl methacrylate (DPAEMA) and an outer block of 2`-acrylamidoethyl-β-D-Galactose tetraacetate (AMEGalOAc). Thus, only the carbohydrate-based moiety was used for the initial polymerizations in solution and at the particle surface.

2.3.1. Synthesis of 2`-acrylamidoethyl-β-D-Galactose tetraacetate (AMEGalOAc)

The synthesis of the 2`-acrylamidoethyl-β-D-Galactose tetraacetate (AMEGalOAc), was achieved by a two-step synthesis based on an acetylation of the sugar moiety followed by a Lewis acid catalyzed glycosylation (Scheme 2.5).

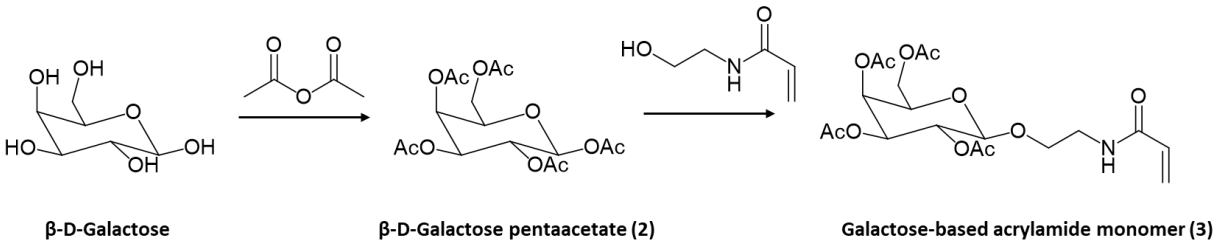

Scheme 2.5 – Synthesis route for the galactose-based acrylamide monomer. 2`-acrylamidoethyl-β-D-Galactose tetraacetate (AMEGalOAc) – compound (**3**). First step – acetylation: Second step – Alkylation.

Starting with the β-D-Galactose, a cheap commercial reagent, a standard procedure of carbohydrate protection was pursued, using sodium acetate as non-nucleophilic base and acetic anhydride. Synthesis of β-D-Galactose pentaacetate **(2)** was confirmed by ^{1}H-NMR (Attachment 6.2) with the appearance of five singlets between 2.1 ppm and 1.9 ppm and a total integration of fifteen protons from the five -CH_3 of the acetate's groups. ^{13}C-NMR, 2D-COSY and 2D-HSQC, (Attachment 6.3-6.5) were performed to fully characterize the compound **(2)**.

The product was recrystallized in ethanol leading to a white powder with a yield of 43%. A quite low yield for this type of reaction [90], since there was no reagent left, confirmed by thin layer chromatography, it was concluded that most of the product was lost during purification.

The second step was the alkylation of the peracetylated galactose by reacting with an alcohol. Acetate oxygens in galactose pentaacetate can act as lewis base, thus by using a lewis acid, in this case, boron trifluoride etherate, the position become electron deficient turning the acetates in excellent leaving groups. This lewis acid was used due to the highly stereoselectivity for the β anomeric form of glycosides. Since anomeric acetates are considerably more reactive than primary and secondary, alkylation takes place mainly at the anomeric position.

The identification and purity of the product **(3)** was confirmed by ^{1}H-NMR (Figure 2.9). The disappearance of a singlet at 2 ppm corresponding to -CH_3 of the acetate group from the anomeric position can be observed. Also, confirmed by the appearance of one duplet and two multiplets between (6.3ppm and 5.5ppm) attributed to the three protons of the acrylamide double bond. After purification by silica gel filtration a white foam was obtained with a yield of 48%. Similar yields were found for allyl alcohols addition to β-D-Galactose using boron trifluoride etherate [91]. ^{13}C-NMR, 2D-COSY and 2D-HSQC, (Attachment 6.6-6.8) were performed to fully characterize the compound **(3)**.

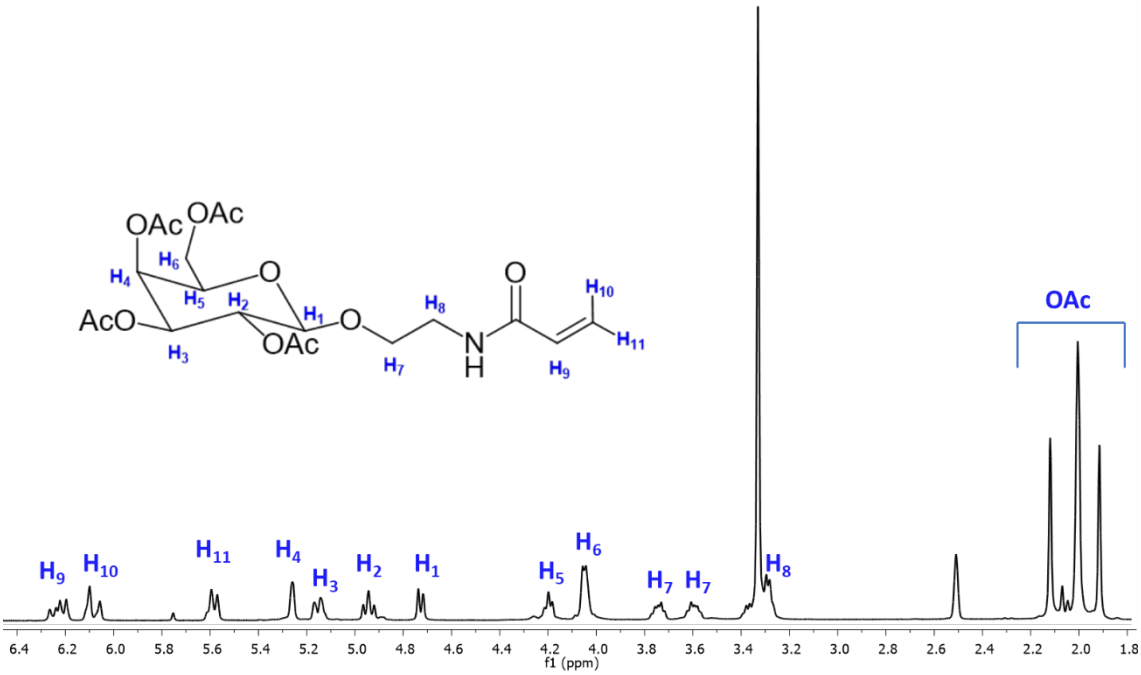

Figure 2.9 – ^{1}H-NMR (400MHz;$(CD_3)_2SO$) obtained for compound 2`-acrylamidoethyl-β-D-Galactose tetraacetate (AMEGalOAc) – compound **(3)**.

2.4. Synthesis of 2-(diiso-propylamino) ethyl methacrylate (DPAEMA)

Although the first attempts of polymerization at the particles surface were based only on the carbohydrate block, the pH-responsive monomer was synthesized in advance. 2-(diiso-propylamino) ethyl methacrylate (DPAEMA) synthesis was performed following a simple nucleophilic addition/elimination between an acyl chloride and alcohol in the presence of a non-nucleophilic base (Figure 2.10).

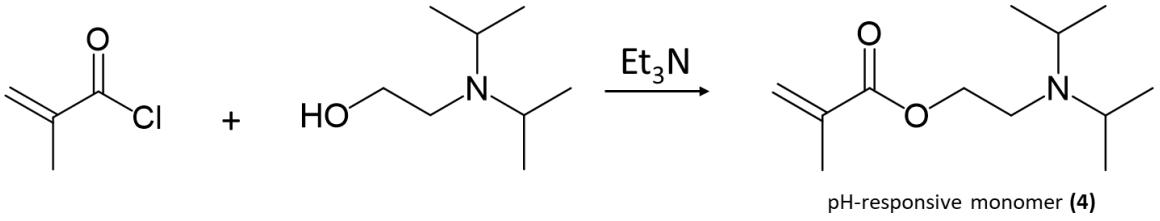

Figure 2.10 – Synthesis of the pH-responsive, 2-(diiso-propylamino) ethyl methacrylate (DPAEMA) – compound **(4)** – by nucleophilic addition/elimination.

Precautions were made to avoid polymerization during reaction by using hydroquinone as a radical sequester. After purification using vacuum distillation a colorless liquid was obtained with a yield of 46%. Structure was confirmed by ^{1}H-NMR (Figure 2.11) and ^{13}C-NMR (Attachment 6.9).

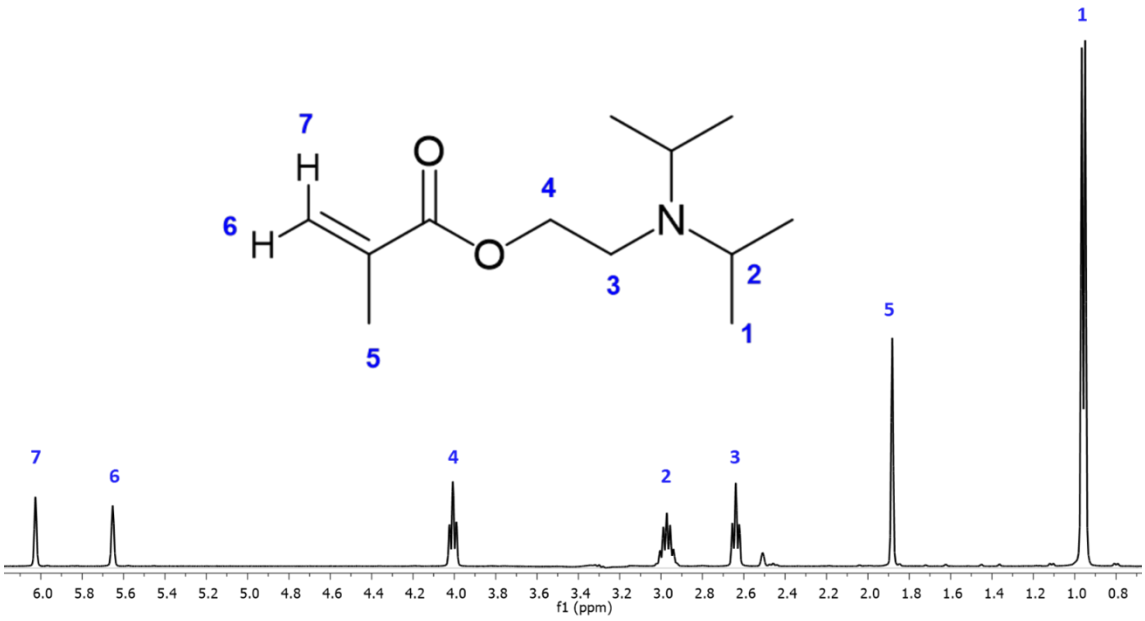

Figure 2.11 – ^{1}H-NMR (400MHz;$(CD_3)_2SO$) obtained for 2-(diiso-propylamino) ethyl methacrylate (DPAEMA) – compound (**4**).

2.5. Polymerization of 2`-acrylamidoethyl-β-D-Galactose tetraacetate

In order to proceed with the polymerization at the nanoparticle surface it was necessary to determine if the CTA and monomer were compatible for RAFT polymerization. Thus, the polymerization was performed in solution with two different [Initiator]/[CTA] ratios. This way evaluation of mass distribution and average molecular weight (Mw) can be studied by changing the initiator concentration. For higher [CTA]/[Initiator] ratio, a better control of the polymerization is expected.

Polymerizations were performed in 1,4-dioxane, with BSPA and AMEGalOAc. For the initiator and internal standard, (2,2′-Azobis) 2-methylpropionitrile (AIBN) and 1,3,5-Trioxane were used respectively. The two different experiments and their conditions can be observed in Table 2.4.

Table 2.4 – Experimental conditions for a controlled polymerization by RAFT in solution, using the acrylamide galactose-based monomer, 2`-acrylamidoethyl-β-D-Galactose tetraacetate (AMEGalOAc) – compound **(3)**.

Variables/Experiment	**1**	**2**
Temperature (°C)	80	
$[AIBN]_0/[CTA]_0/[Monomer]_0$ (mM)	2/10/224	1/10/224
Solvent	1,4-dioxane (3mL)	

These conditions were previously used in the laboratory to synthesize the same polymer with higher AIBN concentration ($[AIBN]_0/[CTA]_0$ = 1/2). Following this procedure, it was possible to synthesize and characterize the polymers by size exclusion chromatography (SEC) and

estimate the molecular weight by UV-Vis. Also, the polymerization kinetics were followed by ^{1}H-NMR to assess the degree of the polymerization over time (Figure 2.12) and built a procedure for polymerization at the particle surface.

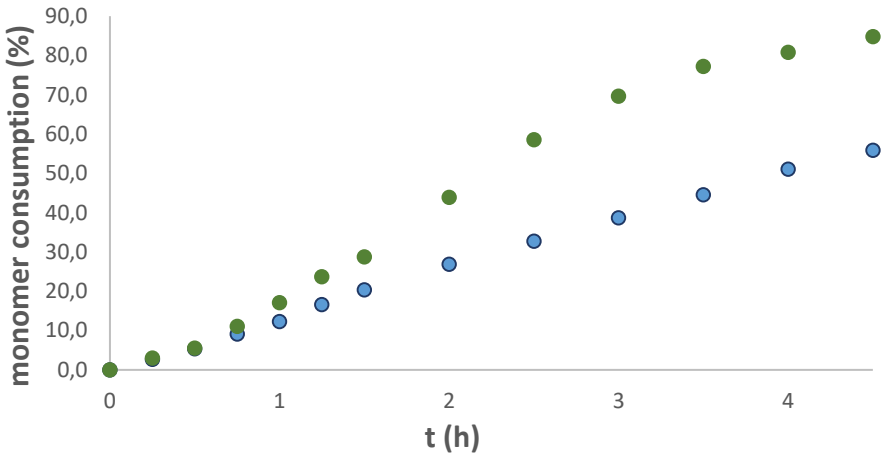

Figure 2.12 – Kinetic plot of acrylamide galactose-based monomer – AMEGalOAc, compound **(3)** - consumption over time for [CTA]/[AIBN] = 5 (green – experiment 1 – table 2.4) and [CTA]/[AIBN] = 10 (blue – experiment 2 – table 2.4) at 80°C in 1,4-dioxane.

From the kinetic data to the lower AIBN concentration (experiment 2 – Table 2.4) a conversion of 56% at 4.5 hours was registered while for higher concentration of initiator (experiment 1 – Table 2.4) a conversion of 85%. By decreasing the initiator concentration (experiment 2 – blue), the number of free radicals is also reduced leading to a slower conversion.

Two approaches were followed to determine the molecular weight. A faster estimative through UV-vis and a more precise method using SEC (Attachment 6.15 to 6.17) able to measure the polymer weight and mass distribution. The results obtained for both methods can be observed in Table 2.5.

Table 2.5 – Molecular weight of the galactose-based polymer (PAMEGalOAc) synthesized in THF, and characterized by UV-Vis and SEC-MALS. Experiment 1 - $[AIBN]_0/[CTA]_0/[Monomer]_0$ = 2/10/224 mM; Experiment 2 - $[AIBN]_0/[CTA]_0/[Monomer]_0$ = 1/10/224 mM.

Experiment	Targeted M_w (kD_a)	M_w (SEC) (kD_a)	M_n (SEC) (kD_a)	Polydispersity (M_w/M_n)	M_w (UV-Vis) (kD_a)
1	10.0	9.5	8.8	1.09	11.2
2		11.5	11.0	1.04	13.2

The molecular weight, by UV-Vis, was estimated by considering that the polymerization occurred in a controlled manner growing all the chains equally. Thus, by using the CTA concentration obtained by UV-Vis (Figure 2.13) and admitting that the number of CTA moles is equal to the repetitive unit of the polymer, it was possible to estimate the molecular weight.

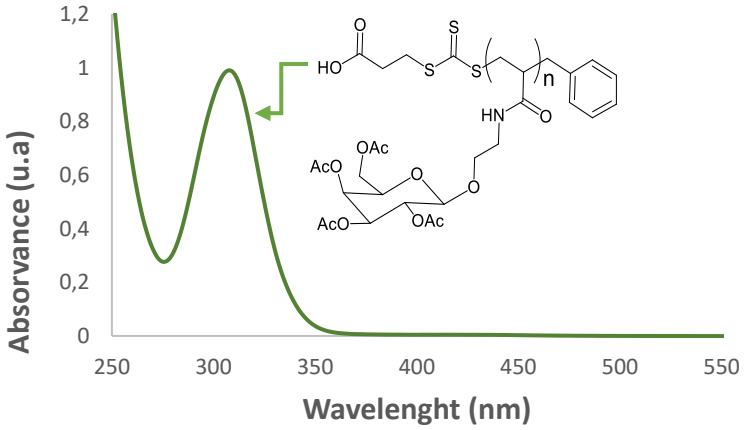

Figure 2.13 – Absorption spectra for galactose-based polymer (PAMEGalOAc) in 1,4-dioxane, obtained from experiment 2 – table 2.5.

The molecular weight determined by SEC, using a refractive index detector (SEC-MALS), was similar to UV-Vis results. There is a difference of approximately 16% between SEC-MALS and UV-Vis results, this could be attributed to experimental error. The Mw obtained for both polymers were very close to what was intended (intended: 10kDa; observed: 11kDa) which corresponds to twenty-five repetitive units in each polymeric chain. By SEC-MALS mass distribution was resolved over elution time (Figure 2.14) obtaining a polydispersity of 1.09 (lower [CTA]/[Initiator] ratio) and 1.04 (higher [CTA]/[Initiator] ratio).

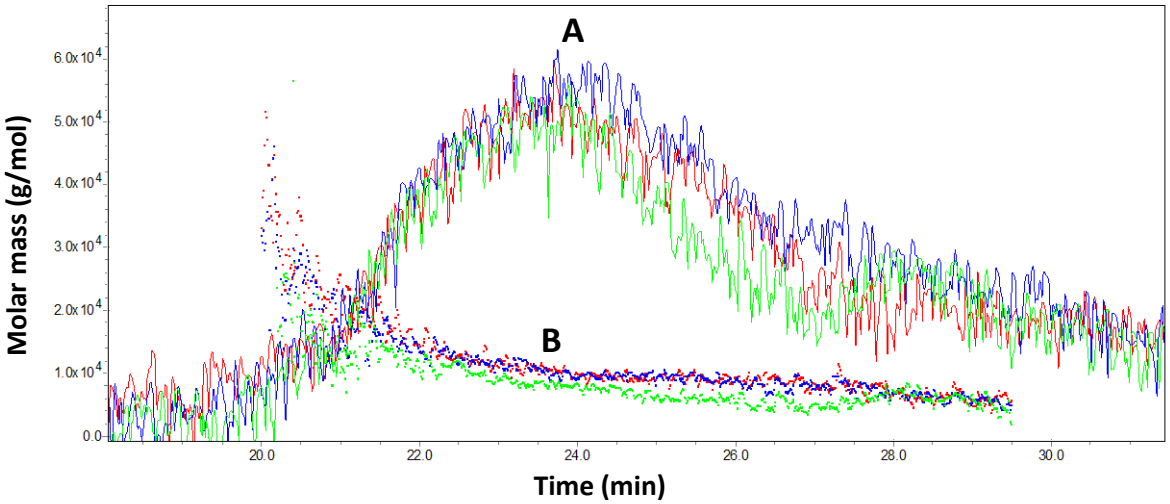

Figure 2.14 – Molecular weight distribution chromatogram for PAMEGalOAc. Elution over time in triplicated assay for experiment 1 – table 2.5 – using 10^2 Å + 10^3 Å columns with a pre-column at 23°C in THF and a refractive index detector.

Galactose-based polymer (PAMEGalOAc) showed a retention time of 24 min (Curve A). Looking at the curve B of the chromatogram is noticeable that mass distribution does not flow significantly over the elution indicating a homogeneous mass distribution. The good narrow

polydispersity can be verified for both polymers with similar values, concluding that the modification in CTA ratio had no significant impact.

2.6. Synthesis of Stöber glyco-nanoparticles

After tracing polymer kinetics and assessed the control of RAFT polymerization in solution, it was possible to synthesize hybrid stöber nanoparticles by growing a glycopolymer from the CTA functionalized nanoparticles. The polymerization was based on a grafting from, by z group approach, or "transfer to", since the CTA is attached covalently by the Z group (Figure 2.15). This approach implicates that the polymer chains grow in solution avoiding intra and intermolecular undesired reaction.

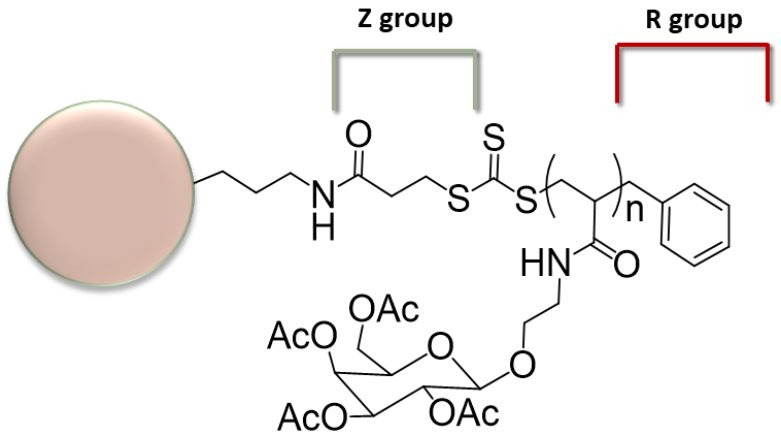

Figure 2.15 – Stöber hybrid silica nanoparticle with a glycopolymeric shell by a "transfer to" approach, highlighting the Z and R group of the CTA.

2.6.1. Grafting densities

The grafting procedure was performed for the different nanoparticles under the same conditions used for experiment 1 (Table 2.4) but in a more diluted environment to achieve a better particle suspension. Due to singlet oxygen that leads to termination of free radicals, a degassing method of bubbling argon was employed. Results for "transfer to" polymerization at the particle surface are expressed in weight percentage per gram of particle (Table 2.6).

Table 2.6 – Quantification of the glycopolymer weight (wt %) grafted onto the particle surface by ^{1}H-NMR.

Particle Batch	CTA Molecules / nm^2	CTA mmol / g of SiNp	Polymer wt (%) / g of SiNp
S_1 (33 nm)	0.4	0.08	1.8
S_2 (61 nm)	0.4	0.08	0.7
S_3 (64 nm)	0.1	0.01	0.5

Polymer weight was quantified by ^{1}H-NMR as mentioned in the section 2.2.1. There is a slightly difference in the total amount of polymer per gram of nanoparticles by changing the CTA concentration (S_2 and S_3). By comparing the degree of polymerization with the CTA chains in both polymerizations, a CTA density eight times lower, led to almost the same polymer weight

percentage. This result can be explained by the fact that a lower CTA concentration are less prompt to termination events, due to the “diffusion-reaction” mechanism, as mentioned in the section 2.2.2. On the other hand, on smaller particles the amount of polymer grafted seems to be higher, this may be correlated with the higher curvature for smaller particles. A higher curvature will create less steric hindrance allowing the polymeric chains to grow freely.

Due to low polymeric density, by ^{1}H-NMR neither alkyl chains nor carbohydrate peaks were observed. However, during particle hydrolysis the acetates groups are also removed, generating acetic acid (1.86 ppm) (Figure 2.16). Thus, grafted polymer density concentration was measured using the product from the acetate groups hydrolysis.

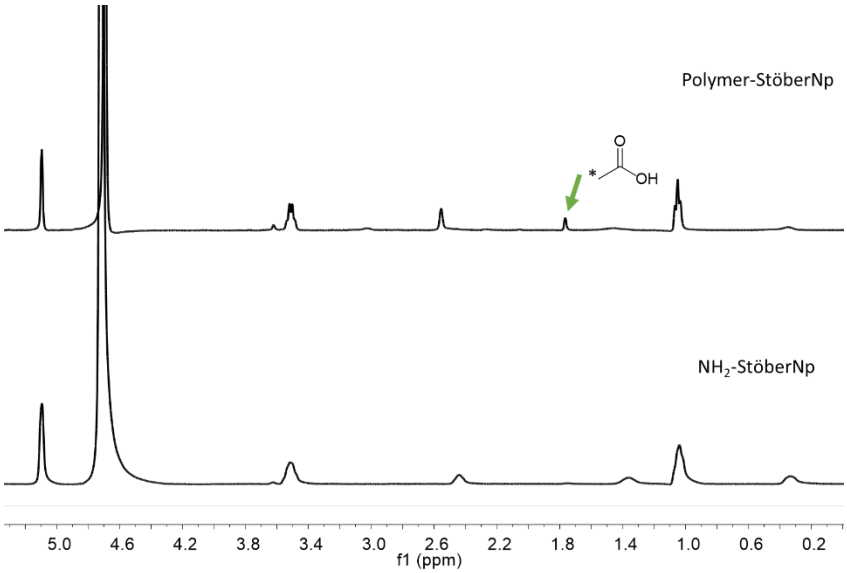

Figure 2.16 – ^{1}H-NMR spectra for the SiNps before and after polymerization. ^{1}H-NMR spectra acquired in D_2O (pH=13) with 1,3,5-Trioxane as internal standard (s, 5.1 ppm) for particles functionalized with amine and after “transfer to” polymerization.

By this method is considered that all acetates in galactose were removed and thus the number of moles of galactose units can be calculated. From that, and knowing the exact number of particles, the weight percentage of the polymer around the nanoparticles can be quantified. A modification from -27 mV to -32 mV was registered in ζ-potential, this effect may be small, but the stability increased as expected by adding a polymer layer.

2.7. Stöber glyco-nanoparticles with dithiobenzoate as CTA

While trying to improve polymer densities at the particle surface, compatibility between trithiocarbonate CTA and methacrylate monomer (pH-responsive monomer - DPAEMA) was tested. Results shown a non-controlled behavior. A molecular weight of 91.8 kD_a was obtained for an intended 10 kD_a polymer. This problem was attributed to the degradation of the trithiocarbonate chain transfer agent during RAFT polymerization by the amines from the pH-responsive methacrylate monomer [92].

Since most pH-responsive polymers with a suitable pK_a for the desired application are based on tertiary amines, a change in CTA had to be done. 4-Cyano-4-

(phenylcarbonothioylthio)pentanoic acid (CPADB) as CTA agent was picked due to their compatibility with 2-(diiso-propylamino)ethyl methacrylate (DPAEMA) [93].

Considering the new CTA, the polymerization of DPAEMA was carried in solution as described in [93] with the addition of 1 equivalent of trifluoroacetic acid. Acid addition was used to reduce the possible aminolysis of the CTA agent by the tertiary amine that could lead to an uncontrolled molecular weight. The reaction was stopped after 5 hours, equivalent to 50% monomer conversion. Resulting polymer (PDPAEMA) was analyzed by SEC (Attachment 6.24 and 6.25) and UV-Vis.

Table 2.7 – Molecular weight for the DPAEMA polymer (PDPAEMA) synthesized in THF, and characterized by SEC-MALS and UV-Vis.

Polymer	*Targeted* M_w *(kDa)*	M_w *(SEC)* *(kDa)*	M_n *(SEC)* *(kDa)*	*Polydispersity* (M_w/M_n)	M_w *(UV-Vis)* *(kDa)*
PDPAEMA	10.0	14.2	14.0	1.01	9.4

Results obtained from the SEC and UV-Vis are slightly discordant. By UV-Vis the polymer obtained had a chain length lower than expected. On the other side, SEC says that the polymer length is higher than expected but the polymerization is well controlled. With the DPAEMA polymerization controlled in solution using CPADB, synthesis of the glyconanoparticles was continued.

Stöber nanoparticles with CPADB as the new CTA agent were synthesized. The particles synthesis and functionalization were proceeded just as previously described for BSPA (Section 2.2.2). Stöber nanoparticles were synthesized with 65 nm ± 4 nm of diameter and functionalized with 1.6 molecules of APTES per nm^2, followed by a CTA density of 0.4 molecules of CTA per nm^2.

Furthermore, the galactose-based monomer (AMEGalOAc) was grown from the surface of CPADB functionalized nanoparticles, using the same conditions as in section 2.5.1. As a result of using CPADB as the new CTA, the polymer now grows from the particle surface (graft from), since the agent is attached by the R-group (4-cyano pentanoic acid). The results for both types of polymerization (transfer to and graft from) can be seen in Table 2.8.

Table 2.8 – Grafted glycopolymer in weight percentage (wt (%)) by controlled RAFT polymerization at stöber nanoparticles functionalized with BSPA (S_3) or CPADB (S_4) as the chain transfer agent.

Particle Batch	CTA Molecules / nm^2	Polymer wt (%) / g of SiNp
S_3 (61 nm)	0.4	0.7
S_4 (64 nm)	0.4	0.5

The polymer density was slightly higher using trithiocarbonate (BSPA). These results may be explained by the CTA reactivity. As CPADB is more reactive than trithiocarbonate (BSPA), it becomes more prompt to hydrolysis affecting the overall quantity of CTA chains available to react. This effect is observable by a color change during polymerization, from pink (CPADB) to yellow (CPADB hydrolyzed). Results from ^{1}H-NMR of CPADB in solution at 80 °C revealed traces of decomposition, but no evidence was found of a by-product. Possibly this effect may aggravate during polymerization and be enough to reduce the graft percentage by a small amount. Kinetic or polymerization were not studied in solution since there is already a well-documented procedure of glycoacrylamide RAFT polymerization using CPADB as the CTA [94].

2.8. Improving "grafting from" polymerization onto stöber nanoparticles

With only half percentage of polymer weight per particle, efforts were made to increase the quantities of polymer per particle. In a recent publication, the authors concluded that addition of CTA in solution would improve polymer grafting percentage [95]. The excess CTA chains in solution creates a steadier polymerization by exchanging oligomeric radicals with grafted CTA. This modification led to an almost two-fold in polymer grafted by adding an equivalent of the grafted CTA to solution.

A new experiment was designed based on the free-CTA principle. The idea was to start growing the polymer in solution without the particles. The particles will be added afterwards, while there still is active growing oligomeric radicals in solution, this way, the CTA transference with the CPADB functionalized nanoparticles is favored. Therefore, a hybridization between "grafting to" and "grafting from" methodologies to improve polymer grafting density was obtained.

Polymerization in solution was made under the conditions of experiment 1 described in section 2.5. (Table 2.4). Monomer concentration was also adjusted to reach higher molecular weights (from 10kD_a to 30kD_a) and free CTA initial concentration was two times higher than the CTA-stöber grafted density. Particles were then added after four hours, which by ^{1}H-NMR was equivalent to 70% monomer consumption. The polymerization with particles stayed under 24 hours to maximize the exchange between solution and grafted CTA.

From ^{1}H-NMR analysis, an almost nine-fold was registered for the hybrid polymer graft when compared with the graft from, polymer percentage increased from 0.5 % to 4.3 % polymer weight per particle. This increment in polymer grafted percentage might not only have to do with the change in grafting method but also with the targeted molecular weight.

Till now we could not characterize the polymer grafted to the nanoparticles due to the small amounts obtainable by the particle hydrolysis. Using this method, it was possible to characterize the polymer left in solution and believed that the grafted polymer is somewhat similar.

By SEC (Attachment 6.18 and 6.19), polymer molecular weight was half than expected with a polydispersity of 1.15. Using these conditions polymerization was not being controlled as pretended. Besides, attempts to remove the acetates group from the carbohydrate moiety without

damaging the nanoparticles structure were all unsuccessful. With basic pH, using sodium hydroxide or potassium carbonate, the silica matrix was hydrolyzed (Figure 2.17). Using an acidic medium (e.g. HCl), the carbohydrate ring would open/close obtaining a mixture of chain and both anomeric closed ring compounds.

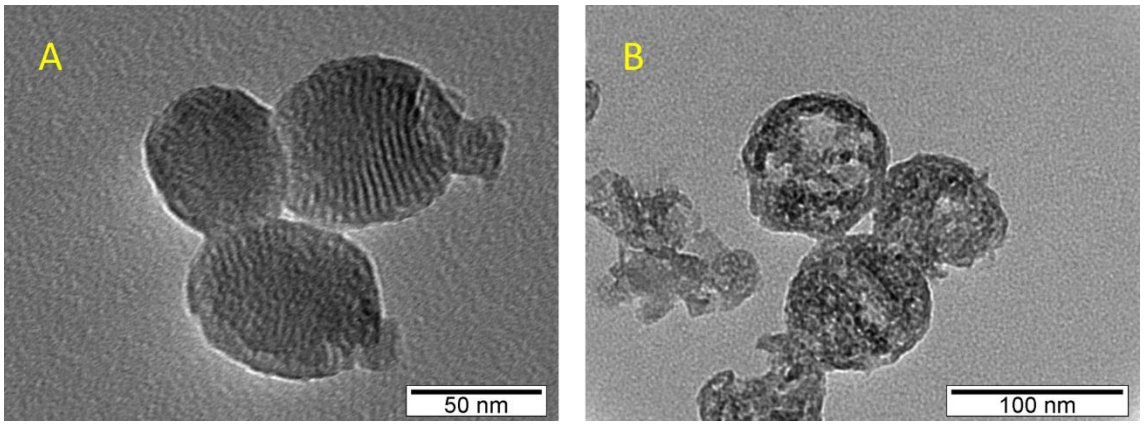

Figure 2.17 – Effect of the basic solution onto the mesoporous silica nanoparticles. TEM image (50 nm scale – left; 100 nm scale – right) of the synthesized mesoporous silica nanoparticles. A) without using the basic solution; B) after removal of the acetate groups using a basic solution.

With the risk of compromising the nanoparticles or carbohydrate moiety the acetates were removed before polymerization using potassium carbonate in methanol (Scheme 2.6). The structure was confirmed by ^{1}H-NMR where there was no signal of the four singlets around 2 ppm corresponding to the CH_3 of the acetate group. A slightly pale-yellow foam was obtained with a yield of 86%, a reasonable yield when compared with the literature [96].

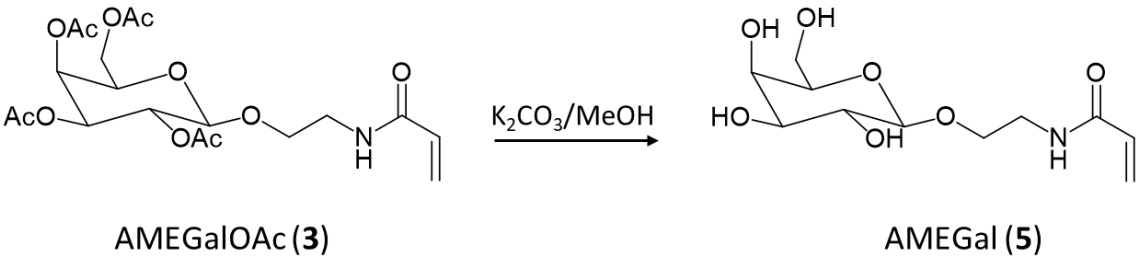

Scheme 2.6 – Deprotection of the galactose-based monomer, 2`-acrylamidoethyl-β-D-Galactose tetraacetate (AMEGalOAc) – compound (**3**) – using potassium carbonate.

Due to changes in solubility of the monomer, polymerization had to be carried in water. Initiator used so far (AIBN) has poor solubility in water, so it was replaced for 4,4'-Azobis (4-cyanopentanoic acid) ACVA. The procedure for the polymerization in solution with the deprotected monomer was carried in the same conditions as described in [94].

After 8 hours, the polymerization was quenched where it was verified a 56% monomer consumption. The resulted polymer was characterized by SEC (Attachment 6.20 and 6.21) and UV-Vis (Table 2.9).

Table 2.9 – Results obtained by SEC-MALS and UV-Vis for the polymerization of the galactose-based deprotected monomer, 2`-acrylamidoethyl-β-D-Galactose (AMEGal) monomer – compound (**5**) – in water.

Polymer	***Targeted M_w (kD_a)***	***M_w (SEC) (kD_a)***	***M_n (SEC) (kD_a)***	***Polydispersity (M_w/M_n)***	***M_w (UV-Vis) (kD_a)***
Galactose monomer (deprotected)	14.0	14.8	14.6	1.01	16.0

Results show that the polymerization was indeed controlled obtaining a very good polydispersity and a molecular weight similar to what was expected.

After the polymerization in solution, the previous hybrid procedure was applied to this monomer. Polymer was grown in solution, following the procedure described in [94]. After four hours, corresponding to 30% monomer conversion, the particles were added. Reaction proceeded for 24 hours and the polymer in solution was characterized by UV-Vis and SEC (Attachment 6.22 and 6.23) to determine the polymer molecular weight and polydispersity (Table 2.10).

Table 2.10 – Results obtained by SEC-MALS and UV-Vis for the polymer obtained in the supernatant of the hybrid RAFT method using the galactose-based deprotected monomer, 2`-acrylamidoethyl-β-D-Galactose (AMEGal) monomer – compound (**5**) – and stöber nanoparticles.

Polymer	***Targeted M_w (kD_a)***	***M_w (SEC) (kD_a)***	***M_n (SEC) (kD_a)***	***Polydispersity (M_w/M_n)***	***M_w (UV-Vis) (kD_a)***
Hybrid - S_5 (62 nm) Galactose-Deprotected	15.0	16.2	15.9	1.02	20.7

Taking into consideration the last hybrid method with galactose-based monomer that was acetylated (PAMEGalOAc) there was an improvement on the polymerization control. Molecular weight was close to what was expected, and polydispersity decreased.

Unfortunately, by the loss of acetate groups the quantification of the polymer graft density around the particle became more difficult. By ^{1}H-NMR (500 MHz) it was possible to verify a small peak referent to the carbohydrate anomeric position at 4.3 ppm. Using this technique, a 1.9% of polymer weight per particle was register but the error may be high due to the signal intensity.

Considering the weight loss by the lack of acetate groups the degree of polymerization seems to be higher. After improving the polymerization conditions, it was time to change from the simpler nanoparticle core (stöber) with glycopolymeric shell to the mesoporous silica nanoparticles with a *co*-polymeric shell.

2.9. Co-polymer synthesis

The designed *co*-polymer with an inner block of pH-responsive polymer (DPAEMA) and galactose-based deprotected monomer (AMEGal) was synthesized in solution. For that, pH-responsive polymer (PDPAEMA) (14.2 kDa) was synthesized in ethanol. From that, the

glycopolymer (targeted M_w of 5 kDa) was grown over the pH-responsive polymer. Only a few protons of both blocks were possible to identify by ^{1}H-NMR (Figure 2.18), partly due to the broadening of the peaks but also by the adopted conformation of the pH-responsive polymer and spatial interaction of the different blocks.

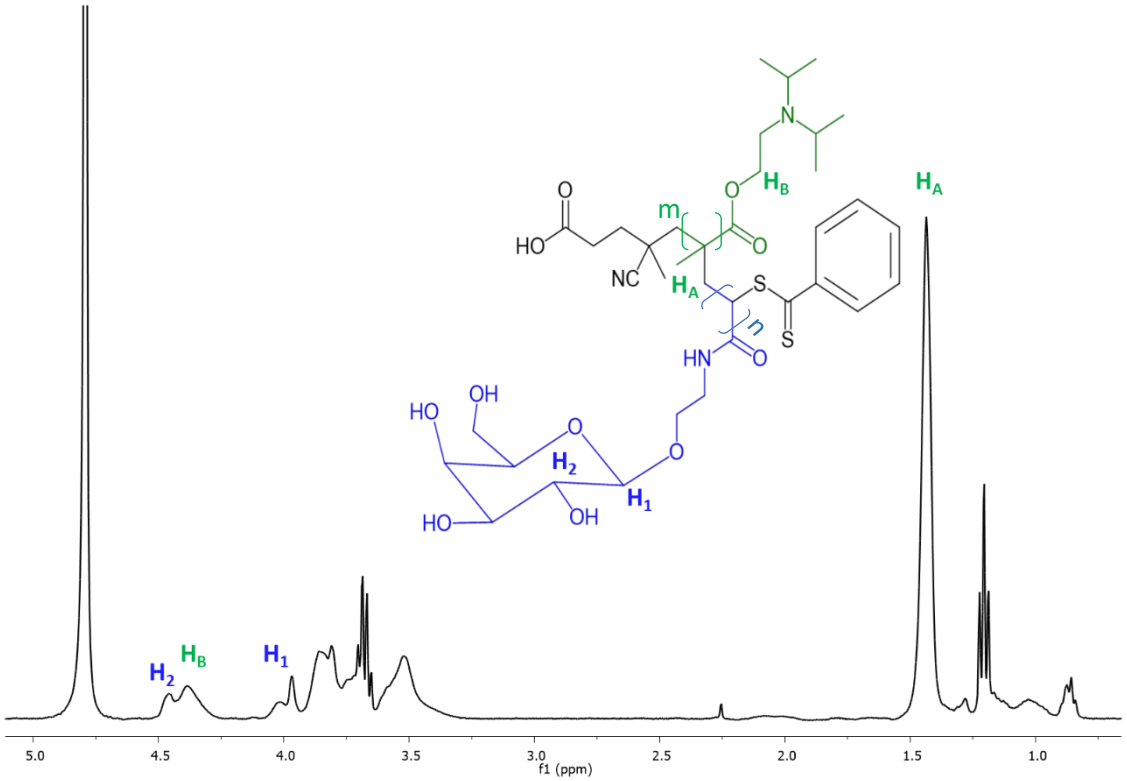

Figure 2.18 – ^{1}H-NMR (400MHz; D_2O) obtained for the *co*-polymer (PDPAEMAM and PAMEGal).

The resulted co-polymer was isolated, the structure was confirmed by ^{1}H-NMR and the polymer weight by UV-Vis and SEC (Attachment 6.26). A molecular weight of 18.4 kDa was obtained for the *co*-polymer, using UV-Vis. From SEC analysis (Figure 2.19) the molecular weight obtained was around 100 kDa but shown a narrow polydispersity of 1.09. This value can be explained by interference between the broad peak of the polymer (2.19-A) and an interference (2.19-B) affecting the analysis of the molecular weight. Considering the UV-Vis results, the polymer weight obtained was fairly similar to what was expected, but by SEC-MALS the results relating to the M_W were inconclusive.

The synthesized *co*-polymer was unviable to the hybrid graft approach due to the monomeric blocks order used (Figure 2.20). A “graft to” reaction was performed using amine functionalized mesoporous silica nanoparticles to couple with the *co*-polymer previously synthesized in solution. The coupling reaction occurred with a low yield, obtaining a total 2% weight of *co*-polymer per particle. From the ^{1}H-NMR (Attachment 6.12), the total grafted polymer

seems to have a 1:2 ratio of grafted pH-responsive to glycopolymer. This result is not concordant with what was expected, the targeted glycopolymer M_w was 5 kDa while for the pH-responsive it was about 10 kDa. Taking into consideration monomers molecular mass and polymer molecular weight it was expected a ratio of 3:1 pH-responsive-glycopolymer. This result indicates that polymerization of the carbohydrate-based monomer give rinse to high molecular weight polymer and that did not happen when the same polymerization was carried without the pH-responsive polymer. No explanation was found for the higher molecular weight of the carbohydrate-based polymer when grown in the presence of the pH-responsive polymer. Regarding the low yield, it was possible, that when the pH-responsive polymer was isolated from a pH below its pK_a, the blocks remained charged and thus, in extended conformation. This chain conformation might block the reactive center, the carbonyl from the acid group in the chain transfer agent, which consequently lowers the amine coupling. Other factor that could contribute to the low yield, is the fact that, to the amine functionalized particles, only 0.1 equivalents (in relation to grafted APTES) of polymer were added. An equimolar of *co*-polymer was not possible to use due to the low amount available.

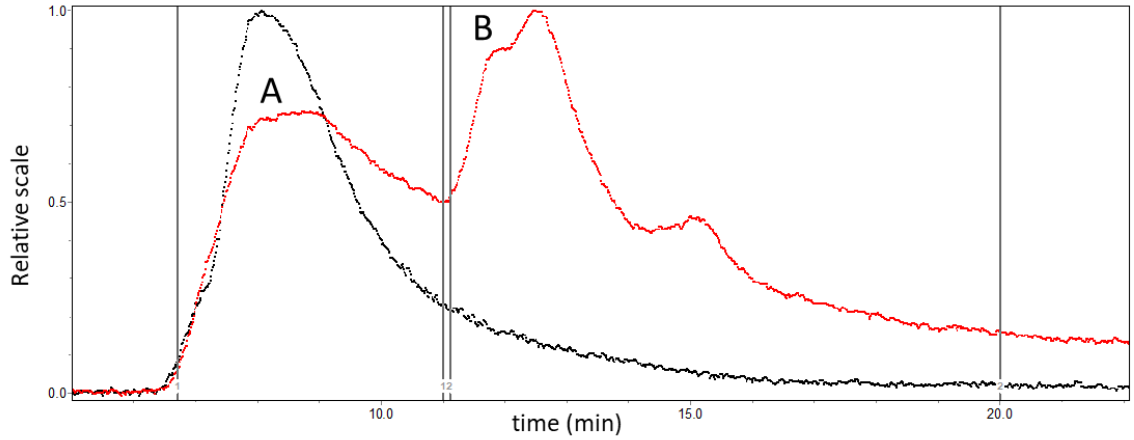

Figure 2.19 – SEC-MALS chromatogram for the co-polymer synthesized in solution. A) co-polymer peak (6.7 min – 11.0 min); B) interference peak (11.1 min - 14.0 min and 14.1 min – 20.0 min). Detectors: ● light scattering; ● raw refractive index.

For the graft of the *co*-polymer into the MSNs by the hybrid method, it was perceived that the monomeric addition had to be inverted (Figure 2.20). The carbohydrate-based polymer (PAMEGal) must be synthesized first and only then the PDPAEMA. As the growing chains are transferred to CTA functionalized particles, the actual growing polymer during the particle addition, must be the pH-responsive. This way the pH-responsive block will be closer to the nanoparticles porous, acting as a gatekeeper, and the carbohydrate moiety will be available on the outer surface of the polymeric shell to further react with the receptor of interest. Inverting the order of the monomers has some implications on the polymerization procedure of the DPAEMA. Because DPAEMA is added during the carbohydrate polymerization, the reaction had to be carried in water. Besides, AIBN as the initiator could no longer be used, due to its insolubility in water.

Considering the order for the *co*-polymerization, DPAEMA polymerization was performed in water and using ACVA as initiator. After 3 hours the polymerization had 89% conversion. The polymer was recovered and analyzed by UV-Vis where a molecular weight of 22.3 kD_a was obtained. This value is two times higher than what expected, and SEC analysis has not yet been done. Thus, the polymerization of DPAEMA must be improved before being possible to graft the polymer, using the hybrid method, into the mesoporous silica nanoparticles.

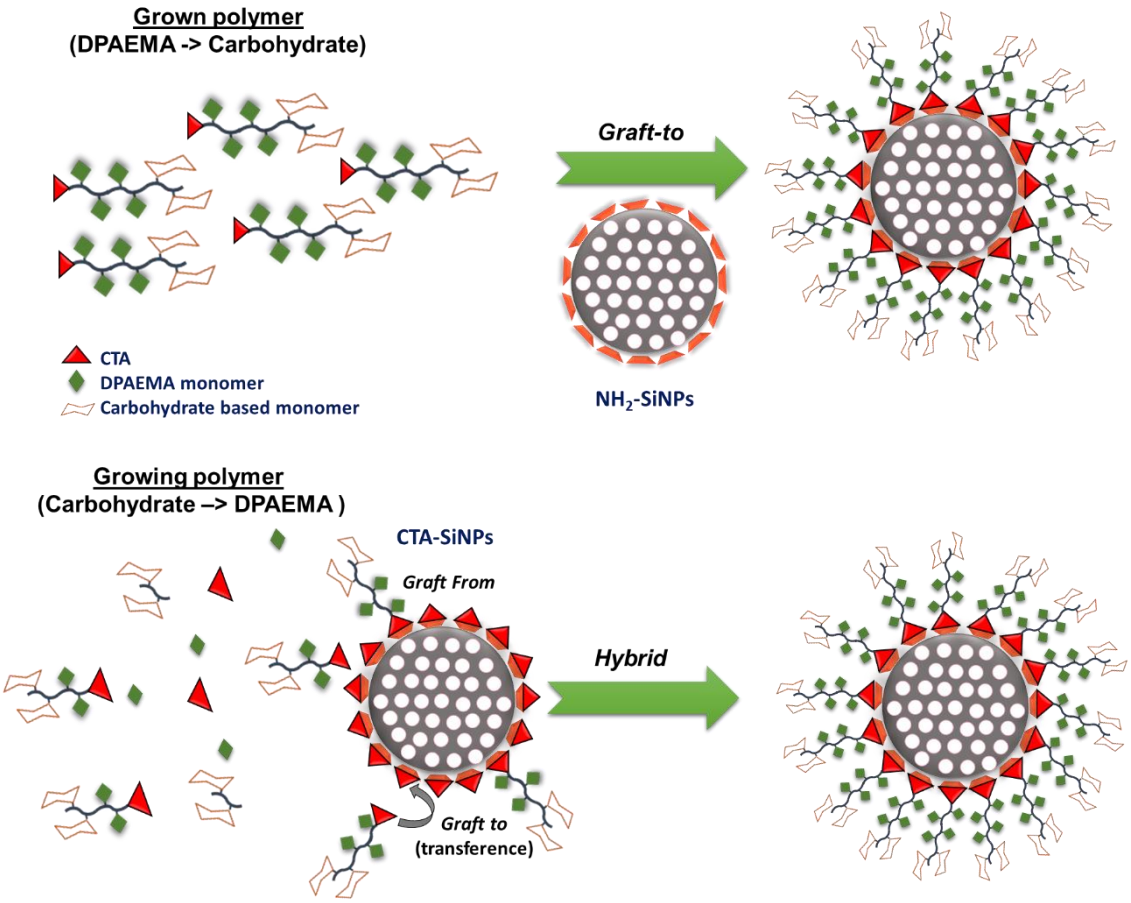

Figure 2.20 – Representative illustration for the hybrid polymerization mechanisms and comparation with the graft-to method.

3. Conclusions and future work

Theranostic nanoplatforms with silica nanoparticles are part of a major group of tools in therapy and diagnosis, especially in the field of cancer theranostic. In recent decades, efforts have been made to design and develop platforms capable of reducing drug side effect and improve their efficacy. In this work, steps towards the synthesis of a new smart and site-specific drug delivery system for theranostics, based on MSNs, were performed.

Fluorescent NPs external surface was modified with amine functional groups by a condensation reaction between bare nanoparticles and APTES molecules. This modification allows the attachment of chain transfer agents (CTA) through the carboxylic acid group of BSPA and CPADB to form an amide, by EDC coupling chemistry. CTA immobilization allow the growth of a carbohydrate-based monomer by a controlled RAFT polymerization from the particle surface.

Fluorescent silica compacted nanoparticles and mesoporous silica nanoparticles were synthesized, with sizes between 30 nm and 65 nm, by controlling pH and temperature. NPs characterization was performed by TEM, and the diameters presented a low size dispersity and well-defined morphology. Amine coverage was quantified by ^{1}H-NMR through the particle hydrolysis in a basic medium, where concentrations between 0.2 and 1.1 mmol of APTES per gram of nanoparticle were achieved. CTA immobilization was assessed using UV-Vis obtaining concentrations between 0.01 and 0.08 mmol per gram of nanoparticle. For lower CTA concentrations a higher degree of polymerization was obtained. Modifications were also followed by ζ-potential, with large variations between bare, amine and CTA functionalized.

A site-specific monomer of galactose ethoxy acrylamide was synthesized to diagnose for a carbohydrate recognition towards cancer cells. For the therapy function, a pH-responsive diisopropylamino ethyl methacrylate monomer (DPAEMA) was synthesized to allow a controlled release mediated by pH. The trithiocarbonate chain transfer agent was also synthesized and as the monomer, characterized by ^{1}H-NMR. Monomers synthesis yield were 21% for the acrylamide monomer, 46% for the methacrylate, and 33% yield for the trithiocarbonate chain transfer agent. Different degrees of monomer conversion were obtained for the polymerization in solution. Relating to the acetylated acrylamide monomer, an 85% conversion was obtained in 1,4-dioxane with BSPA as chain transfer agent. For the deacetylated monomer the polymerization was only performed in water with CPADB as CTA with 56% monomer conversion. Regarding the methacrylate monomer, the best result was obtained in water with CPADB as CTA obtaining 89% conversion. Characterization by UV-Vis and size exclusion chromatography, shown that most of the polymers had a narrow polydispersity and were fairly close to the expected molecular weight, an indication of the good control of the RAFT polymerization.

Glyconanoparticles, based on the stöber nanoparticles, were synthesized using a “grafting from” and “transfer to” methodologies. Polymer grafted density was quantified by ^{1}H-NMR, obtaining 0.5 to 1.8% weight percentage of polymer. Lower grafted CTA densities have shown a higher degree of polymerization. Also, for smaller particles, a larger polymer weight percentage

per particles was achieved. Besides, a hybrid method developed between polymerization in solution and “grafting from”, allowed an improvement in the grafted polymer density by almost a nine-fold.

Co-polymer synthesis was performed in solution, using CPADB as CTA agent. The co-polymer was synthesized by growing the galactose-based monomer (AMEGal) over the DPAEMA polymer. UV-Vis and SEC analysis shown a narrow dispersity, but the SEC led us to believe that the co-polymer has a higher carbohydrate content than expected. The co-polymer was attached into the mesoporous silica nanoparticles by a “graft to” approach yielding a 2% polymer weight. Before proceeding with the co-polymerization at the particle surface, by the optimized hybrid method, a reversed order *co*-polymer - inner block of AMEGal and outter block of DPAEMA - must be synthesized by controlled RAFT polymerization.

Through the progress of this work, several milestones were achieved. To begin with, the carbohydrate monomer and homo polymer were synthesized in solution with a narrow polydispersity, the same can be said for the pH-responsive block. Then, stöber nanoparticles and MSN were synthesized and functionalized with different CTA densities, which allowed to understand their influence onto the polymerization. After that, glyconanoparticles were synthesized and used as a simpler model to improve the amount of polymer grafted onto the nanoparticles and a hybrid method of polymerization was developed. Although the *co*-polymeric MSNs were not achieved by the improved hybrid method here reported, it has shown to be more efficient than the “transfer to” and “graft from” methodologies. Finally, the *co*-polymer was synthesized in solution and attached onto the mesoporous silica nanoparticles by a coupling reaction (graft to) and is expected to fulfil the function of therapy and diagnosis. To sum up, the goal of this work was fulfilled since it was possible to synthesize smart hybrid glyconanoparticles.

As futures perspectives, it would be interesting to test the glyconanoparticles in *in vitro* studies using cancer hepatic cells. For that, galactose-nanoparticles synthesized, would be used to target lectins at Hep G2 cell line (human hepatocyte carcinoma), and glucose-nanoparticles, that could be synthesized using the same procedure, as the negative control. This way, specificity of the carbohydrate block and biodistribution of the glyconanoparticles would be evaluated. It should also be of a great interest, to optimize the *co*-polymerization, to apply it in on the RAFT hybrid method here described. Additionally, another attempt onto the “graft to” methodology of the co-polymer to the MSNs should be performed, by controlling the pH and consequently conformation of the pH-responsive polymer to study its influence onto the grafting. Furthermore, after the smart hybrid MSNs synthesis, *in vitro* studies of the release mechanism and uptake of the nanoparticles should be tested. This way, when compared with the conventional therapies and diagnose methodologies for cancer, an assess of the advantages for this novel theranostics nanocarrier could be made.

4. Experimental section

4.1. Reagents and solvents

N-cetyltrimethylammonium bromide BioXtra 99% (CTAB), tetraethylorthosilicate 98% (TEOS), (3-aminopropyl) triethoxysilane 98% (APTES), 1-ethyl-3-(3-dimethylaminopropyl)-carbodiimide hydrochloride (EDC.HCl), 4-(Dimethylamino) pyridine 99% (DMAP), 4-Cyano-4-(phenylcarbonothioylthio)pentanoic acid 97% (CPADB), azobisisobutyronitrile 99% (AIBN), hydroquinone 99%, 4,4′-Azobis(4-cyanopentanoic acid) 98% (ACVA), methacryloyl chloride 97%, 2–(diisopropylamino) ethanol 98%, and D-(+)-Galactose, N-hydroxyethyl acrylamide 97% (HEAA), boron trifluoride diethyl etherate, were purchased from Sigma-Aldrich. 1,3,5-trioxane was purchased from Fluka.

Absolute ethanol (EtOH) was purchased from Fisher Chemical. Toluene, 1,4-dioxane, tetrahydrofuran, dichloromethane, aqueous ammonium hydroxide (25 wt %; NH_4OH) and concentrated hydrochloric acid (HCl, 37%) were purchased from Sigma Aldrich. Sodium hydroxide (NaOH) was purchased from EKA Pellets. Absolute ethanol 99.5% (EtOH) was purchased from Fisher Chemical. Spectroscopy 1,4-dioxane 99%+ was purchased from Acros organics. Chloroform-D ($CDCl_3$, 99.8%) and deuterium oxide (D_2O, 99.9%) was purchased from Cambridge Isotope Laboratories. Trifluoroacetic acid 99% (TFA) was purchased from Merck. Toluene, dichloromethane and triethylamine were refluxed over calcium hydride for 24 hours and then distilled prior to use. Tetrahydrofuran was refluxed over sodium benzophenone ketyl for 24 hours and then distilled prior to use. AIBN was recrystallized in methanol and ACVA in dichloromethane. The PDI derivative was synthesized according to the literature [97]. Deionized water purified using a Millipore Milli-Q system to a resistivity of 18.2 MΩ was used throughout the experiments unless otherwise stated. Argon (Ar) gas (Alphagaz 1, 99,999%) was purchased from Air Liquid. Unless otherwise specified, all chemicals were used as received without further purification. Column chromatography was performed with the designated solvents using E. Merck silica gel 60 (particle size 0.035–0.070 mm).

4.2. Equipment

4.2.1. Centrifuge

Avanti J – 30I Centrifuge (Beckman Coulter, California, USA), rotor JA – 30.50 Ti, was used for washing bare stöber and MSNs. For the centrifugations, 50 mL centrifuge tubes from the same manufacturer were used. Centrifugal Refrigerator (3-16K) (Sigma Zentrifugen, Osterode am Harz Germany), rotor 12141, was used for washing modified silica nanoparticles. Disposable 10 mL polypropylene tubes were used for the centrifugations.

4.2.2. Transmission Electronic Microscopy (TEM)

TEM images were obtained on a Hitachi transmission electron microscope (Hitachi High – technologies, Tokyo, Japan), model H-8100, with a LaB6 filament (Hitachi) complemented with an accelerator voltage of 200 kV and a current of 20μA. A camera KeenView (Soft Imaging

System, Münster, Germany) is incorporated in this equipment, which through iTEM software, allows acquiring TEM images. A drop of the ethanolic nanoparticle suspension was deposited onto Formvar carbon coated copper grid 200 mesh (Ted Pella, Redding, CA) and excess solution was tapped with filter papers. Then, the thin-film solution was dried under ambient conditions. The size/dimension, polydispersity, and morphology of the particles were estimated by evaluating 100 nanoparticles by ImageJ software.

4.2.3. Nuclear magnetic resonance (NMR)

Solution proton NMR data were collected on a Bruker Avance III 400 spectrometer (Bruker BioSpin GmbH, Rheinstetten, Germany) operating at 400 MHz. Quantification of particle surface coverage using ^{1}H-NMR was performed according to the literature [83].

4.2.4. UV-Vis spectroscopy

UV-660 UV-VIS Spectrophotometer (JASCO International, Tokyo, Japan), supplied with a double monochromator and a photomultiplier detector for higher resolution, was employed for UV-Vis spectroscopy assays, using a 1 cm path length quartz cuvette. The absorption spectrum was measured from 750 nm to 250 nm at a scan rate of 400 nm/min and a step size of 1 nm against an air/air background sample.

4.2.5. ζ-Potential

Zeta potential was measured on a Zetasizer (Malvern Instruments) with a 50 mW laser source operating at 532 nm, after appropriate dilution with Milli-Q water (1 mg/mL). For each sample, the measurement was performer three times at room temperature in Milli-Q water, and the values reported as the average ± standard error.

4.2.6. Size Exclusion Chromatography (SEC)

Polymer molecular weight and their size dispersity were determined by size exclusion chromatography with multi-angle static light-scattering (SEC-MALS). Three detectors in series were used: a Shimadzu Prominence RF-20A fluorimetric detector (λ_{exc} = 280 nm), a multi-angle static light-scattering Wyatt MiniDawn Treos detector, and a Shimadzu RID-10A Refractive Index detector (internal temperature 40.0 ºC). Two chromatography Phenolgel analytical columns (30 cm × 7.8 mm, pore sizes of 10^2 and 10^3 Å) and a Phenolgel linear precolumn from Phenomenex were used, with water or dry tetrahydrofuran as mobile phase at a flow rate of 0.8 mL/min. Columns were thermostatically at 23 °C in a Shimadzu CTO-20AC columns oven.

4.3. Experimental procedure

4.3.1. Synthesis of fluorescent stöber silica nanoparticles

Stöber nanoparticles were synthesized by the stöber method [25]. 6-8 mg of PDI derivative was add to 4 mL of absolute ethanol and sonicated for 30 minutes. Result was filtrated into 0.4 micron cellulose filter, solution concentration was measured by absorbance (Ɛ(522nm) = 41053 $M^{-1}cm^{-1}$) . Onto a 250 mL polypropylene flask, absolute ethanol (104.5 mL), distillated water (9.2 mL) and ammonia solution (1.5 mL, 25-28% v/v) were added, the mixture was stirred at 30°C.

PDI solution and TEOS (4.5 mL) were mixed and added drop wise to the flask while the solution was stirred at precise and constant velocity. Stöber nanoparticles were recovered by centrifugation and washed three times with ethanol at 19,000 rpm for 20 min at room temperature. Particle precipitate was dried at 50 °C overnight and afterwards vacuum dried to obtain a slightly pale orange powder.

4.3.2. Synthesis of fluorescent mesoporous silica nanoparticles

MSN synthesis was performed by a modified sol-gel procedure. In a 15 mL polypropylene flask PDI (6 mg) and CTAB (500 mg) were dissolved in tetrahydrofuran (6 mL). The solution was stirred at 40 °C for 24h, to obtain a powder mixture of CTAB and PDI adsorbed. In a 500 mL polypropylene flask, Milli Q water (240 mL) and 1.7 M NaOH solution (1.75 mL) were added. The solution was stirred at 30 °C, until the temperature inside was stable. The mixture of CTAB and PDI, were added followed by TEOS (2.5 mL) was added drop wise. After 4 minutes the solution becomes clouded, with formation of a precipitate after 12 mins, the reaction was left stirring for 2h. After two hours, the particles were recovered by centrifugation, and washed three times with ethanol at 20,000 rpm for 20 min at room temperature. Particle precipitate was dried at 50 °C overnight and afterwards vacuum dried to obtain a slightly pink powder.

4.3.3. Modification of silica nanoparticles surface

To functionalize the particle outer surface with amines, particles were dispersed in dry toluene (4.5 mL per 0.1 g of particles) and sonicated for 30 mins. To the particle suspension, APTES (MSN: 30 µL; stöber: 5 µL; per 0.1 g of particle) was added drop wise and refluxed for 24h under argon atmosphere. APTES volumes were calculated based on a target surface coverage of 2 reagent molecules/nm^2 and on particles density (MSN: 0.34 g/cm^3; Stöber: 1.6 g/cm^3), further information in attachment 6.13. Particles were recovered by centrifugation and washed three times with ethanol at 15,000 rpm for 10 min at room temperature. Particle precipitate was dried at 50°C overnight and afterwards vacuum dried to obtain a slightly pink powder. Quantification was performed by ^{1}H-NMR in D_2O (pH=13) using an internal standard, as the described procedure at [83].

^{1}H-NMR (400MHz, D_2O) **(NH_2-SiNP)** δ(ppm): *J*(Hz): 2.6 (t, 2H, *J*= 7.0, C**H_2**-NH_2); 1.5 (m, 2H, CH_2-C**H_2**-CH_2); 0.5 (t, 2H, *J*=8.4, Si-C**H_2**). ^{1}H-NMR spectra in figure 2.4.

For MSN, surfactant was removed from NH_2-MSN porous using a 0.5 M HCl ethanolic solution (5 mL per 0.1 g of particle). The solution was left stirred at 50 °C for 24h. Particles were recovered by centrifugation, washed twice with an ammonia solution (7% v/v) and three times with ethanol at 15,000 rpm for 10 min at room temperature. Particle precipitate was dried at 50°C overnight and afterwards vacuum dried to obtain a slightly pink powder.

To anchor CTA molecules to the nanoparticle surface, NH_2-SiNPs were suspended in dry dichloromethane (6 mL per 0.1 g of nanoparticles) and sonicated for 30 mins. Reaction was cooled down with ice and 3-(benzylsulfanylthiocarbonylsulfanyl) propionic acid (BSPA) or 4-Cyano-4-(phenylcarbonothioylthio) pentanoic acid (CPADB) was added in equimolar of grafted

APTES quantities. At the same time, EDC.HCl (1.2 eq), and in some cases DMAP (1.2 eq) were also added. After 30 minutes the ice was removed, and the reaction proceeded for 24h at room temperature. Particles were recovered by centrifugation and washed three times with ethanol at 15,000 rpm for 10 min at room temperature. Particle precipitate was dried at 50°C overnight and afterwards vacuum dried to obtain a pink powder (for CPADB) and a yellow powder (for BSPA). CTA grafted concentration was measured by UV-Vis (BSPA: (Ɛ(310nm) = 13976 $M^{-1}cm^{-1}$); CPADB: (Ɛ(303nm) = 10480 $M^{-1}cm^{-1}$)).

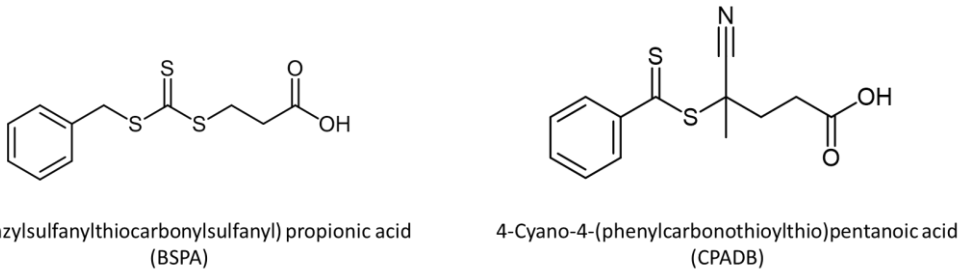

3-(benzylsulfanylthiocarbonylsulfanyl) propionic acid (BSPA)

4-Cyano-4-(phenylcarbonothioylthio)pentanoic acid (CPADB)

Figure 4.1 – Both CTAs chemical structure used to anchor at the particle surface: 3-(benzylsulfanylthiocarbonylsulfanyl) propionic acid (BSPA) and 4-Cyano-4-(phenylcarbonothioylthio) pentanoic acid (CPADB)

4.3.4. Synthesis of 3-(benzylsulfanylthiocarbonylsulfanyl) propionic acid (BSPA)

3-Mercaptopropionic acid (4 mL, 50 mmol) was added drop wise to a stirring solution of potassium hydroxide (5.1 g, 10 mmol) in water (50 mL). Then, carbon disulfide (30 mL, 500 mmol) was added drop wise for 45 minutes and the reaction was left stirring during 5h. Subsequently, benzyl bromide (6 mL, 50 mmol) was added to the reaction and left overnight at room temperature, the reaction had changed from an orange solution to a yellow foam after one hour. After cooling, dichloromethane (200 mL) was added to the reaction followed by acidification with HCl (37%) until the organic phase became yellow. Then, the mixture was extracted with dichloromethane and washed with a brine solution and water. The organic layers were then dried with sodium sulfate, filtrated and concentrated. The product was recrystallized in dichloromethane, obtaining a yellow powder (4.3 g, 17 mmol) with a 33% yield.

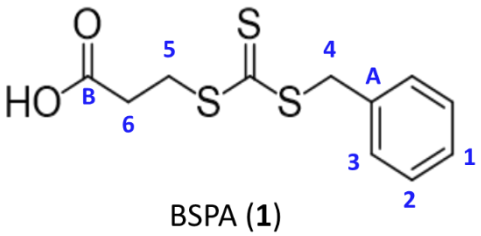

BSPA (**1**)

^{1}H-NMR (400MHz; $CDCl_3$) **(3-(benzylsulfanylthiocarbonylsulfanyl) propionic acid) (1)** δ(ppm): J(Hz): 7.3-7.2 (m, 5H, H-1, H-2, H-3); 4.6 (s, 2H, H-4); 3.6 (s, 2H, H-5); 2.8 (s, 2H, H-6). ^{1}H-NMR spectra in figure 2.6.

^{13}C-NMR (400MHz; $(CD_3)_2SO$) **(3-(benzylsulfanylthiocarbonylsulfanyl) propionic acid (1)** δ(ppm): 172.8 (C-B); 135.6 (C-A); 129.6, 129.1, 128.2 (C-1, C-2, C-3); 40.8 (C-4); 32.9 (C-5); 31.9 (C-6). ^{13}C-NMR spectra in attachment 6.1.

4.3.5. Carbohydrate-based ethoxy acrylamide monomer

4.3.5.1. Synthesis of β-D-Galactose pentaacetate (GalOAc)

Potassium acetate (2.95 g, 30 mmol) was added in acetic anhydride (50 mL), the solution was stirred and heated to 120 °C for 30 min, then β-D-Galactose (5 g, 28 mmol) was added. After two hours, the mixture was poured into ice and washed with a saturated sodium bicarbonate saturated solution, to neutral pH. A white precipitated was obtained and separated from the mixture. The mixture was extracted with dichloromethane, and the organic phases were washed with brine solution and water. Then, the organic layer was dried using sodium sulfate, filtrated and concentrated. A while solid was obtained and recrystallized in ethanol to obtain β-D-Galactose pentaacetate (4.6 g, 12 mmol) with a 43% yield.

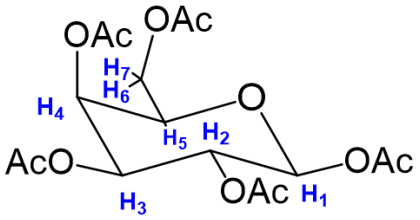

β-D-GalOAc (**2**)

^{1}H-NMR (400 MHz, $(CD_3)_2SO$) (**β-D-Galactose pentaacetate**) **(2)** δ(ppm): J(Hz): 5.90 (d, 1H, *J*= 8.4, H-1); 5.37-5.30 (m, 1H, H-4); 5.09 (t, 1H, *J*= 10.7, H-2); 5.02 (d, 1H, *J*= 4.6, H-3); 4.42 (t, 1H, J= 4.3; H-5) ; 2.13, 2.06, 2.02, 1.99, 1.92 (s, 15H, OAc). ^{1}H-NMR spectra as attachment 6.2.

^{13}C-NMR (400 MHz; $(CD_3)_2SO$) **(β-D-Galactose pentaacetate) (2)** δ(ppm): 170.5, 170.2, 170.1, 169.7, 169.5 (**C**OO-CH3) 91.8 (C-1); 82.8 (C-5), 80.0 (C-2), 76.6 (C-3), 69.5 (C-4), 62.4 (C-6), 20.9 (**C**H_3-COO-). ^{13}C-NMR spectra as attachment 6.3.

4.3.5.2. Synthesis of 2`-acrylamidoethyl-β-D-Galactose tetraacetate (AMEGalOAc)

β-D-Galactose pentaacetate (2.0 g, 5.1 mmol) and 2-hydroxyethyl acrylamide (0.6 g, 4.6 mmol) were added in dry dichloromethane (10 mL) and stirred for 10 mins under argon atmosphere. Then, $BF_3.Et_2O$ (1.9 mL, 15.4 mmol) was added and the reaction proceeded for 1h under sonication. The mixture was diluted with dichloromethane (20 mL) and washed with a brine solution and water. The organic layers were then dried with sodium sulfate and concentrated. The compound was adsorbed to silica flash by solvent evaporation and followed by silica gel filtration. A mixture of hexane-ethyl acetate 3:2 was used to remove impurities while ethyl acetate was used to extract the compound (Rf = 0.2; diethyl eter-ethyl acetate (3:1)). 2`-acrylamido ethyl-β-D-Galactose tetra acetate was obtained as white foam (1.2 g, 2.2 mmol) with a 48% yield.

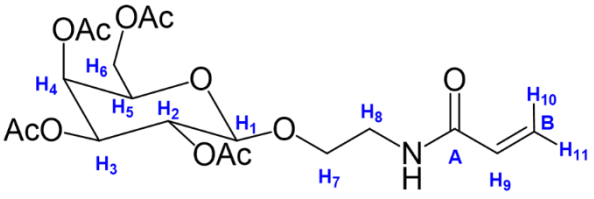

AMEGalOAc (**3**)

^{1}H-NMR (400MHz; $(CD_3)_2SO$) **(2`-acrylamidoethyl-β-D-Galactose tetraacetate) (3)** δ(ppm): J(Hz): 6.26-6.20 (m, 1H, H-9); 6.07 (d, 1H, *J*= 17.4, H-10); 5.58 (d, 1H, *J*= 9.9, H-11); 5.26 (s, 1H, H-4); 5.16 (d, 1H, *J*= 12.1, H-3); 4.94 (t, 1H, *J*= 9.4, H-2); 4.73 (d, 1H, *J*= 7.9, H-1); 4.20 (t, 1H, *J*=6.6, H-5); 4.05 (d, 2H, *J*=6.0, H-6); 3.78-3.71 (m, 1H, H-7) 3.62-3.57 (m, 1H, H-7); 3.29 (d, 2H, *J*= 5.5, H-8); 2.12, 2.01, 2.00, 1.92 (s, 12H). ^{1}H-NMR spectra in figure 2.9.

^{13}C-NMR (400MHz; $(CD_3)_2SO$) **(2`-acrylamidoethyl-β-D-Galactose tetraacetate) (3)** δ(ppm): 170.4, 170.3, 169.9, 169.6 (**C**OO-CH_3); 165.2 (C-A); 132.0 (C-9); 125.6 (C-B); 100.5 (C-1); 70.8 (C-3); 70.4 (C-5); 69.0 (C-2); 68.1 (C-7); 67.8 (C-4); 61.8 (C-6); 39.2 (C-8); 21.2, 20.9, 20.8, 20,7 (**C**H_3-COO). ^{13}C-NMR spectra in attachment 6.6.

4.3.6. Synthesis of 2-(diisopropylamino) ethyl methacrylate (DPAEMA)

Hydroquinone (40 mg, 0.4 mmol) and 2-(diisopropylamino) ethanol (4.8 mL, 28 mmol) were added into dry tetrahydrofuran (40 mL) under argon atmosphere. Subsequently, the reaction was cooled down and dry triethylamine (4 mL, 28 mmol) was added. Then, methacryloyl chloride (2.8 mL, 28 mmol) were added drop wise and refluxed for 2 hours. The reaction was filtered and concentrated, to obtain a yellow oil. The product was distillated under reduced pressure at 130°C, obtaining a translucid oil (2.6 g, 12.9 mmol) with a 46% yield. ^{1}H-NMR spectra in figure 2.11.

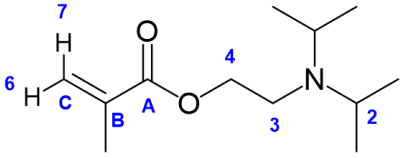

DPAEMA **(4)**

^{1}H-NMR (400MHz; $(CD_3)_2SO$) **(2-(diisopropylamino) ethyl methacrylate) (4)** δ(ppm): J(Hz): 6.2 (s, 1H, H-7); 5.7 (s, 1H, H-6); 4.0 (t, 2H, *J*= 6.6, H-4); 3.0-2.9 (m, 1H, H-2); 2.64 (t, 2H, *J*= 6.7, H-3); 1.9 (s, 3H, H-5); 0.9 (d, 12H, H-1). ^{1}H-NMR spectra in figure 2.11.

^{13}C-NMR (400MHz; $(CD_3)_2SO$) **(2-(diisopropylamino) ethyl methacrylate) (4)** δ(ppm): 166.8 (C-A); 136.4 (C-B); 125.9 (C-C); 65.3 (C-4); 48.8 (C-2); 43.2 (C-3); 20.9 (C-5) 18.3 (C-1). ^{13}C-NMR spectra in attachment 6.9.

4.3.7. Deprotection of 2`-acrylamidoethyl-β-D-Galactose tetraacetate

2`-acrylamidoethyl-β-D-Galactose tetraacetate (1.0 g, 2.6 mmol) and potassium bicarbonate (0.3 g, 2.1 mmol) was dissolved in methanol (10 mL). The reaction was stirred at room temperature for 15 mins and then filtrated. To the mixture, an ion-exchange resin, pre-washed in methanol, was added and left stirred for 15 mins. Subsequently, the resin was filtrated, and the mixture was concentrated. 2S-acrylamide-ethoxy-β-D-Galactose was obtained as a pale-yellow foam (0.54 g, 2.2 mmol) with 86% yield.

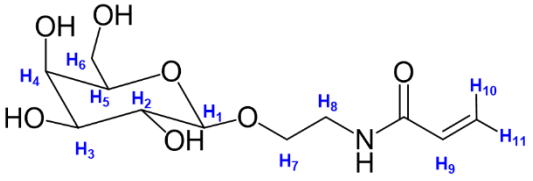

AMEGal (**5**)

^{1}H-NMR (400MHz; (D_2O) **(2`-acrylamidoethyl-β-D-Galactose) (5)** δ(ppm): J(Hz): 6.28-6.21 (m, 1H, H-9); 6.11-6.04 (m, 1H, H-10); 5.61-5.55 (m, 1H, H-11); 4.90-4.65 (m, 2H, H-4;H-3); 4.39 (s, 1H, H-2); 4.09 (d, 1H, *J*= 8.3, H-1); 3.78-3.72 (m, 1H, H-5); 3.62 (s, 1H, H-6); 3.36-3.26 (m, 4H, H-7;H-8). ^{1}H-NMR spectra as attachment 6.10.

4.3.8. RAFT polymerization in solution

4.3.8.1. 2`-acrylamidoethyl-β-D-Galactose tetraacetate polymerization in 1,4-dioxane

A mixture of BSPA (8.7 mg, 0.032 mmol), 2`-acrylamidoethyl-β-D-Galactose tetraacetate (300 mg, 0.67 mmol), 1,3,5-trioxane (20 mg) in 1,4-dioxane (2.9 mL) was added in a schlenk tube.

At the same time, AIBN solution ([AIBN] = 10 mg/mL) in 1,4-dioxane was added (0.1 mL, 0.006 mmol). Then, the schlenk was sealed with a rubber septum and purged with argon for one hour. Subsequently, the Schlenk tube was immersed in bath at 80°C. After 4.5 hours, the reaction was quenched in cold water and exposed to air. The polymer was isolated by drop wise addition of the reaction mixture to n-hexane. The polymer was then dissolved in dichloromethane, concentrated and dried under vacuum. A yellow foam was obtained. Besides this procedure, a different CTA/AIBN ratio was tested, instead of 1:5 [AIBN]/[CTA], a 1:10 [AIBN]/[CTA] (0.0032 mmol of AIBN) was used. After 4.5 hours, 85% monomer consumption was registered using the 1:5 [AIBN]/[CTA] procedure and 56% to the 1:10 [AIBN]/[CTA]. Polymer purity was confirmed by ^{1}H-NMR, while polydispersity and molecular weight were assessed using SEC-MALS (Attachment 6.14 to 6.17) and UV-Vis.

For kinetics, samples of 80µL were taken every 15 mins during the first hour and every 30 mins after the first hour, during 4 hours, the samples were stored at low temperatures and then analyzed by ^{1}H-NMR. Monomer consumption over time (Figure 2.12) was followed using an internal standard (1,3,5-trioxane) as a reference.

4.3.8.2. 2`-acrylamidoethyl-β-D-galactose polymerization in water

The RAFT polymerization of the carbohydrate-based monomer was proceeded in water using a similar procedure as described above (4.3.8.1). The reaction was carried out by adding to the schlenk tube, 2`-acrylamidoethyl-β-D-galactose (302.0 mg, 1.0 mmol), CPDB (6.1 mg, 0.022 mmol), ACVA (1.2mg, 0.0044 mmol), 1,3,5-trioxane (20 mg) and Milli-Q water (1 mL). The reaction was degassed with five freeze-pump thaw cycles, followed by immersion in an 80 °C bath under stirring. The reaction was stopped after 8h with an equivalent monomer consumption of 56%. Polymer was isolated by a drop wise addition of the mixture to acetone. Polymer purity was confirmed by ^{1}H-NMR, while polydispersity and molecular weight were assessed using SEC-MALS (Attachment 6.20 and 6.21) and UV-Vis.

4.3.8.3. DPAEMA polymerization in ethanol

Polymerizations were conducted using CPADB or BSPA (0.05 mmol), AIBN (1.7 mg, 0.01 mmol), DPAEMA (515.4 mg, 2.42 mmol), 1,3,5-trioxane (20 mg) in a previously acidified absolute ethanol (3 mL) with one equivalent of TFA. The reaction was degassed with five freeze-pump thaw cycles, followed by immersion in an 85°C bath under stirring. After 5h, the reaction was quenched and a monomer consumption of 50% was registered. Polymer was isolated by a drop wise addition of the mixture to diethyl ether. Polymer purity was confirmed by ^{1}H-NMR, while polydispersity and molecular weight were assessed using SEC-MALS (Attachment 6.24 and 6.25) and UV-Vis.

4.3.8.4. DPAEMA polymerization in water

The RAFT polymerization of DPAEMA in water was proceeded as follows: DPAEMA (280 mg, 1.3 mmol) was stirred in ketone (2 mL) with TFA (0.1 mL, 1.3 mmol) for 30 mins. Then, ketone was removed by evaporation. The mixture was transferred to a schlenk tube, using Milli-Q water

(2x5mL), followed by the addition of CPADB (7.8 mg, 0.028 mmol) and ACVA (1.9 mg, 0.007 mmol). Then, the reaction was degassed with five freeze-pump thaw cycles and immersed in an 85°C bath under stirring. After 3 hours the reaction was quenched with a monomer conversion of 90%. Polymer was isolated by a drop wise addition of the mixture to diethyl ether. Polymer purity was confirmed by ^{1}H-NMR, while molecular weight was assessed using UV-Vis. The polymer was not yet analyzed by SEC-MALS,

4.3.8.5. Co-polymerization in solution

To the schlenk tube, poly-DPAEMA (100 mg, 10.7 mmol) - synthesized using the procedures described in 4.3.8.3 -, ACPA (0.6 mg, 0.002 mmol), 2`-acrylamidoethyl-β-D-galactose (69.9 mg, 0.25 mmol) and 1,3,5-trioxane (20 mg) were added in Milli-Q water (1 mL). The reaction was degassed with five freeze-pump thaw cycles, followed by immersion in an 80°C bath under stirring. The reaction was quenched after 16h with a monomer consumption of 88%. Polymer was diluted in ethanol (10 mL) and diethyl ether (20 mL) and centrifuged. Polymer purity was confirmed by ^{1}H-NMR, while polydispersity and molecular weight were assessed using SEC-MALS (Attachment 6.26 and Figure 2.19) and UV-Vis.

4.3.9. Polymeric grafting at SiNPs surface

4.3.9.1. "Graft from" and "transfer to" polymerization method

To a schlenk tube, AIBN (one fifth of particle CTA grafted concentration) were added, followed by 2`-acrylamidoethyl-β-D-galactose (160 mg, 0.36 mmol), 1,3,5-trioxane (20 mg) and 1,4-dioxane (7 mL). The schlenk was sealed with a rubber septum and degassed using five freeze-pump thaw cycles. The mixture was then transferred to a different schlenk tube containing CTA-SiNPs (0.1 g), followed by immersion in an 80 °C bath under stirring. Reaction was quenched after 24h and an aliquot of the mixture was stored to obtain the monomer conversion by ^{1}H-NMR. Particles were recovered by centrifugation and washed three times with ethanol at 10,000 rpm for 10 min at room temperature. Particle precipitate was dried at 50°C overnight and afterwards vacuum dried. Polymer weight percentage was quantified by ^{1}H-NMR in D_2O (pH=13) using an internal standard, as the described procedure at [75].

4.3.9.2. Hybrid polymerization method

RAFT polymerization by the hybrid method, was conducted by a mixture between the "graft from" methodology and polymerization in solution. Firstly, polymerization in solution was performed using a two times higher CTA concentration when compared with the CTA grafted to the particles. CTA, AIBN (one fifth of the CTA concentration in solution), 2`-acrylamidoethyl-β-D-galactose (101 mg, 0.23 mmol) and 1,3,5-trioxane (20 mg) were added on a schlenk tube **(1)** with 1,4-dioxane (2 mL). The reaction was degassed with five freeze-pump thaw cycles, followed by immersion in an 80 °C bath under stirring.

On a different schlenk tube **(2)**, CTA-SiNPs (50 mg), AIBN (one fifth of the CTA concentration in schlenk 1) and 1,4-dioxane (5 mL) were sealed and degasses with five freeze-pump thaw cycles. The mixture from the schlenk **(1)** was transferred to schlenk **(2)**, with a cannula

using argon pressure, when monomer conversion values were between 30% to 70%. Then, the reaction proceeded for 24h at 80 °C bath under stirring. Particles were recovered by centrifugation and washed three times with ethanol at 10,000 rpm for 10 min at room temperature. Particle precipitate was dried at 50 °C overnight and afterwards vacuum dried. Polymer weight percentage was quantified by ^{1}H-NMR in D_2O (pH=13) using an internal standard, as the described procedure at [75]. The polymer obtained from the supernatant at the schlenk **(2)** was precipitated in according to the monomer used and as described previously. Polymer molecular weight and polydispersity was assessed using UV-Vis and SEC-MALS [Attachment 6.18 and 6.19 (PAMEGalOAc) and Attachment 6.22 and 6.23 (PAMEGal)].

4.3.9.3. Graft to polymerization method

Graft to polymerization method was performed in a similar procedure to the CTA coupling with amine functionalized particles. Into a round flask in argon atmosphere, NH_2-MSN (50 mg, 0.96 mmol of APTES per gram of MSN) were dispersed in anhydrous acetonitrile (2 mL) and sonicated for 30 mins. To the particle suspension, a solution of DMAP (0.2 eq.), EDC.HCl (1.5 eq.) and the DPAEMA and AMEGal co-polymer (0.1 eq.) was dissolved in anhydrous acetonitrile (1 mL) and added. Every 24h, a new mixture of EDC.HCl (1.0 eq) and DMAP (0.2 eq) in anhydrous acetonitrile (1 mL) was added to the reaction mixture, the reaction proceeded for 96h. Particles were recovered by centrifugation and washed three times with ethanol at 10,000 rpm for 10 min at room temperature. Particle precipitate was dried at 50°C overnight and afterwards it was vacuum dried to obtain a slightly orange powder. Quantification was performed by ^{1}H-NMR in D_2O (pH=13) using an internal standard as the described procedure at [83].

THIS

PAGE INTENTIONALLY

LEFT BLANK

5. References

[1] G. A. Silva, “Introduction to nanotechnology and its applications to medicine,” *Surg. Neurol.*, vol. 61, no. 3, pp. 216–220, 2004.

[2] D. F. Emerich and C. G. Thanos, “Nanotechnology and medicine,” *Expert Opin. Biol. Ther.*, vol. 3, no. 4, pp. 655–663, 2003.

[3] K. Strebhardt and A. Ullrich, “Paul Ehrlich ’ s magic bullet concept : 100 years of progress,” *Nat. Rev. cancer*, vol. 8, no. june, pp. 473–480, 2008.

[4] S. A. A. Rizvi and A. M. Saleh, “Applications of nanoparticle systems in drug delivery technology,” *Saudi Pharm. J.*, vol. 26, no. 1, pp. 64–70, 2017.

[5] H. Shimoda, K. Taniguchi, M. Nishimura, K. Matsuura, T. Tsukioka, H. Yamashita, N. Inagaki, K. Hirano, M. Yamamoto, Y. Kinosada, and Y. Itoh, “Preparation of a fast dissolving oral thin film containing dexamethasone: A possible application to antiemesis during cancer chemotherapy,” *Eur. J. Pharm. Biopharm.*, vol. 73, no. 3, pp. 361–365, 2009.

[6] T. Iwamoto, “Clinical Application of Drug Delivery Systems in Cancer Chemotherapy: Review of the Efficacy and Side Effects of Approved Drugs,” *Biol. Pharm. Bull.*, vol. 36, no. 5, pp. 715–718, 2013.

[7] R. L. and O. F. L Zhang, FX Gu, JM Chan, Az Wang, “Nanoparticles in Medicine: Therapeutic Applications and Developments,” *Clin. Pharmacol. Ther.*, vol. 83, no. 5, pp. 761–769, 2008.

[8] C. Baleizão and J. P. S. Farinha, “Hybrid smart mesoporous silica nanoparticles for theranostics,” *Nanomedicine*, vol. 10, no. 15, pp. 2311–2314, 2015.

[9] C. Park, K. Oh, S. C. Lee, and C. Kim, “Controlled release of guest molecules from mesoporous silica particles based on a pH-responsive polypseudorotaxane motif,” *Angew. Chemie - Int. Ed.*, vol. 46, no. 9, pp. 1455–1457, 2007.

[10] X. Shi, K. Sun, and J. R. Baker, “Spontaneous formation of functionalized dendrimer-stabilized gold nanoparticles,” *J. Phys. Chem. C*, vol. 112, no. 22, pp. 8251–8258, 2008.

[11] I. Journal, “Liposomes and nanotechnology in drug development : Focus on ocular targets Liposomes and nanotechnology in drug development : focus on ocular targets,” no. February, pp. 495–504, 2013.

[12] A. Bianco, “Carbon nanotubes for the delivery of therapeutic molecules,” *Expert Opinion on Drug Delivery*, 2004. [Online]. Available: http://www.tandfonline.com/doi/full/10.1517/17425247.1.1.57. [Accessed: 23-Aug-2018].

[13] S. Kapse-Mistry, T. Govender, R. Srivastava, and M. Yergeri, “Nanodrug delivery in reversing multidrug resistance in cancer cells,” *Front. Pharmacol.*, vol. 5, no. 159, pp. 1–22, 2014.

[14] K. Hussain and T. Hussain, “Gold Nanoparticles: A Boon to Drug Delivery System,” *South Indian J. Biol. Sci.*, vol. 1, no. 3, p. 128, 2015.

[15] P. S. Z. and M. R. H. Mahdi Karimi, Hamed Mirshekari, Masoumeh Aliakbari, “Smart mesoporous silica nanoparticles for controlled-release drug delivery,” *Nanotechnol. Rev.*, vol. 5, no. 2, 2016.

[16] C. Oerlemans, W. Bult, M. Bos, G. Storm, J. F. W. Nijsen, and W. E. Hennink, “Polymeric micelles in anticancer therapy: Targeting, imaging and triggered release,” *Pharm. Res.*, vol. 27, no. 12, pp. 2569–2589, 2010.

[17] C. L. Lay, J. Liu, and Y. Liu, “Functionalized carbon nanotubes for anticancer drug delivery,” *Expert Rev. Med. Devices*, vol. 8, no. 5, pp. 561–566, 2011.

[18] M. Fang, C. Peng, D. Pang, and Y. Li, “Quantum Dots for Cancer Research : Current

Status , Remaining Issues , and Future Perspectives Characteristics of QDs for Biomedical," *Cancer Biol Med*, vol. 9, no. 3, pp. 151–163, 2012.

[19] C. Bharti, N. Gulati, U. Nagaich, and A. Pal, "Mesoporous silica nanoparticles in target drug delivery system: A review," *Int. J. Pharm. Investig.*, vol. 5, no. 3, p. 124, 2015.

[20] D. L. Green, J. S. Lin, Y. F. Lam, M. Z. C. Hu, D. W. Schaefer, and M. T. Harris, "Size, volume fraction, and nucleation of Stober silica nanoparticles," *J. Colloid Interface Sci.*, vol. 266, no. 2, pp. 346–358, 2003.

[21] I. A. Rahman and V. Padavettan, "Synthesis of Silica nanoparticles by Sol-Gel: Size-dependent properties, surface modification, and applications in silica-polymer nanocompositesa review," *Journal of Nanomaterials*. pp. 1–15, 2012.

[22] C. C. M. C. Carcouët, M.W.P. van de Put, B. Mezari, P. C. M. M. Magusin, J. Laven, P. H. H, Bomans, H. Friedrich, A. C. A. Esteves, N. A. J. M. Sommerdijk, R. A. T. M. van Benthem, and G. de With, "Nucleation and growth of monodisperse silica nanoparticles: Supporting Info," *Nano Lett.*, vol. 14, no. 3, pp. 1433–1438, 2014.

[23] T. Matsoukas and E. Gulari, "Dynamics of growth of silica particles from ammonia-catalyzed hydrolysis of tetra-ethyl-orthosilicate," *J. Colloid Interface Sci.*, vol. 124, no. 1, pp. 252–261, 1988.

[24] G. H. Bogush and C. F. Zukoski IV, "Uniform silica particle precipitation: An aggregative growth model," *J. Colloid Interface Sci.*, vol. 142, no. 1, pp. 19–34, 1991.

[25] W. Stober and A. Fink, "Controlled Growth of Monodispersed Silica Spheres in the Micron Size Range," *J. Colloid Interface Sci.*, vol. 26, pp. 62–69, 1968.

[26] S. Bhakta, C. K. Dixit, I. Bist, K. A. Jalil, S. L. Suib, and J. F. Rusling, "Sodium hydroxide catalyzed monodispersed high surface area silica nanoparticles," *Mater. Res. Express*, vol. 3, no. 7, 2016.

[27] C. T. Kresge, M. E. Leonowicz, W. J. Roth, J. C. Vartuli, and J. S. Beck, "Ordered mesoporous molecular sieves synthesized by a liquid-crystal template mechanism," *Nature*, vol. 359, no. 6397, pp. 710–712, 1992.

[28] S. Abbott, *Surfactant Science: Principles and Practice*, 2016. [Online]. Available: http://Www.Stevenabbott.Co.Uk/Practical-Surfactants/the-Book.Php. [Accessed: 23-Aug-2018]

[29] F. Hoffmann, M. Cornelius, J. Morell, and M. Fröba, "Silica-based mesoporous organic-inorganic hybrid materials," *Angew. Chemie - Int. Ed.*, vol. 45, no. 20, pp. 3216–3251, 2006.

[30] M. Vallet-Regi, A. Rámila, R. P. del Real, and J. Pérez-Pariente, "A New Property of MCM-41:Drug Delivery System," *Chem. Mater.*, vol. 13, no. 2, pp. 308–311, 2000.

[31] J. H. Park, L. Gu, G. Von Maltzahn, E. Ruoslahti, S. N. Bhatia, and M. J. Sailor, "Biodegradable luminescent porous silicon nanoparticles for in vivo applications," *Nat. Mater.*, vol. 8, no. 4, pp. 331–336, 2009.

[32] Q. He, Z. Zhang, F. Gao, Y. Li, and J. Shi, "In vivo biodistribution and urinary excretion of mesoporous silica nanoparticles: Effects of particle size and PEGylation," *Small*, vol. 7, no. 2, pp. 271–280, 2011.

[33] J. Lu, M. Liong, Z. Li, J. I. Zink, and F. Tamanoi, "Biocompatibility, biodistribution, and drug-delivery efficiency of mesoporous silica nanoparticles for cancer therapy in animals," *Small*, vol. 6, no. 16, pp. 1794–1805, 2010.

[34] J. Peng, K. Wang, W. Tan, X. He, C. He, P. Wu, and F. Liu, "Identification of live liver cancer cells in a mixed cell system using galactose-conjugated fluorescent nanoparticles," *Talanta*, vol. 71, no. 2, pp. 833–840, 2007.

[35] T. Ribeiro, S. Raja, A. S. Rodrigues, F. Fernandes, C. Baleizão, and J. P. S. Farinha, "NIR

and visible perylenediimide-silica nanoparticles for laser scanning bioimaging," *Dye. Pigment.*, vol. 110, pp. 227–234, 2014.

[36] T. Ribeiro, E. Coutinho, A. S. Rodrigues, C. Baleizão, and J. P. S. Farinha, "Hybrid mesoporous silica nanocarriers with thermovalve-regulated controlled release," *Nanoscale*, vol. 9, no. 36, pp. 13485–13494, 2017.

[37] T. Ribeiro, C. Baleizão, and J. P. S. Farinha, "Synthesis and Characterization of Perylenediimide Labeled Core - Shell Hybrid Silica - Polymer Nanoparticles," *J. Phys. Chem. C*, vol. 113, no. 42, pp. 18082–18090, 2009.

[38] T. Ribeiro, A. Fedorov, C. Baleizão, and J. P. S. Farinha, "Formation of hybrid films from perylenediimide-labeled core-shell silica-polymer nanoparticles," *J. Colloid Interface Sci.*, vol. 401, pp. 14–22, 2013.

[39] T. Ribeiro, S. Raja, A. S. Rodrigues, F. Fernandes, J. P. S. Farinha, and C. Baleizão, "High performance NIR fluorescent silica nanoparticles for bioimaging," *RSC Adv.*, vol. 3, no. 24, pp. 9171–9174, 2013.

[40] A. Ravve, *Principles of polymer chemistry, Volume 1*. Ithaca and London: Cornell University Press, 2000.

[41] M. A. Hillmyer, *Polymer Synthesis*, vol. 1. Elsevier B.V., 2012.

[42] T. Otsu, M. Yoshida, and T. Tazaki, "A model for living radical polymerization," *Die Makromol. Chemie, Rapid Commun.*, vol. 3, no. 2, pp. 133–140, 1982.

[43] D. H. Solomon, E. Rizzardo, and P. U. S. Cacioli, "Patent 4,581,429," 102, 221335q, 1985.

[44] M. K. Georges, R. P. N. Veregin, P. M. Kazmaier, and G. K. Hamer, "Narrow Molecular Weight Resins by a Free-Radical Polymerization Process," *Macromolecules*, vol. 26, no. 11, pp. 2987–2988, 1993.

[45] H. Fischer and M. Souaille, "The persistent radical effect in living radical polymerization - Borderline cases and side-reactions," *Macromol. Symp.*, vol. 174, no. 97, pp. 231–240, 2001.

[46] J. S. Wang and K. Matyjaszewski, "Controlled/'Living' Radical Polymerization. Atom Transfer Radical Polymerization in the Presence of Transition-Metal Complexes," *J. Am. Chem. Soc.*, vol. 117, no. 20, pp. 5614–5615, 1995.

[47] H. Bergenudd (2011), "Understanding the mechanisms behind atom transfer radical polymerization : exploring the limit of control," (Doctoral Dissertation).

[48] J. Chiefari, Y. K. B. Chong, F. Ercole, J. Krstina, J. Jeffery, T. P. T. Le, R. T. A. Mayadunne, G. F. Meijs, C. L. Moad, G. Moad, E. Rizzardo, and S.H. Thang, "Living Free-Radical Polymerization by Reversible Addition - Fragmentation Chain Transfer : The RAFT Process We wish to report a new living free-radical polymer- ization of exceptional effectiveness and versatility . 1 The living character is conferred by," *Macromolecules*, vol. 31, no. 16, pp. 5559–5562, 1998.

[49] G. Moad, "Radical Polymerization," in *Polymer Science: A Comprehensive Reference, 10 Volume Set*, vol. 3, 2012, pp. 59–118.

[50] P. Science, "Polymer Science RAFT : Choosing the Right Agent to Achieve Controlled Polymerization," 2016. [Online]. Available: https://www.sigmaaldrich.com/technical-documents/articles/materials-science/polymer-science/raft-polymerization.html. [Accessed: 23-Aug-2018].

[51] J. Xiao, W. Chen, F. Wang, and J. Du, "Polymer / TiO 2 Hybrid Nanoparticles with Highly E ff ective UV- Screening but Eliminated Photocatalytic Activity," *Macromolecules*, vol. 46, pp. 375–383, 2013.

[52] J. S. Suk, Q. Xu, N. Kim, J. Hanes, and L. M. Ensign, "PEGylation as a strategy for improving nanoparticle-based drug and gene delivery," *Adv. Drug Deliv. Rev.*, vol. 99, pp.

28–51, 2016.

[53] G. Poźniak, I. Gancarz, and W. Tylus, “Modified poly(phenylene oxide) membranes in ultrafiltration and micellar-enhanced ultrafiltration of organic compounds,” *Desalination*, vol. 198, pp. 215–224, 2006.

[54] S. Kango, S. Kalia, A. Celli, J. Njuguna, Y. Habibi, and R. Kumar, “Surface modification of inorganic nanoparticles for development of organic-inorganic nanocomposites - A review,” *Prog. Polym. Sci.*, vol. 38, no. 8, pp. 1232–1261, 2013.

[55] J. C. Foster, S. C. Radzinski, and J. B. Matson, “Graft polymer synthesis by RAFT transfer-to,” *J. Polym. Sci. Part A Polym. Chem.*, vol. 55, no. 18, pp. 2865–2876, 2017.

[56] J. Liu, V. Bulmus, D. L. Herlambang, C. Barner-Kowollik, M. H. Stenzel, and T. P. Davis, “In situ formation of protein-polymer conjugates through reversible addition fragmentation chain transfer polymerization,” *Angew. Chemie - Int. Ed.*, vol. 46, no. 17, pp. 3099–3103, 2007.

[57] M. Xie, H. Shi, K. Ma, H. Shen, B. Li, S. Shen, X. Wang, and Y. Jin, “Hybrid nanoparticles for drug delivery and bioimaging: Mesoporous silica nanoparticles functionalized with carboxyl groups and a near-infrared fluorescent dye,” *J. Colloid Interface Sci.*, vol. 395, no. 1, pp. 306–314, 2013.

[58] C. Dai, H. Guo, J. Lu, J. Shi, J. Wei, and C. Liu, “Osteogenic evaluation of calcium/magnesium-doped mesoporous silica scaffold with incorporation of rhBMP-2 by synchrotron radiation-based μCT,” *Biomaterials*, vol. 32, no. 33, pp. 8506–8517, 2011.

[59] A. Taheri, R. Dinarvand, F. Ahadi, M. R. Khorramizadeh, and F. Atyabi, “The in vivo antitumor activity of LHRH targeted methotrexate-human serum albumin nanoparticles in 4T1 tumor-bearing Balb/c mice,” *Int. J. Pharm.*, vol. 431, no. 1–2, pp. 183–189, 2012.

[60] A. Guaragna, A. Chiaviello, C. Paolella, D. DAlonzo, G. Palumbo, and G. Palumbo, “Synthesis and evaluation of folate-based chlorambucil delivery systems for tumor-targeted chemotherapy,” *Bioconjug. Chem.*, vol. 23, no. 1, pp. 84–96, 2012.

[61] Y. C. Wang, X. Q. Liu, T. M. Sun, M. H. Xiong, and J. Wang, “Functionalized micelles from block copolymer of polyphosphoester and poly(e{open}-caprolactone) for receptor-mediated drug delivery,” *J. Control. Release*, vol. 128, no. 1, pp. 32–40, 2008.

[62] W. Cheng, J. Nie, L. Xu, C. Liang, Y. Peng, G. Liu, T. Wang, L. Mei, L. Huang, and X. Zeng, “pH-Sensitive Delivery Vehicle Based on Folic Acid-Conjugated Polydopamine-Modified Mesoporous Silica Nanoparticles for Targeted Cancer Therapy,” *ACS Appl. Mater. Interfaces*, vol. 9, no. 22, pp. 18462–18473, 2017.

[63] H. Ghazarian, B. Idoni, and S. B. Oppenheimer, “A glycobiology review: Carbohydrates, lectins and implications in cancer therapeutics,” *Acta Histochem.*, vol. 113, no. 3, pp. 236–247, 2011.

[64] A. A. D’Souza and P. V. Devarajan, “Asialoglycoprotein receptor mediated hepatocyte targeting - Strategies and applications,” *J. Control. Release*, vol. 203, pp. 126–139, 2015.

[65] J. Ding, C. Xiao, Y. Li, Y. Cheng, N. Wang, C. He, X. Zhuang, X. Zhu, and X. Chen, “Efficacious hepatoma-targeted nanomedicine self-assembled from galactopeptide and doxorubicin driven by two-stage physical interactions,” *J. Control. Release*, vol. 169, no. 3, pp. 193–203, 2013.

[66] G. Sahay, D. Y. Alakhova, and A. V. Kabanov, “Endocytosis of nanomedicines,” *J. Control. Release*, vol. 145, no. 3, pp. 182–195, 2010.

[67] G. Quan, X. Pan, Z. Wang, Q. Wu, G. Li, L. Dian, B. Chen, and C. Wu, “Lactosaminated mesoporous silica nanoparticles for asialoglycoprotein receptor targeted anticancer drug delivery,” *J. Nanobiotechnology*, vol. 13, no. 1, pp. 1–12, 2015.

[68] H. J. H. Amir K. Varkouhi, Marije Scholte, Gert Storm, “Endosomal escape pathways for delivery of biologicals,” *J. Control. Release*, vol. 151, no. 3, pp. 220–228, 2011.

[69] B. Martins Estevão, I. Miletto, L. Marchese, and E. Gianotti, “Optimized Rhodamine B labeled mesoporous silica nanoparticles as fluorescent scaffolds for the immobilization of photosensitizers: A theranostic platform for optical imaging and photodynamic therapy,” *Phys. Chem. Chem. Phys.*, vol. 18, no. 13, pp. 9042–9052, 2016.

[70] M. A. Mumin, W. Z. Xu, and P. A. Charpentier, “Quantum dots/silica/polymer nanocomposite films with high visible light transmission and UV shielding properties,” *Nanotechnology*, vol. 26, no. 31, p. 14, 2015.

[71] K. M. L. Taylor, J. S. Kim, W. J. Rieter, H. An, W. Lin, and W. Lin, “Mesoporous silica nanospheres as highly efficient MRI contrast agents,” *J. Am. Chem. Soc.*, vol. 130, no. 7, pp. 2154–2155, 2008.

[72] S. Giri, B. G. Trewyn, M. P. Stellmaker, and V. S. Y. Lin, “Stimuli-responsive controlled-release delivery system based on mesoporous silica nanorods capped with magnetic nanoparticles,” *Angew. Chemie - Int. Ed.*, vol. 44, no. 32, pp. 5038–5044, 2005.

[73] F. Torney, B. G. Trewyn, V. S. Y. Lin, and K. Wang, “Mesoporous silica nanoparticles deliver DNA and chemicals into plants,” *Nat. Nanotechnol.*, vol. 2, no. 5, pp. 295–300, 2007.

[74] T. D. Nguyen, H-S. Tseng, P. C. Celestre, A. H. Flood, Y. Liu, J. F. Stoddart, and J. I. Zink, “A reversible molecular valve,” *Proc. Natl. Acad. Sci. U. S. A.*, vol. 102, no. 29, pp. 10029–34, 2005.

[75] N. K. Mal, M. Fujiwara, and Y. Tanaka, “Photocontrolled reversible release of guest molecules from coumarin- modified mesoporous silica,” *Nature*, vol. 421, no. 23, pp. 350–353, 2003.

[76] R. Casasús, M. D. Marcos, R. Martínez-Máñez, J. V. Ros-Lis, J. Soto, L. A. Villaescusa, P. Amorós, D. Beltrán, C. Guillem, and J. Latorre, “Toward the development of ionically controlled nanoscopic molecular gates,” *J. Am. Chem. Soc.*, vol. 126, no. 28, pp. 8612–8613, 2004.

[77] S. M. Simon, “Role of oganelle ph in tumor cell biology and drug resistance,” *Drug Discov. Today*, vol. 4, no. 1, pp. 32–38, 1999.

[78] G. Kocak, C. Tuncer, and V. Bütün, “PH-Responsive polymers,” *Polym. Chem.*, vol. 8, no. 1, pp. 144–176, 2017.

[79] L. Zhu, S. Powell, and S. G. Boyes, “Synthesis of tertiary amine-based pH-responsive polymers by RAFT Polymerization,” *J. Polym. Sci. Part A Polym. Chem.*, vol. 53, no. 8, pp. 1010–1022, 2015.

[80] M. G. Gouveia, “Aggregation behavior of a temperature- and pH-responsive diblock copolymer in aqueous solution,” 2016.

[81] J. M. Rosenholm, A. Meinander, E. Peuhu, R. Niemi, J. E. Eriksson, C. Sahlgren, and M. Lindén, “Targeting of porous hybrid silica nanoparticles to cancer cells,” *ACS Nano*, vol. 3, no. 1, pp. 197–206, 2009.

[82] T. G. Kim, G. S. An, J. S. Han, J. U. Hur, B. G. Park, and S. C. Choi, “Synthesis of size controlled spherical silica nanoparticles via sol-gel process within hydrophilic solvent,” *J. Korean Ceram. Soc.*, vol. 54, no. 1, pp. 49–54, 2017.

[83] C. I. C. Crucho, C. Baleizão, and J. P. S. Farinha, “Functional Group Coverage and Conversion Quantification in Nanostructured Silica by1H NMR,” *Anal. Chem.*, vol. 89, no. 1, pp. 681–687, 2017.

[84] K. S. and J. T. Liz G. Williams, “Select RAFT Agents for Making Well-Defined Functionalized Polymers.” [Online]. Available: https://www.sigmaaldrich.com/technical-documents/articles/technology-spotlights/raft-agents-for-functionalized-polymers.html. [Accessed: 02-Sep-2018].

[85] E. Bicciocchi, Y. K. Chong, L. Giorgini, G. Moad, E. Rizzardo, and S. H. Thang,

"Substituent effects on RAFT polymerization with benzyl aryl trithiocarbonates," *Macromol. Chem. Phys.*, vol. 211, no. 5, pp. 529–538, 2010.

[86] J. Li, J. Ren, Y. Cao, and W. Yuan, "Synthesis of biodegradable pentaarmed star-block copolymers via an asymmetric BIS-TRIS core by combination of ROP and RAFT: From star architectures to double responsive micelles," *Polymer (Guildf).*, vol. 51, no. 6, pp. 1301–1310, 2010.

[87] A. M. Santiago, T. Ribeiro, A. S. Rodrigues, B. Ribeiro, R. F. M. Frade, C. Baleizão, and J. P. S. Farinha, "Multifunctional Hybrid Silica Nanoparticles with a Fluorescent Core and Active Targeting Shell for Fluorescence Imaging Biodiagnostic Applications," *Eur. J. Inorg. Chem.*, vol. 2015, no. 27, pp. 4579–4587, 2015.

[88] Y. Tsujii, M. Ejaz, K. Sato, A. Goto, and T. Fukuda, "Mechanism and kinetics of RAFT-mediated graft polymerization of styrene on a solid surface. 1. Experimental evidence of surface radical migration," *Macromolecules*, vol. 34, no. 26, pp. 8872–8878, 2001.

[89] S. Bhattacharjee, "DLS and zeta potential - What they are and what they are not?," *J. Control. Release*, vol. 235, pp. 337–351, 2016.

[90] Z. Y. Zhu, D. Cui, H. Gao, F. Y. Dong, X. C. Liu, F. Liu, L. Chen, and Y. M. Zhang, "Efficient synthesis and activity of beneficial intestinal flora of two lactulose-derived oligosaccharides," *Eur. J. Med. Chem.*, vol. 114, pp. 8–13, 2016.

[91] G. Zheng, A. Graham, M. Shibata, J. R. Missert, A. R. Oseroff, T. J. Dougherty, and R. K. Pandey, "Synthesis of β-galactose-conjugated chlorins derived by enyne metathesis as galectin-specific photosensitizers for photodynamic therapy," *J. Org. Chem.*, vol. 66, no. 26, pp. 8709–8716, 2001.

[92] B. A. Abel and C. L. McCormick, "Mechanistic Insights into Temperature-Dependent Trithiocarbonate Chain-End Degradation during the RAFT Polymerization of N-Arylmethacrylamides," *Macromolecules*, vol. 49, no. 2, pp. 465–474, 2016.

[93] Y. Q. Hu, M. S. Kim, B. S. Kim, and D. S. Lee, "Synthesis and pH-dependent micellization of 2-(diisopropylamino)ethyl methacrylate based amphiphilic diblock copolymers via RAFT polymerization," *Polymer (Guildf).*, vol. 48, no. 12, pp. 3437–3443, 2007.

[94] M. Álvarez-Paino, V. Bordegé, R. Cuervo-Rodríguez, A. Muñoz-Bonilla, and M. Fernández-García, "Well-defined glycopolymers via raft polymerization: Stabilization of gold nanoparticles," *Macromol. Chem. Phys.*, vol. 215, no. 19, pp. 1915–1924, 2014.

[95] S. N. R. Kutcherlapati, R. Koyilapu, U. M. R. Boddu, D. Datta, R. S. Perali, M. J. Swamy, and T. Jana, "Glycopolymer-Grafted Nanoparticles: Synthesis Using RAFT Polymerization and Binding Study with Lectin," *Macromolecules*, vol. 50, no. 18, pp. 7309–7320, 2017.

[96] X. Ding and P. Wang, "Using the 3-Diethylaminobenzyl Group as a Photocage in Aqueous Solution," *J. Org. Chem.*, vol. 83, no. 14, pp. 7459–7466, 2018.

[97] Y. Luo and J. Lin, "Solvent induced different morphologies of bis(propyl)triethoxysilane substituted perylenediimide and their optical properties," *J. Colloid Interface Sci.*, vol. 297, no. 2, pp. 625–630, 2006.

6. Attachments

6.1. NMR Spectra

6.1.1. BSPA

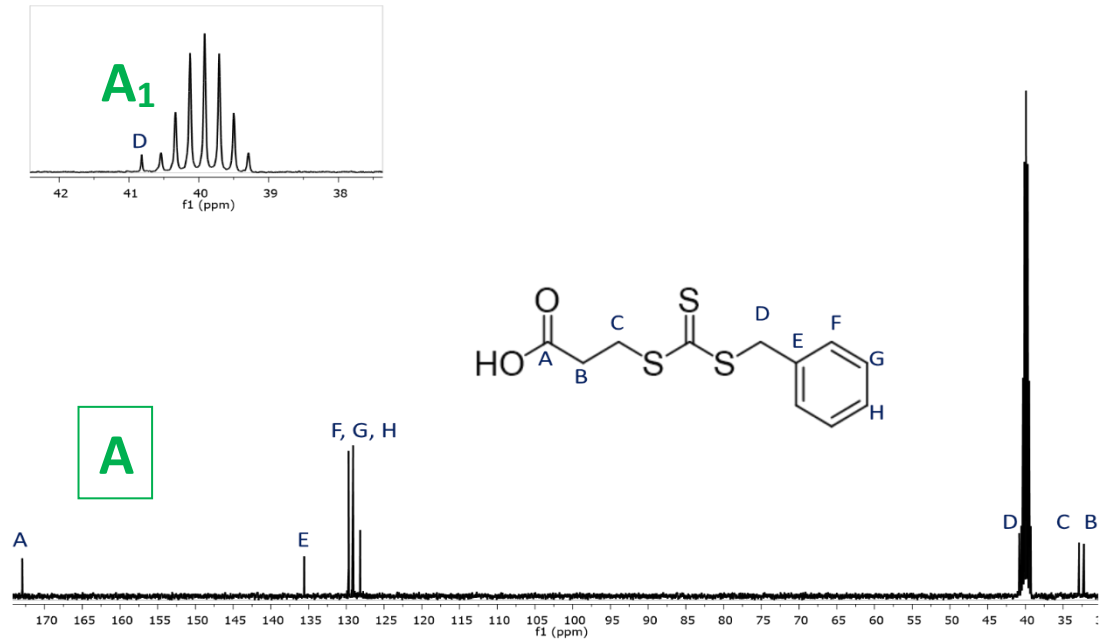

Attachment 6.1 – ^{13}C-NMR (400MHz; $(CD_3)_2SO$) for 3-(benzylsulfanylthiocarbonylsulfanyl) propionic acid (BSPA) (4.3.4). A_1 – expansion between 42-38ppm, to highlight Carbon-D, next to DMSO peaks. ^{1}H-NMR (400MHz; ($CDCl_3$)) in figure 2.6.

6.1.2. β-D-Galactose pentaacetate *(GalOAc)*

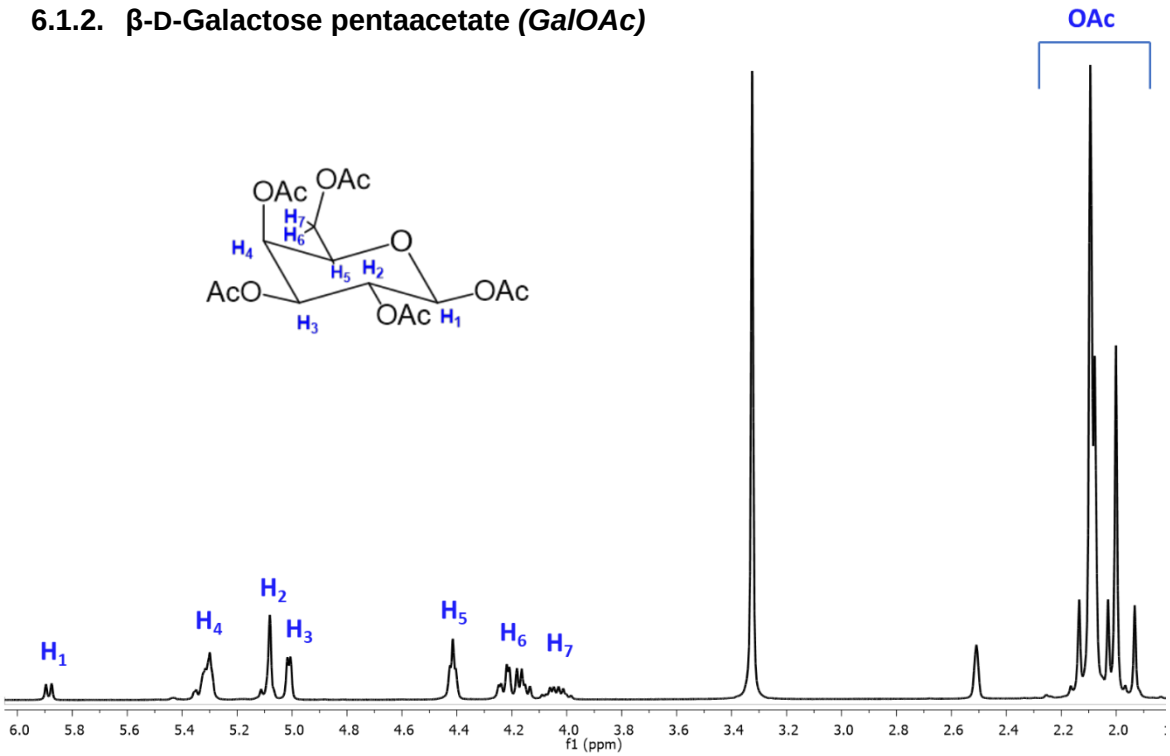

Attachment 6.2 – ^{1}H-NMR (400MHz; $(CD_3)_2SO$) for β-D-Galactose pentaacetate (4.3.5.1).

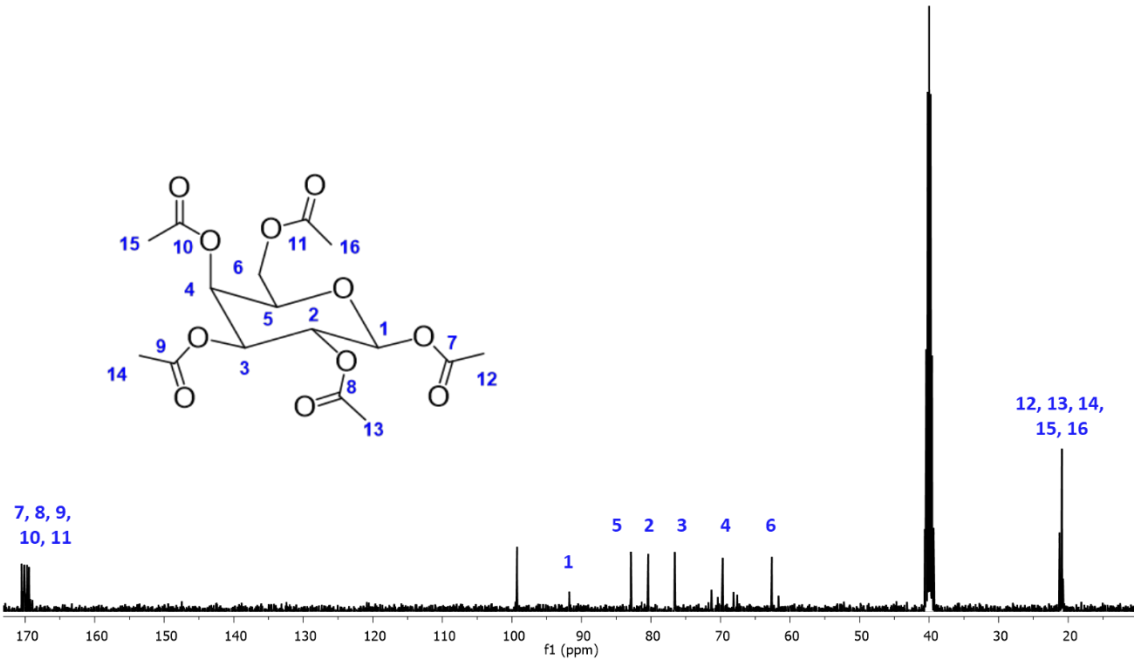

Attachment 6.3 – ^{13}C-NMR (400MHz; $(CD_3)_2SO$) for β-D-Galactose pentaacetate (4.3.5.1).

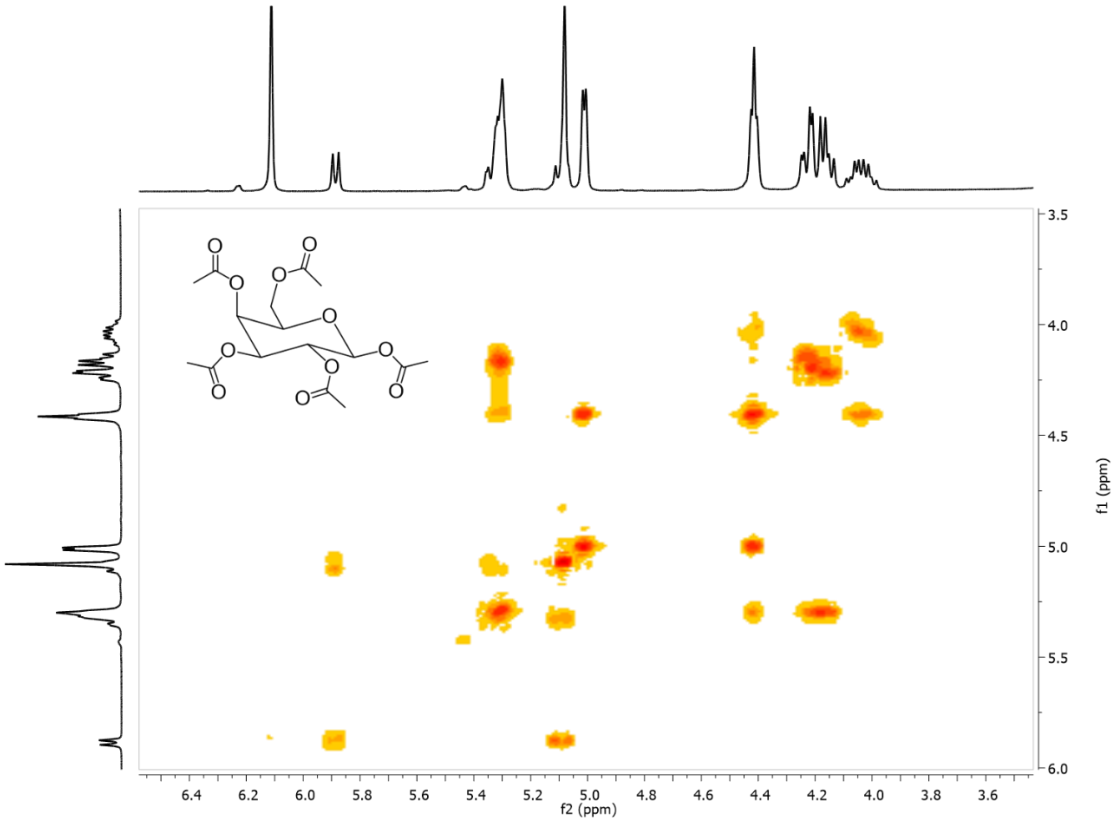

Attachment 6.4 – 2D-COSY (400MHz; $(CD_3)_2SO$) for β-D-Galactose pentaacetate (4.3.5.1).

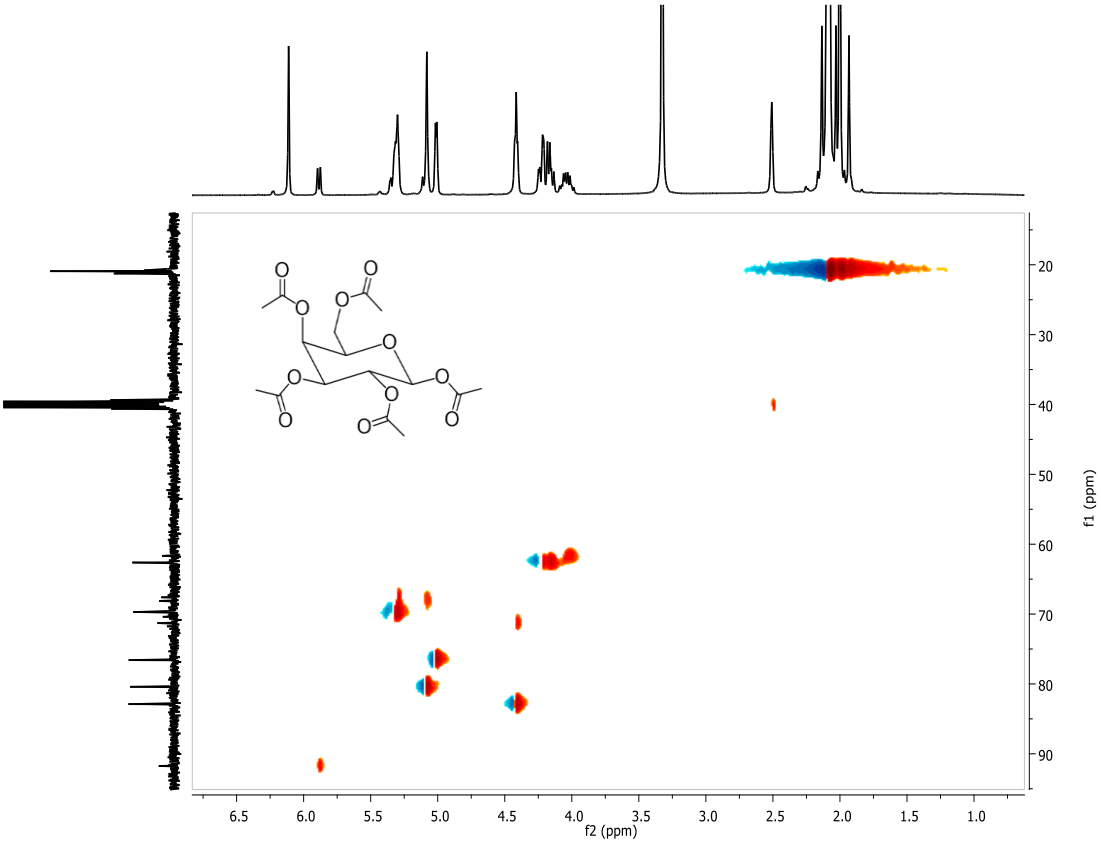

Attachment 6.5 – 2D-HSQC (400MHz; $(CD_3)_2SO$) for β-D-Galactose pentaacetate (4.3.5.1).

6.1.3. 2`-acrylamidoethyl-β-D-Galactose tetraacetate *(AMEGalOAc)*

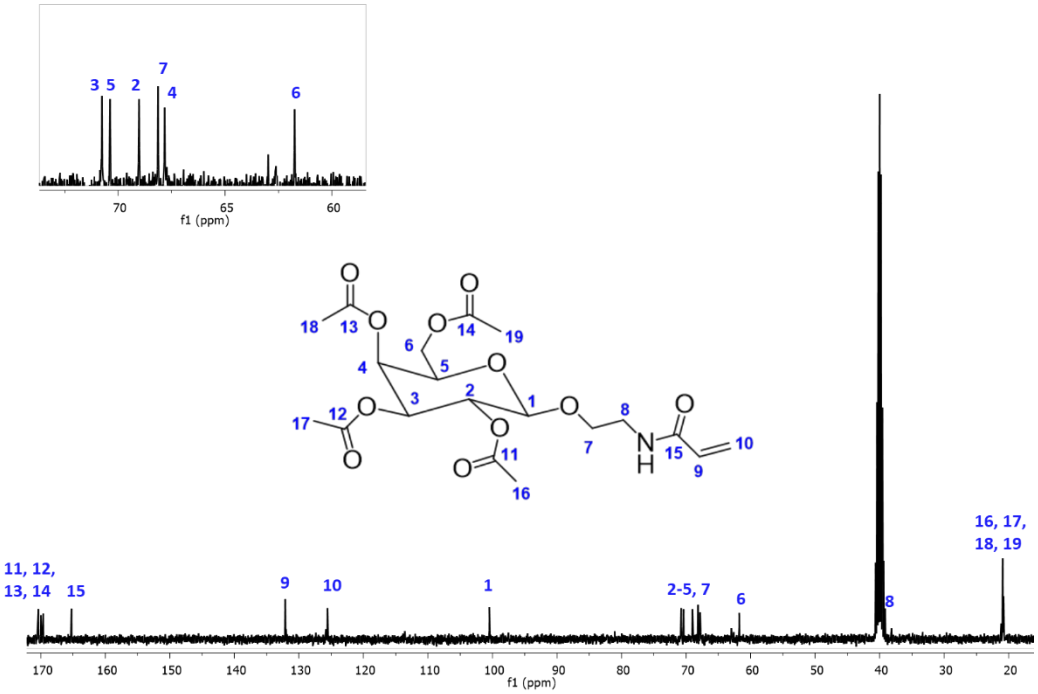

Attachment 6.6 – ^{13}C-NMR (400MHz; $(CD_3)_2SO$) for 2`-acrylamidoethyl-β-D-Galactose tetraacetate (AMEGalOAc) (4.3.5.2). ^{1}H-NMR (400MHz; $(CDCl_3)$) in figure 2.9.

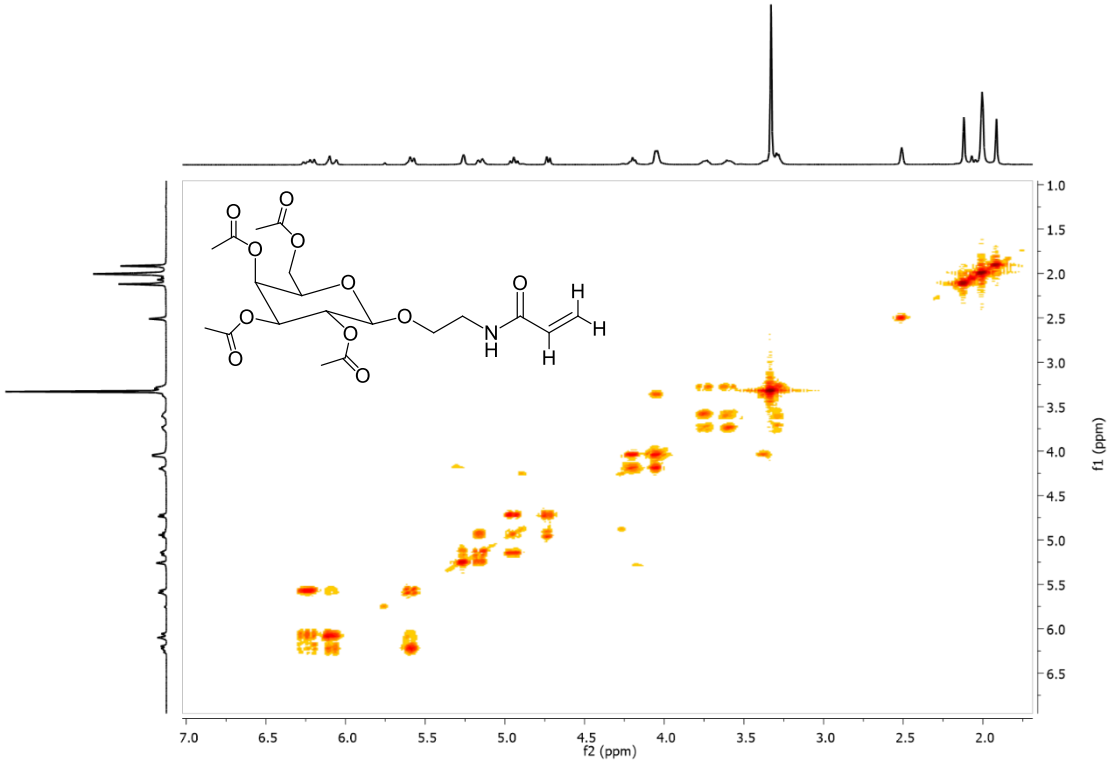

Attachment 6.7 – 2D-COSY (400MHz; $(CD_3)_2SO$) for 2`-acrylamidoethyl-β-D-Galactose tetraacetate (AMEGalOAc) (4.3.5.2).

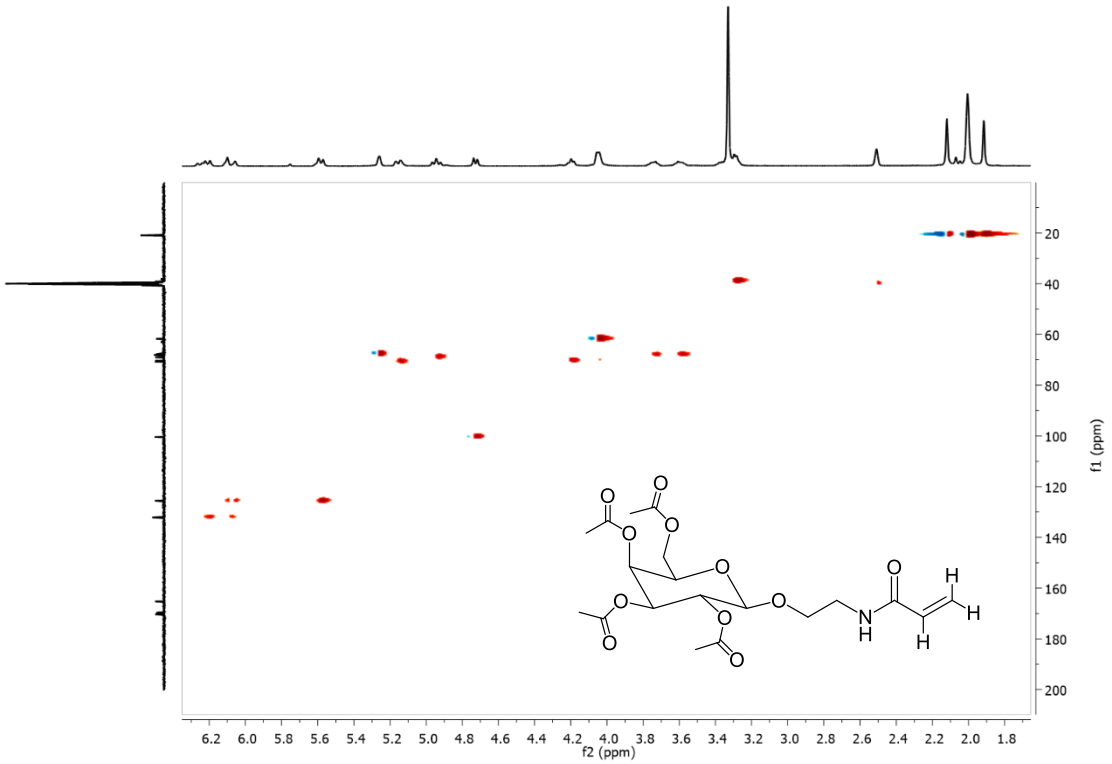

Attachment 6.8 – 2D-HSQC (400MHz; $(CD_3)_2SO$) for 2`-acrylamidoethyl-β-D-Galactose tetraacetate (AMEGalOAc) (4.3.5.2).

6.1.4. 2-(diiso-propylamino) ethyl methacrylate (DPAEMA)

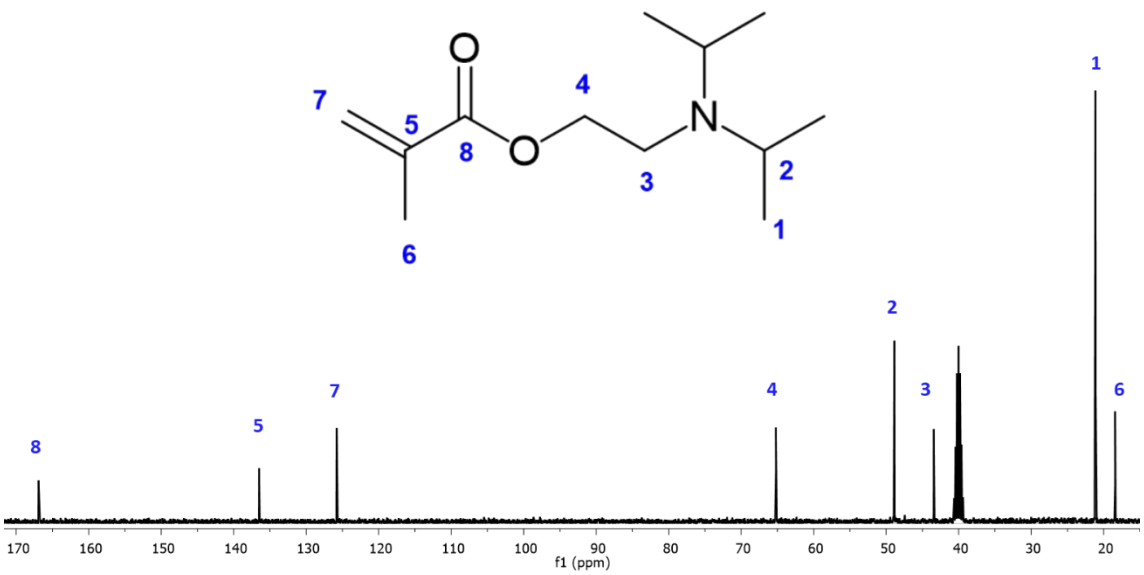

Attachment 6.9 – ^{13}C-NMR (400MHz; $(CD_3)_2SO$) for 2-(diiso-propylamino) ethyl methacrylate (DPAEMA) (4.3.6). ^{1}H-NMR (400MHz; $(CDCl_3)$) in figure 2.11.

6.1.5. 2`-acrylamidoethyl-β-D-Galactose *(AMEGal)*

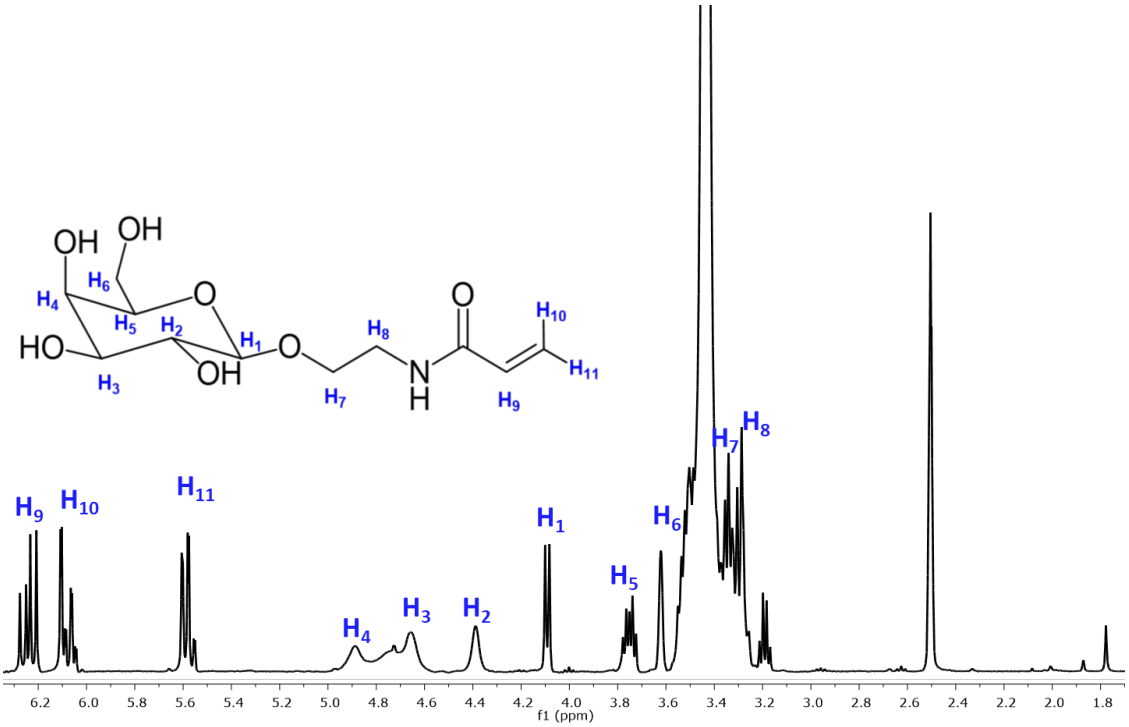

Attachment 6.10 – ^{1}H-NMR (400MHz; $(CD_3)_2SO$) for 2`-acrylamidoethyl-β-D-Galactose (4.3.7).

6.1.6. Particle grafted polymer

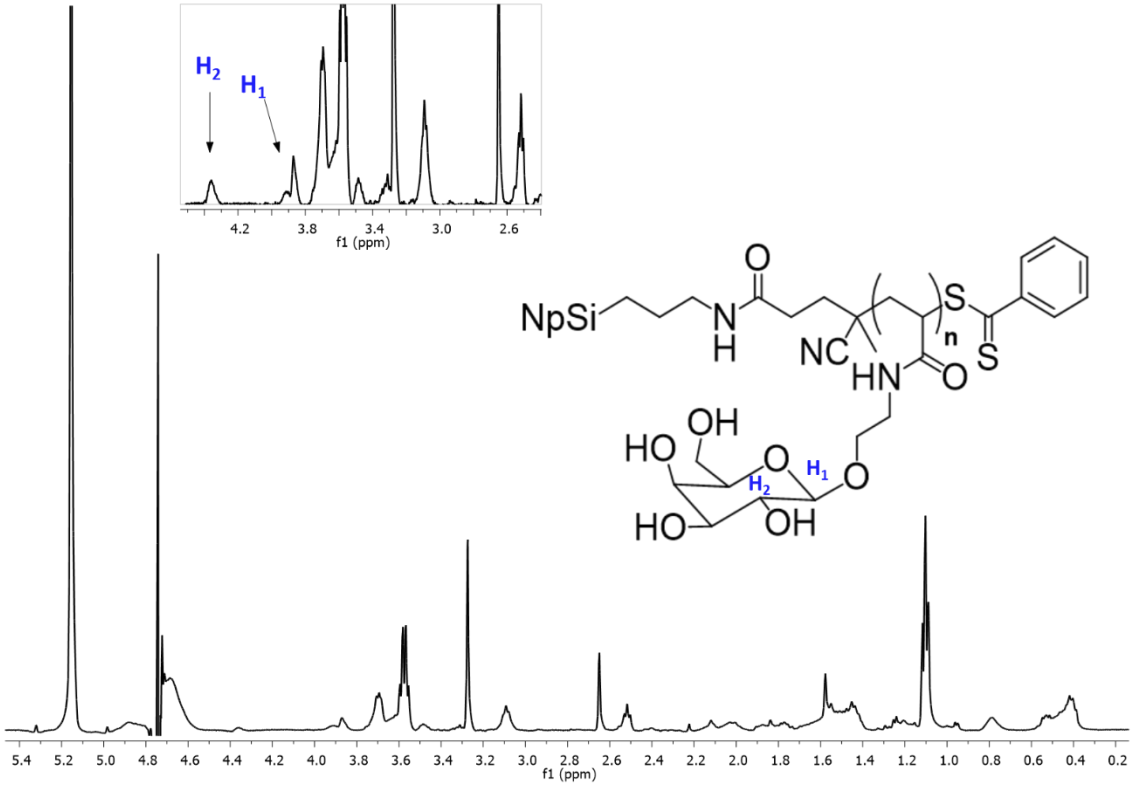

Attachment 6.11 – ^{1}H-NMR (500MHz; (D_2O) for 2`-acrylamidoethyl-β-D-Galactose polymer grafted onto stöber nanoparticles by the hybrid method (4.3.9.2). Solvent peak (4.79 ppm) was reversed to allow a better quantification.

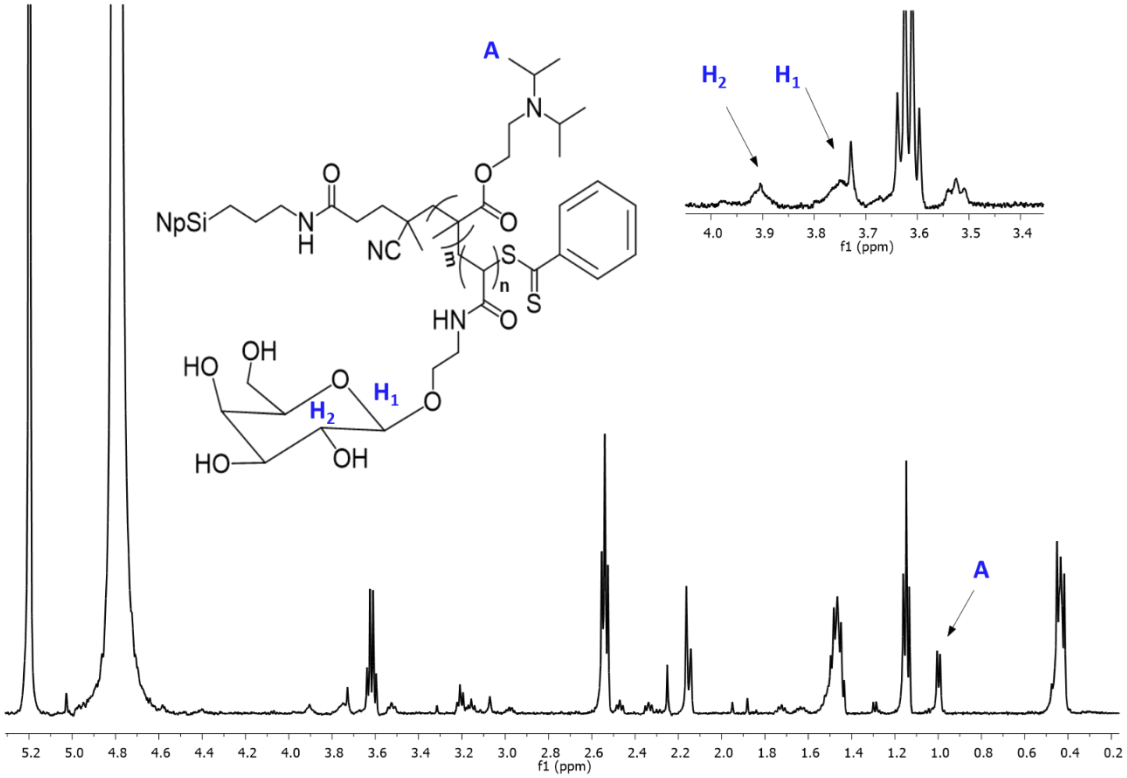

Attachment 6.12 – ^{1}H-NMR (500MHz; (D_2O) for the copolymer (PDPAEMA and PAMEGal) grafted onto MSN nanoparticles by the hybrid method (4.3.9.2).

6.2. Calculation of the surface coverage

$$V = \frac{4}{3}\pi r^3 \qquad d = \frac{m_p}{V} \qquad N_{NP} = \frac{1}{m_p} \qquad A_s = 4\pi r^2 \qquad A_T = A_s * N_{NP} \qquad n = \frac{m}{M}$$

Attachment 6.13 – Calculation of the particle surface coverage (mmol/nm^2). Particle volume (V) was calculated with the particle radius (r) followed by the particle mass (m_p) calculation using their density (d) (stöber 1.6g/mL; MSN 0.34g/mL - from [83]). Thus, reaching the number of particles per gram (N_{NP}), the surface area (A_s) and the total surface area (A_T) available per gram can be estimated. From this point, quantification by ^{1}H-NMR can be possible by determination of molecules (mol) per area.

6.3. Chromatograms

6.3.1. Polymer of 2`-acrylamidoethyl-β-D-Galactose tetraacetate *(PAMEGalOAc)*

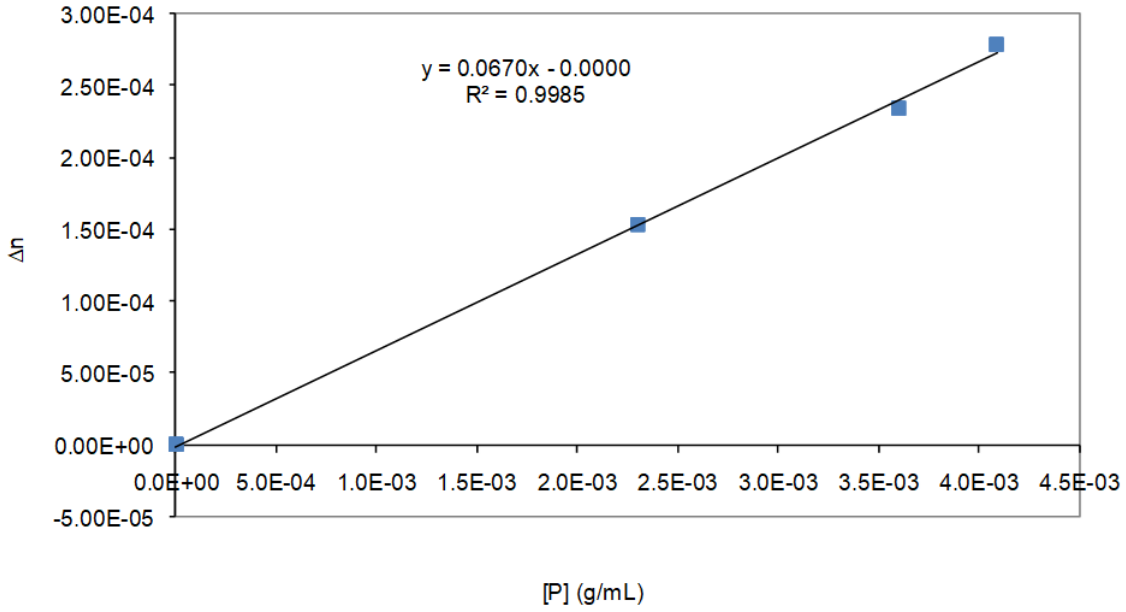

Attachment 6.14 - *dn/dc* (slope) calculation for the PAMEGalOAc. Refractive index measured in a refractometer at 40°C using different concentration solutions.

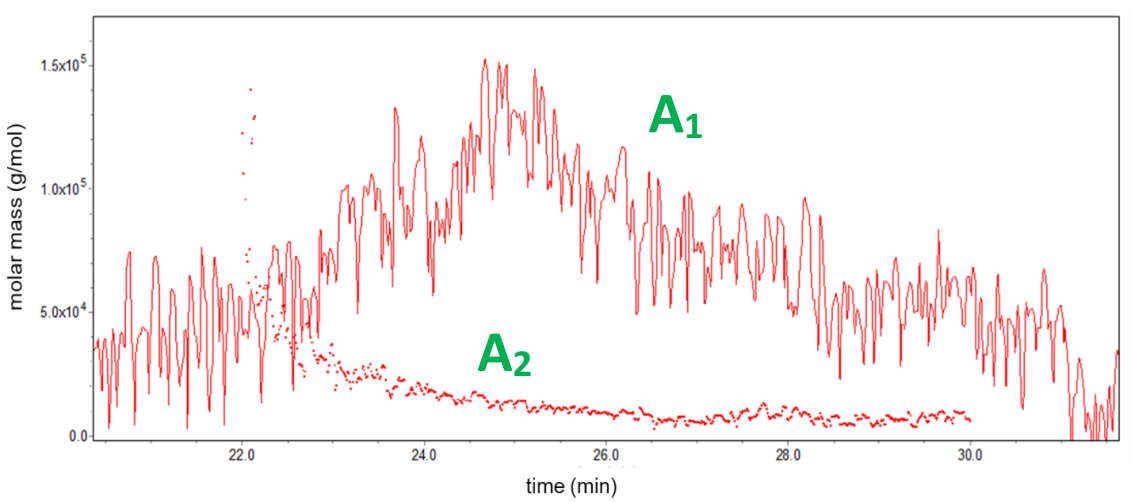

Attachment 6.15 – Chromatogram of the molecular weight distribution over elution time for PAMEGalOAc with (1/10) [initiator]/[CTA] ratio (4.3.8.1). Chromatogram of the molecular weight distribution over elution time for the (1/5) [initiator]/[CTA] ratio (4.3.8.1) is showed in figure 2.14. A_1 - Polymer elution over time (retention time limits 21.0 - 29.5 mins); A_2 - mass distribution over the elution.

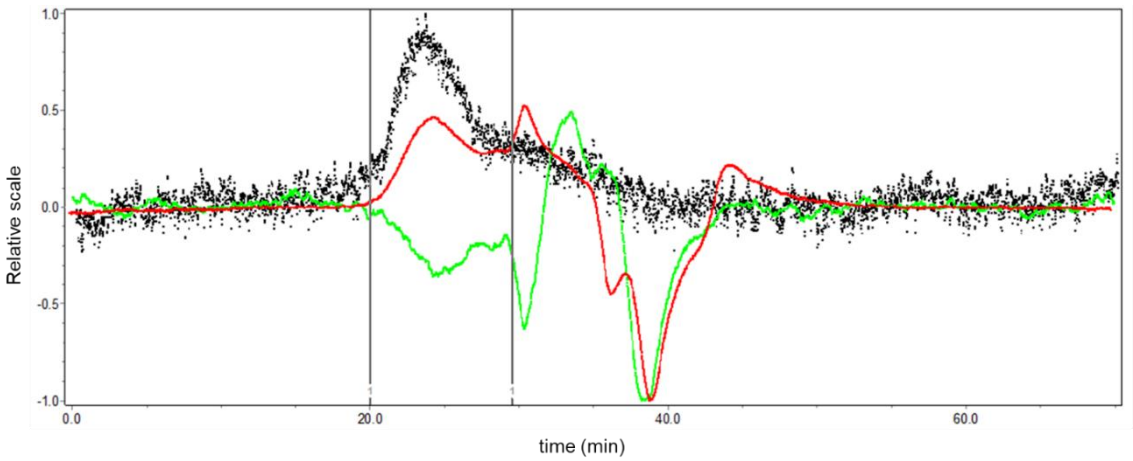

Attachment 6.16 – SEC-MALS results in THF, from the polymerization in solution using 2`-acrylamidoethyl-β-D-Galactose tetraacetate and BSPA as the CTA agent in a [initiator]/[CTA] ratio of 1 to 5 (4.3.8.1). Detectors: ● light scattering; ● raw refractive index; ● raw UV absorbance data.

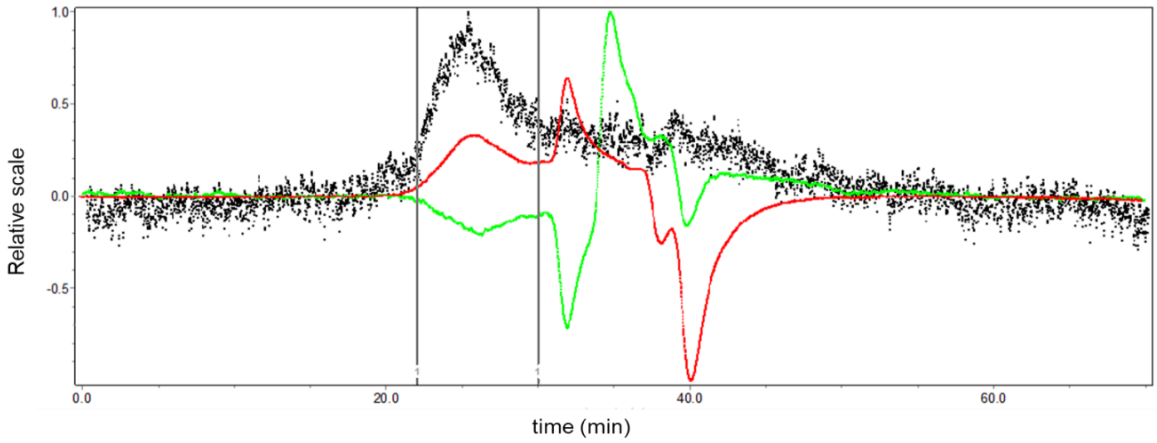

Attachment 6.17 – SEC-MALS results in THF, from the polymerization in solution using 2`-acrylamidoethyl-β-D-Galactose tetraacetate and BSPA as the CTA agent in a [initiator]/[CTA] ratio of 1 to 10 (4.3.8.1). Detectors: ● light scattering; ● raw refractive index; ● raw UV absorbance data.

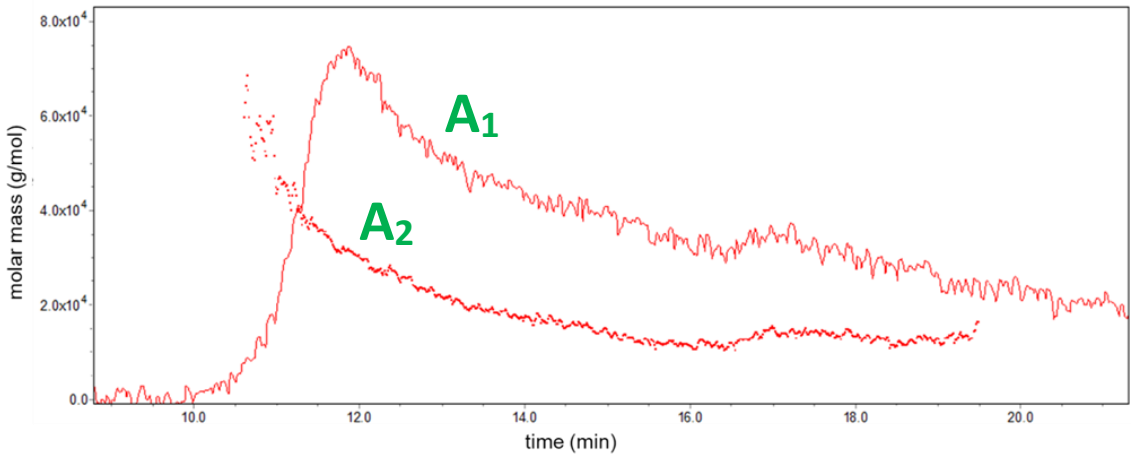

Attachment 6.18 – Chromatogram of the molecular weight distribution over elution time for PAMEGalOAc grown at the particle surface using the hybrid method (4.3.9.2) with CPADB as the CTA agent. A_1 - polymer elution over time (retention time limits 10.8 - 19.3 mins); A_2 - mass distribution over the elution.

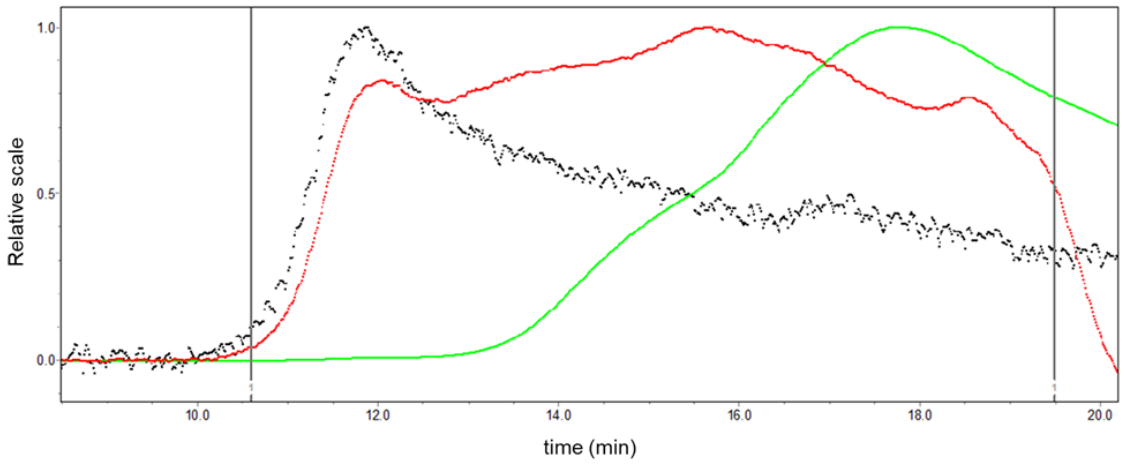

Attachment 6.19 – SEC-MALS results in THF, for the PAMEGalOAc grown at the particle surface using the hybrid method (4.3.9.2) with CPADB as the CTA agent. Detectors: ● light scattering; ● raw refractive index; ● raw UV absorbance data.

6.3.2. Polymer of 2`-acrylamidoethyl-β-D-Galactose *(PAMEGal)*

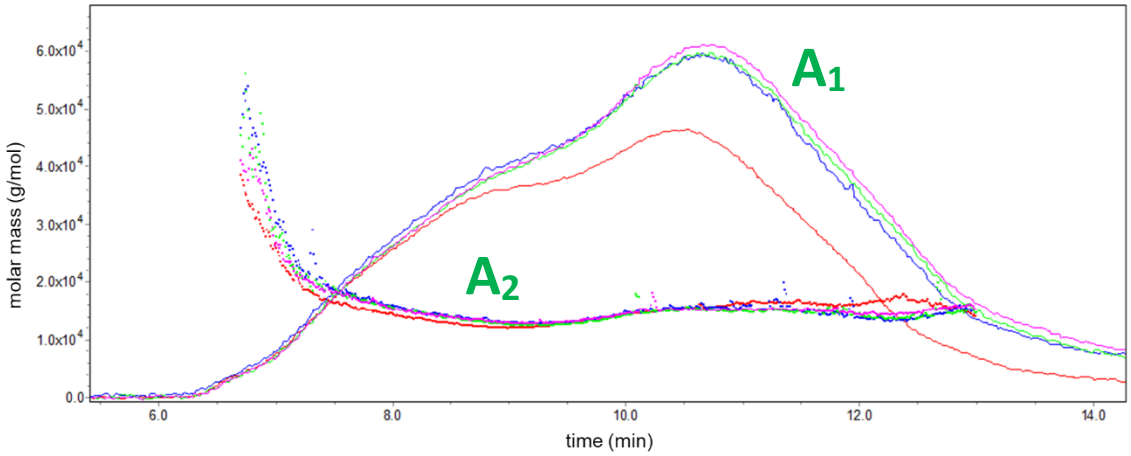

Attachment 6.20 – Chromatogram of the molecular weight distribution over elution time for PAMEGal grown in solution (4.3.8.2) with CPADB as the CTA agent. A_1 - polymer elution over time (retention time limits 6.7 – 13.0 mins); A_2 - mass distribution over the elution.

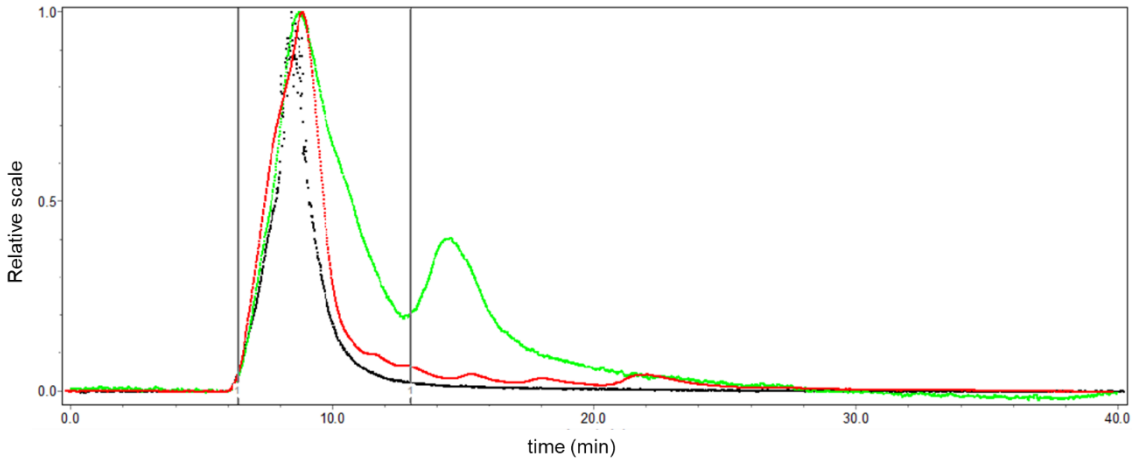

Attachment 6.21 – SEC-MALS results in H_2O, for the PAMEGal grown in solution (4.3.8.2) with CPADB as the CTA agent. Detectors: ● light scattering; ● raw refractive index; ● raw UV absorbance data.

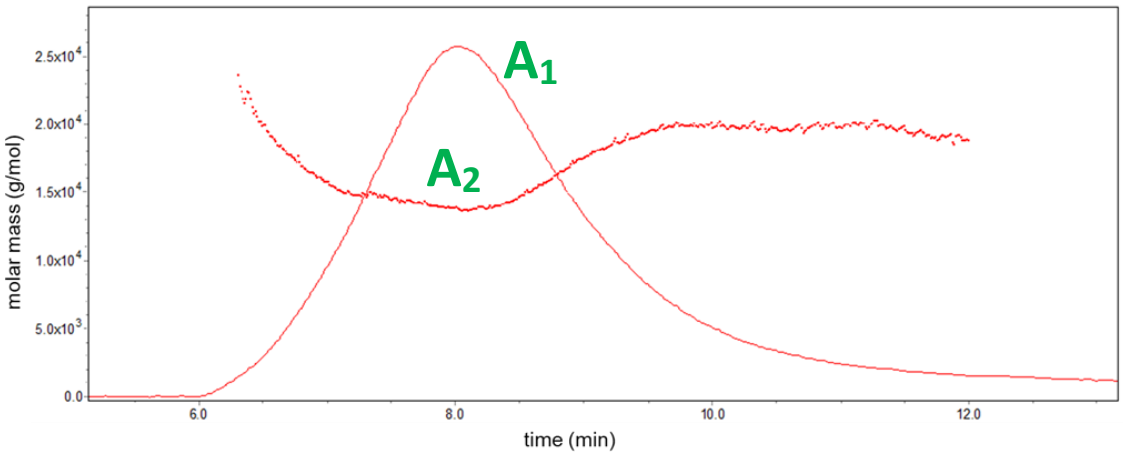

Attachment 6.22 – Chromatogram of the molecular weight distribution over elution time for PAMEGal grown at the particle surface using the hybrid method (4.3.9.2) with CPADB as the CTA agent. A_1 - polymer elution over time (retention time limits 6.7 - 11.7 mins); A_2 - mass distribution over the elution.

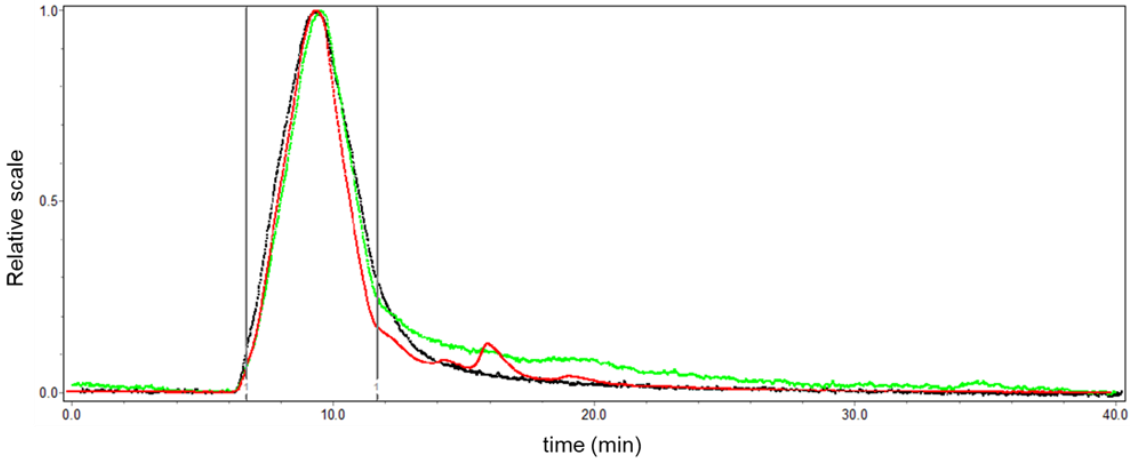

Attachment 6.23 – SEC-MALS results in H_2O, for the PAMEGal grown at the particle surface using the hybrid method (4.3.9.2) with CPADB as the CTA agent. Detectors: ● light scattering; ● raw refractive index; ● raw UV absorbance data.

6.3.3. Polymer for 2-(diiso-propylamino) ethyl methacrylate (PDPAEMA)

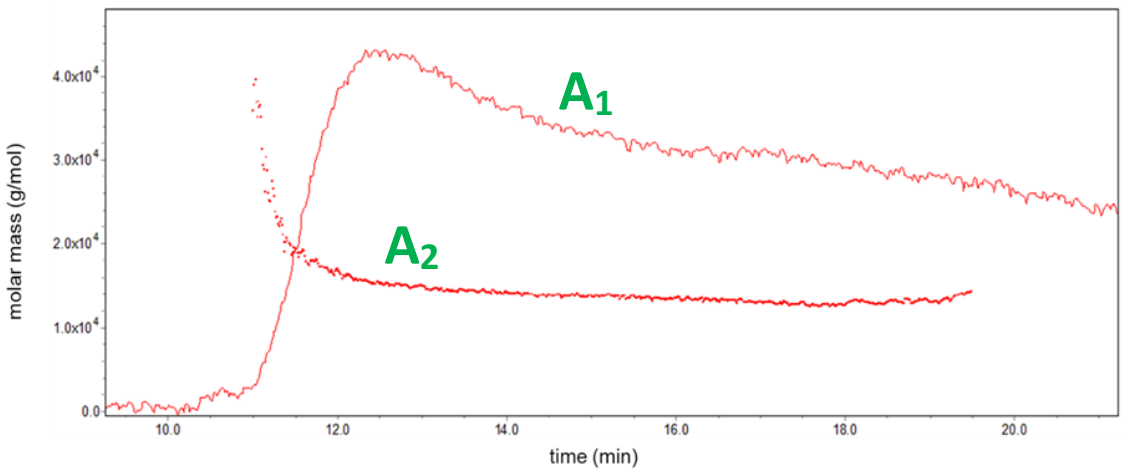

Attachment 6.24 – Chromatogram of the molecular weight distribution over elution time for PDPAEMA grown in solution with CPADB as the CTA agent. A_1 - polymer elution over time (retention time limits 12.0 – 20.0 mins); A_2 - mass distribution over the elution.

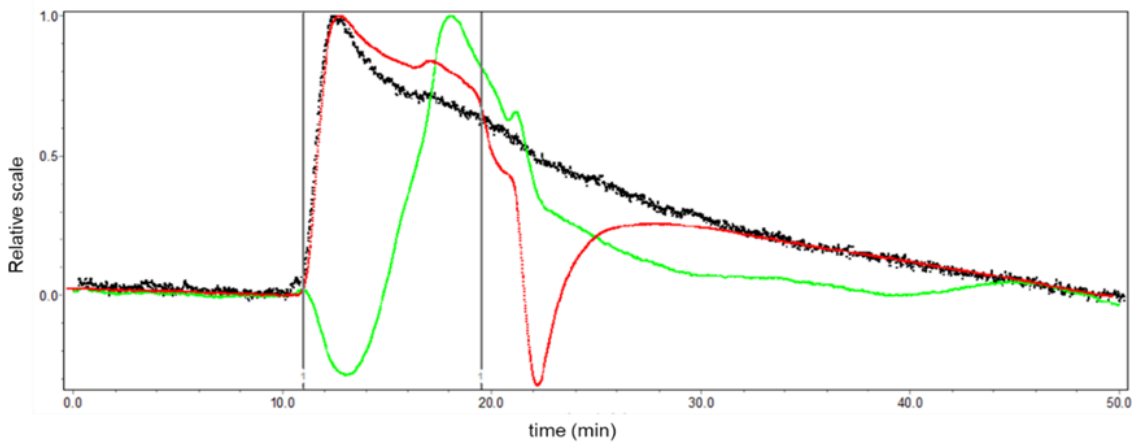

Attachment 6.25 – SEC-MALS results in THF, for the PDPAEMA grown in solution with CPADB as the CTA agent. Detectors: ● light scattering; ● raw refractive index; ● raw UV absorbance data.

6.3.4. Co-Polymerization of DPAEMA and AMEGal

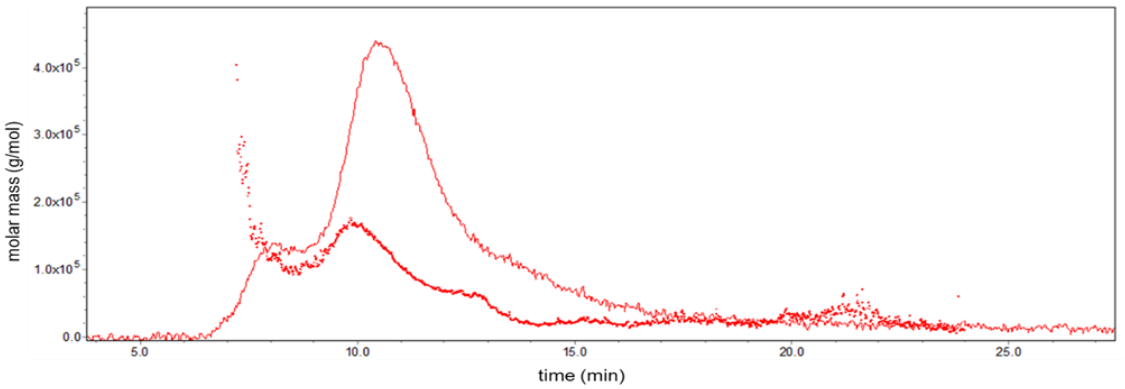

Attachment 6.26 – Chromatogram of the molecular weight distribution over elution time in H_2O for the co-polymer grown in solution (4.3.8.5) with CPADB as the CTA agent. A_1 - Polymer elution over time (retention time limits 6.7 - 11.0); A_2 - mass distribution over the elution time. SEC-MALS chromatogram for the co-polymer in figure 2.19.